

Diss. ETH No. 16173

**Assessing the carbon and water vapor fluxes in a temperate
grassland using $^{13}\text{CO}_2$ and H_2^{18}O as system tracers**

A dissertation submitted to the

SWISS FEDERAL INSTITUTE OF TECHNOLOGY ZURICH

for the degree of

DOCTOR OF SCIENCES

presented by

Daniel Ethan Theis

dipl. microbiol., University of Zurich

born 29th August 1972

citizen of Winterthur (ZH) and Schaffhausen (SH)

accepted on the recommendation of

Prof. Dr. Emmanuel Frossard, examiner

Prof. Dr. Hans Schnyder, TU Munich, co-examiner

Dr. Rolf Siegwolf, PSI Villigen, co-examiner

2005

II

Table of contents

Summary.....	V
Zusammenfassung.....	VIII
1 General introduction.....	1
1.1 Rising atmospheric CO ₂ and the global carbon cycle.....	1
1.2 Grassland.....	2
1.2.1 Grassland soils.....	2
1.2.2 The FACE experiment.....	3
1.3 Ecosystem-scale studies using stable isotopes.....	4
1.4 Objectives of this study.....	5
2 A portable automated system for trace gas sampling in the field and stable isotope analysis in the laboratory.....	6
2.1 Summary.....	7
2.2 Introduction.....	8
2.3 System design.....	9
2.3.1 Overview.....	9
2.3.2 Operation.....	10
2.3.3 Computer control.....	11
2.3.3.1 Sampling.....	11
2.3.3.2 Analysis.....	12
2.4 System performance.....	13
2.4.1 Calibration of the Mass Spectrometer.....	13
2.4.2 Laboratory performance.....	14
2.4.2.1 Storage effects.....	16
2.4.2.2 Automated compared to manual gas sampling and analysis.....	17
2.4.2.3 CO and CH ₄ isotope analysis.....	18
2.4.3 Field performance.....	20
2.5 Conclusions.....	21
2.6 Acknowledgements.....	21
3 Dynamics of soil organic matter turnover and soil respired CO ₂ in a temperate grassland labelled with carbon-13.....	22
3.1 Summary.....	23
3.2 Introduction.....	24
3.3 Materials and methods.....	26
3.3.1 Experimental site.....	26
3.3.2 Sampling and analysis.....	27
3.3.2.1 Bulk Soil.....	27
3.3.2.2 Soil air.....	28

3.3.2.3	Plant tissue.....	29
3.3.2.4	Calculation of remaining labelled carbon.....	29
3.3.2.5	Calculation of rhizosphere respiration.....	30
3.3.2.6	Statistical analysis.....	30
3.4	Results.....	30
3.4.1	Plant material.....	30
3.4.2	Soil organic matter (SOM).....	31
3.4.3	Calculation of new carbon after fumigation.....	35
3.4.4	Soil respired CO ₂	36
3.5	Discussion.....	38
3.5.1	SOM carbon content and isotopic disequilibrium.....	38
3.5.2	Soil carbon exchange after fumigation.....	38
3.5.3	Effects of the dry summer 2003 on SOM and soil respiration.....	39
3.5.4	Soil respired CO ₂	40
3.6	Conclusions.....	41
3.7	Acknowledgements.....	42
4	Partitioning of CO ₂ and H ₂ O-vapor fluxes in a temperate grassland using stable isotopes.....	43
4.1	Summary.....	44
4.2	Introduction.....	46
4.3	Materials and Methods.....	47
4.3.1	Experimental site.....	47
4.3.2	Sampling and analysis.....	48
4.3.2.1	Net ecosystem exchange (NEE).....	48
4.3.2.2	Air samples.....	49
4.3.2.3	Water vapor.....	49
4.3.2.4	Soil water.....	50
4.3.2.5	Plant water and carbon.....	50
4.3.2.6	Meteorological data.....	51
4.3.3	Calculations.....	51
4.3.3.1	Partitioning of CO ₂ fluxes.....	51
4.3.3.2	Partitioning of water vapor into evaporation and transpiration.....	53
4.3.3.3	Calculating canopy discrimination.....	55
4.3.4	Statistical analysis.....	58
4.4	Results.....	58
4.4.1	NEE and micrometeorology.....	58
4.4.2	Water vapor flux partitioning.....	60
4.4.3	Canopy discrimination.....	62
4.4.3.1	Influence of transpiration on canopy discrimination.....	65
4.4.4	CO ₂ flux partitioning.....	67

IV

4.4.4.1	Day – night course of CO ₂ and δ ¹³ C	67
4.4.4.2	Keeling plots	68
4.4.4.3	Assessment of CO ₂ fluxes F _R and F _A	72
4.5	Discussion	77
4.5.1	Water vapor flux partitioning	77
4.5.1.1	Keeling plots of H ₂ O	78
4.5.2	Discrimination	78
4.5.3	Diurnal and inter-diurnal variations of Keeling plot intercepts	80
4.5.4	CO ₂ flux partitioning	82
4.5.5	Sensitivity analysis	83
4.5.5.1	Calculation of Δ _{canopy}	83
4.5.5.2	Calculation of F _R and F _A	83
4.5.6	Pooling of data	85
4.5.6.1	Pooling of different (former) CO ₂ treatments from FACE	85
4.5.6.2	Pooling of different nitrogen fertilization levels	86
4.6	Conclusions	86
4.7	Acknowledgements	87
5	General Discussion	88
5.1	A novel tool for air sampling	88
5.2	CO ₂ and H ₂ O flux partitioning	89
5.3	Carbon sequestration	90
5.4	¹³ C as a system tracer	91
5.5	Outlook	91
6	References	93
	Appendix – A short introduction to stable isotopes and their applications:	99
	Acknowledgements	102
	Curriculum vitae	103

Summary

In a managed temperate grassland site in Switzerland (Eschikon, ZH, 550 m a.s.l.), formerly under ten years of “free air carbon dioxide enrichment” (FACE), a series of experiments was conducted to investigate carbon fluxes and pools within this ecosystem. The study was carried out for better quantifying the gross fluxes that are not fully understood at present. This is a serious constraint towards the development of reliable models for estimating the impact of future climate change and of rising CO₂ concentrations.

A new approach to partition the net flux of CO₂ (NEE) into assimilation (F_A) and respiratory fluxes (F_R) using ¹³CO₂ and H₂¹⁸O was tested. Discrimination of the plant canopy (Δ_{canopy}) against ¹³CO₂, which is a crucial parameter in the calculation of the gross fluxes F_A and F_R , was assessed by combining well-known equations describing photosynthesis and stomatal conductance. The sole parameter needed to calculate Δ_{canopy} that can not be directly measured on a canopy scale is the transpiration flux. This was further addressed by partitioning the evapotranspiration flux of water into plant transpiration and soil evaporation utilizing the different H₂¹⁸O signature of these two gross sub-fluxes. Uncertainties concerning the isotopic signature of the transpiration flux are related to the assumption of leaf ¹⁸O isotopic steady state. This led to a new approach where leaf water ¹⁸O enrichment was included. The model was discussed in detail and subjected to a sensitivity analysis. The obtained results for the H₂O flux partitioning with this new model were within the expected range and yielded results for Δ_{canopy} between 13.6 and 23.8‰. The calculated Δ_{canopy} showed a close correlation to water vapor pressure deficit (c_i / c_a vs. VPD, $r^2 = 0.81$) and net carbon assimilation on two days with changing cloud cover ($r^2 = 0.69$). The proposed model is thought to serve as a basis for a further refinement of the H₂O partitioning method.

Data from ¹³CO₂ samples provided information on ecosystem processes concerning assimilation and respiration. A close link between the $\delta^{13}C$ signature of assimilation and respiration during the following night was found, indicating that day time photosynthesis could be the driving force for night time respiration. Between day and night, differences in the isotopic source value as derived from a two-component mixing model (“Keeling plot”) were between 4.1 and 6.7‰. Additionally, night time source value (δ_R) correlated to meteorological conditions (VPD) 3-4 days prior to sampling.

VI

Optimal time slots for $^{13}\text{CO}_2$ sampling in an investigated ecosystem could be determined. The most stable results for Keeling plot analysis were obtained when transition times at sunrise and sunset were excluded. Furthermore, a sensitivity analysis of the equation used in the partitioning of CO_2 fluxes was done. Variations of day and night time Keeling plot intercepts (δ_N and δ_R) showed only little influence if the isotopic disequilibrium between the assimilation and respiration flux was strong (δ_A and δ_R). A high sensitivity to ambient $^{13}\text{CO}_2$ values was found, showing that locations for sampling of ambient CO_2 at flux sites should be carefully chosen.

No significant difference in the soil carbon pool size between the CO_2 fumigated and the control plots was found after ten years of the FACE experiment. The results strongly suggest that most of the new belowground C-deposition (during the FACE) was residing in labile C-pools and only a minute amount within the recalcitrant fraction.

A strong ^{13}C label of 3.4‰ was found on the formerly fumigated FACE plots within soil organic matter (SOM) in 0-12 cm soil depth at the end of the ten-year fumigation. This was a result of the ^{13}C depletion of the used CO_2 (-28.8‰). The uptake of non-labeled carbon and the decay of the fumigation signal after the end of the FACE-experiment was used as an inverse labeling experiment. The input of fresh carbon two years after the end of the CO_2 fumigation was calculated to be 45% of the total carbon in 0-12cm soil depth, according to the rapidly decreasing magnitude of the ^{13}C label. Annual carbon input was estimated to $9.8 \pm 3.7 \text{ Mg ha}^{-1}$. From the isotopic disequilibrium between the plants and the soil in the last year of the CO_2 fumigation, the proportion of rhizosphere respiration within total soil respiration could be determined to 61%.

To further facilitate sampling of trace gases for stable isotope analysis a portable, automated air sampler (ASA) was developed. It allows for 33 air samples of 300 mL to be taken at freely programmable sampling times. Analysis for ^{13}C and ^{18}O of CO_2 from all 33 flasks is possible in a little less than six hours without the need of handling the samples individually. The ASA works like an autosampler at the mass spectrometer and is ready again for sampling as soon as an analysis is completed. The achieved precision was shown to be twice as high as with manual single-flask analysis, 0.03‰ for $\delta^{13}\text{C}$ and 0.02‰ for $\delta^{18}\text{O}$ of CO_2 (standard errors *SE*, $n=11$). The ASA is also a useful tool for sampling and analysis of other trace gases with

smaller concentrations than CO₂ (e.g. CO, CH₄, NO_x, SO_x). Storage of samples is possible for 2-3 days without experiencing isotopic drifts, but potentially much longer when manually closing the stopcocks of the glass flasks used to store the samples. Programmable and reliable sampling greatly enhances the possibilities in particular for night-time sampling, which is a prerequisite for the application of the CO₂ flux partitioning method.

Zusammenfassung

Auf einer bewirtschafteten Graslandfläche in der Schweiz (Eschikon, ZH, 550 m ü M), welche vorher 10 Jahre lang Teil eines Versuches zur “Freiluft-Kohlendioxid-Anreicherung” (FACE) gewesen war, wurde eine Reihe von Experimenten durchgeführt um die Kohlenstoffflüsse und -reservoirs innerhalb einer Graslandfläche zu untersuchen. Die vorliegende Studie wurde mit dem Ziel gemacht, die quantitativen Verhältnisse der einzelnen Teilflüsse besser verstehen zu lernen. Die Wissenslücke betreffend der Grösse der einzelnen Kohlenstoff-Teilflüsse hindert die Entwicklung von zuverlässigen Klimamodellen und CO₂-Prognosen.

Ein neuer Ansatz innerhalb der stabilen-Isotopen-Methode, die zur Auftrennung des CO₂ Nettoflusses mittels ¹³CO₂ und H₂¹⁸O in Assimilation (F_A) und Respiration (F_R) verwendet wird, kam zur Anwendung. Die Diskriminierung eines Pflanzenbestandes gegenüber ¹³CO₂ (Δ_{canopy}) ist dabei ein entscheidender Parameter. Dieser wurde durch kombinieren von wohlbekannten Gleichungen betreffend Fotosynthese und Stomata-Leitfähigkeit hergeleitet. Der einzige Parameter in der resultierenden Gleichung der nicht direkt gemessen werden kann ist die Transpiration des Pflanzenbestandes. Um die Transpiration berechnen zu können wurde die Evapotranspiration in ihre Teilflüsse Transpiration und Evaporation aufgetrennt; dies unter Ausnützung der verschiedenen H₂¹⁸O Isotopensignaturen dieser zwei Teilflüsse. Aufgrund der Annahme eines isotopisch stationären Zustandes zwischen Blattwasser und Transpirationsstrom bestehen Unsicherheiten was die genaue isotopische Zusammensetzung des transpirierten Wassers betrifft. Wir haben deshalb erstmalig einen neuen Ansatz gewählt der die ¹⁸O Anreicherung im Blattwasser während des Tages berücksichtigt. Dieses neue Modell wurde in der vorliegenden Arbeit im Detail diskutiert und einer Sensitivitätsanalyse unterzogen. Die Resultate die das neue Modell für die H₂O Flusstrennung geliefert hat lagen im erwarteten Bereich (63% Transpiration bezogen auf Evapotranspiration, kurz nach einer Niederschlagsperiode). Das daraus errechnete Δ_{canopy} lag zwischen 13.6 und 23.8‰. Δ_{canopy} zeigte eine gute Korrelation zum Wasserdampf-Sättigungs-Defizit (VPD) der Luft (c_i / c_a gegen VPD, $r^2 = 0.81$) und zur Nettofotosynthese an zwei Tagen mit wechselnder Bewölkung ($r^2 = 0.69$). Das präsentierte Modell betreffend Transpiration soll als Basis für eine weiter Verfeinerung der H₂O Flusstrennungs-Methode dienen.

Anhand von Daten aus $^{13}\text{CO}_2$ Messungen konnten Informationen über Assimilation und Respiration gewonnen werden. Ein enger Zusammenhang zwischen der $\delta^{13}\text{C}$ Signatur der Assimilation und der Respiration während der folgenden Nacht wurde gefunden. Dies zeigt, dass die Fotosynthese die treibende Kraft hinter der (ihr folgenden) nächtlichen Respiration sein könnte. Werte aus dem Zwei-Komponenten Mischungsmodell (Keeling plot) des Tages und der folgenden Nacht unterschieden sich zwischen 4.1 und 6.7‰. Zusätzlich wurde ein Zusammenhang der nächtlichen $\delta^{13}\text{C}$ Signatur mit dem VPD 3-4 Tage vor den Probenahmen gefunden.

Für Keeling plot Anwendungen konnten optimale Zeitfenster für $^{13}\text{CO}_2$ Probenahmen eruiert werden. Die stabilsten Resultate wurden erzielt wenn die Übergangszeiten zwischen Tag und Nacht weggelassen wurden. Die Gleichung die für die CO_2 Flusstrennung verwendet wird wurde einer Sensitivitätsanalyse unterzogen. Variationen innerhalb der Tag und Nacht Keeling plot Werte (δ_N und δ_R) hatten nur eine geringe Auswirkung auf das Endergebnis der Berechnungen unter der Voraussetzung dass das isotopische Ungleichgewicht zwischen dem Assimilations- und dem Respirationsfluss genügend gross war. Hingegen wurde eine hohe Sensitivität gegenüber dem $^{13}\text{CO}_2$ Wert der Umgebungsluft festgestellt. Dies hat zur Folge dass Orte für die Probenahme von Umgebungsluft sorgfältig ausgewählt werden sollten.

Es konnten nach zehnjähriger CO_2 Begasung keine Unterschiede betreffend der Kohlenstoff Reservoirs zwischen den begasten und unbegasten Flächen des FACE Versuches festgestellt werden. Die Resultate deuten stark darauf hin, dass praktisch der gesamte während des FACE Experiments neu eingetragene Kohlenstoff in labilen Reservoirs abgelagert wurde.

Eine starke Markierung des Bodens mit ^{13}C wurde nach zehn Jahren FACE gefunden (3.4‰ in 0-12 cm Bodentiefe). Die Ursache dafür war das stark ^{13}C abgereicherte CO_2 welches für die Begasung benutzt wurde (-28.8‰). Die nach dem Ende der Begasung sich schlagartig veränderte ^{13}C Signatur in den Pflanzen wurde als inverses Markierungsexperiment verwendet. Der Eintrag von neuem Kohlenstoff zwei Jahre nach Ende der Begasung wurde auf 45% des Gesamtkohlenstoffs in 0-12 cm Tiefe bestimmt, dies aufgrund der festgestellten raschen Abnahme der ^{13}C Markierung im Boden. Der jährliche Kohlenstoffeintrag betrug $9.8 \pm 3.7 \text{ Mg ha}^{-1}$. Aufgrund des isotopischen Ungleichgewichts zwischen den Pflanzen und dem Boden (im letzten Sommer der Begasung) konnte der Anteil der Rhizosphären-Respiration an der totalen Bodenrespiration auf 61% bestimmt werden.

X

Um die Probenahme von atmosphärischen Spurengasen weiter zu vereinfachen wurde ein portabler, automatisierter Luftprobenehmer (ASA) entwickelt. 33 Proben zu je 300 mL können so zu frei programmierbaren Zeitpunkten gesammelt werden. Ohne die Proben aus dem Gerät nehmen zu müssen können sie am Massenspektrometer innerhalb von weniger als sechs Stunden auf ^{13}C und ^{18}O (von CO_2) analysiert werden und der ASA ist gleich nach der Analyse wieder einsatzfähig. Die Genauigkeit der CO_2 Analyse beim Gebrauch des ASA beträgt 0.03‰ für $\delta^{13}\text{C}$ und 0.02‰ für $\delta^{18}\text{O}$ (Standardfehler, n=11). Dies ist doppelt so hoch wie bei einer Probenahme mit Einzelflaschen von Hand. Mit dem ASA können Luftproben auch auf Spurengase mit kleineren Konzentrationen als CO_2 analysiert werden, z.B. CO , CH_4 , NO_x und SO_x . Die Proben können 2-3 Tage ohne Veränderung der Isotopenzusammensetzung aufbewahrt werden. Längere Zeiträume sind prinzipiell auch möglich wenn die Ventile an den Glasflaschen von Hand zgedreht werden. Der ASA eröffnet durch seine freie Programmierbarkeit und Genauigkeit grosse Möglichkeiten bei der Planung insbesondere von Nachtprobenahmen, welche eine Grundvoraussetzung für die Anwendung der CO_2 Flusstrennungs-Methode sind.

Chapter 1

1 General introduction

1.1 Rising atmospheric CO₂ and the global carbon cycle

During the last 420'000 years global climatic conditions oscillated between warm and cool periods (“ice ages”), differing by 9-12 °C (Petit *et al.*, 1999). These oscillations are thought to be mainly caused by fluctuations of solar forcing on the earth’s climate system (Bond *et al.*, 2001), enhanced or attenuated by feedback mechanisms of terrestrial processes like cloud cover, atmospheric transport mechanisms, biomass production and “greenhouse gas” concentrations (Beer *et al.*, 2000). Since the industrialization around 1750, greenhouse trace gases (CO₂, CH₄, N₂O) are considered to be a major factor of radiative forcing on the global climate (Houghton *et al.*, 2001), due to their increasing concentrations. Nevertheless it should be pointed out that the magnitude of influence from other contributing factors like aerosols, clouds or land albedo is yet uncertain. CO₂ has the largest influence on radiative forcing of the fore mentioned trace gases, since its concentration within the atmosphere is by far the highest. As retrieved from Antarctic ice core data covering the past 420 k years, the carbon dioxide (CO₂) concentration in the atmosphere has presently reached an unprecedented high concentration of 370 ppm (Petit *et al.*, 1999).

The global carbon cycle is quite well understood regarding the pathways, but concerning the magnitude of the individual fluxes there are still some uncertainties. The largest carbon pool is found in the oceans, predominantly in deep waters layers. At present, the oceans are a sink for carbon by dissolving atmospheric CO₂ in cold polar waters and conveying it to deep layers (North Atlantic deep water formation, NADW, Broecker & Peng, 1992). Without the NADW and deep sea currents as its driving force, the atmospheric CO₂ concentrations are estimated to be 200 ppm higher than the present level (Maier-Reimer *et al.*, 1996).

That the observed increase in atmospheric CO₂ is indeed primarily caused by (anthropogenic) fossil fuel burning was demonstrated by the “Süss-effect”. Carbon of fossil origin contains no more of the radioisotope ¹⁴C (since its half-life is only 5600 years) and concurrently shows a low ratio of the stable isotopes ¹³C/¹²C due to its plant origin (see below). Since roughly 200 years, as retrieved from ice core data, the atmospheric ¹⁴C content has been decreasing,

disturbed only by a short-term, but large increase after 1945 caused by the surface testing of nuclear weapons. The same was found for the $^{13}\text{C}/^{12}\text{C}$ ratio in the atmosphere, but without the “bomb peak” (Friedli *et al.*, 1986).

Roughly one fourth of the annual anthropogenic CO_2 release (7.5 Gt C a^{-1}) is entering the oceans, whereas an estimated 50% resides in the atmosphere. The remaining 2 Gt C a^{-1} are still unaccounted for (Gifford, 1994) within the global C budget and thus referred to as the “missing sink”. It is thought that this carbon is sequestered into soil organic matter (SOM) via an increased biomass production. This seems feasible since SOM contains twice the amount of carbon as the atmosphere and three times as much as the terrestrial vegetation (Houghton *et al.*, 2001). This lack of knowledge concerning the missing sink reduces the reliability of modeled predictions for future CO_2 and climate scenarios and is therefore a topic of current research.

1.2 Grassland

Grasslands cover an estimated 24% of the global land surface (Sims & Risser, 2000) and 20% of the land area in Europe (Soussana *et al.*, 2004). The majority of grassland areas in temperate regions are not climax vegetation but a result of agricultural activities. In temperate climate zones these semi-natural grasslands growing on fertile soils, are often dominated by *Lolium perenne* (perennial ryegrass). The significance of grassland within the global carbon cycle has probably been underestimated. Since grasslands are rarely tilled and generally covered by dense vegetation throughout the year, their soils have a larger C storage capacity than tilled soils under annual crops (Soussana *et al.*, 2004).

1.2.1 Grassland soils

In grassland ecosystems up to 98% of the total carbon can be found belowground (Hungate *et al.*, 1997). Soil organic matter (SOM) in general contains twice the amount of carbon found in the atmosphere (Post *et al.*, 1982). Within the context of the expected future rise of the atmospheric CO_2 content and possible changes of climatic conditions, it is still uncertain if the soil carbon pools will be a future source or sink. Two distinctly different turnover rates for SOM are found within soils: a labile fraction with turnover rates of years to decades and a more inert fraction with turnover rates of centuries (Balesdent & Mariotti, 1987). Older SOM pools, such as stable non-hydrolysable humus fractions, show a low susceptibility towards

microbial decomposition, thus causing the low turnover rate. These pools are considered to be conservative in regard to new carbon input (Pelz *et al.*, 2005).

Between soils and the atmosphere a large annual turnover of 60 Gt C a⁻¹ has been estimated (Houghton *et al.*, 2001). A large proportion of the carbon entering the soil is therefore returned to the atmosphere by soil respiration (Jones & Donnelly, 2004), either directly, derived from fresh inputs (root and rhizosphere respiration) or indirectly, from older SOM (heterotrophic SOM respiration). Soil respiration is therefore considered to be a key factor for soil carbon turnover and the allocation of the fore mentioned C-fractions to the underlying processes is of particular interest.

The sum of respiration by living roots, their associated mycorrhizal fungi and heterotrophic respiratory transformation of root exudates is termed as “rhizosphere respiration” and shows a strong dependency on the magnitude of assimilation by the plants (Ekblad *et al.*, 2005). The proportions of the individual contributions to soil respiration are still uncertain and highly variable results have been obtained from the few conducted studies. For grassland, rhizosphere respiration was reported to account for 16 to 95% of total soil respiration (Jones *et al.*, 2004). Recent studies found rhizosphere respiration to be the dominating fraction, accounting for 54 to 70% of total soil respiration within cropland and forest ecosystems (Högberg *et al.*, 2001, Soe *et al.*, 2004).

1.2.2 The FACE experiment

The physiological effects on plants due to elevated CO₂ are well known under laboratory conditions (Nösberger *et al.*, 2000). However, predictions on ecosystem responses to elevated CO₂ levels are limited from these studies. The Swiss free-air CO₂ enrichment (FACE) experiment in Eschikon (ZH) was established in 1993 to investigate the response of a grassland ecosystem to elevated CO₂. The increased CO₂ level of 600 ppm was maintained during ten years until the end of the growing season 2002 (see Zanetti *et al.*, 1996 for further details). It was the longest-running FACE experiment on a managed grassland site.

The response of plants to elevated CO₂ within the FACE was found to change with time due to feedback mechanisms in the soil, which were only revealed after several years (Schneider *et al.*, 2004). Aeschlimann *et al.*, 2005 found no increase of net ecosystem carbon input after nine years of elevated CO₂, even though net assimilation was higher. Since respiratory releases were also increased, no net change was observed, but the C-flow in the ecosystem was enhanced.

A different set of experiments became possible after the long-term exposure to elevated CO₂, since the added CO₂ originated from the combustion of fossil carbon sources and was therefore depleted in ¹³C ($\delta^{13}\text{C} = -28.8\text{‰}$ in the year 2002). This caused a strong ¹³C label within the SOM after a few growing seasons, allowing for studies of carbon input and turnover to be done (Nitschelm *et al.*, 1997, Six *et al.*, 2001, Van Kessel *et al.*, 2000). In accordance to the findings of Aeschlimann *et al.*, 2005, no significant differences between the size of the SOM pools in the fumigated and the control plots were found.

1.3 Ecosystem-scale studies using stable isotopes

Net ecosystem exchange (NEE) of CO₂ and H₂O is being measured by means of the eddy-covariance technique (Baldocchi *et al.*, 1988) at over 100 sites around the world. However, net fluxes provide only marginal information on the underlying gross sub-fluxes photosynthesis and day time respiration (or transpiration and evaporation in the case of H₂O). On the leaf-level, the gross CO₂ and H₂O sub-fluxes can be measured with high precision (Percy *et al.*, 1989), but with poor spatial representation. Since it is these sub-fluxes that are primarily influenced by weather and climatic conditions, an understanding of the interrelationships on an ecosystem scale is of great interest.

During the photosynthetic process the CO₂ fixing enzyme ribulose-1-5-biphosphate-carboxylase (RUBISCO) exerts a discrimination against ¹³CO₂. The carbon in plants is therefore depleted in ¹³C relative to the atmosphere; with the magnitude of this depletion depending on the photosynthetic pathway (C₃, C₄) of the plants (Smith & Epstein, 1971). The carbon in C₃ plants has an average $\delta^{13}\text{C}$ value of -27‰ whereas plants with the C₄-pathway show a much smaller discrimination resulting in an isotopic value of about -12‰ for their carbon-13 ($\delta^{13}\text{C}$ of atmospheric CO₂ is -8‰). The realization that during photosynthesis the air around a plant canopy is locally enriched in ¹³C due to the discrimination (Farquhar *et al.*, 1989), led to the development of methods to deploy this characteristic to partition the net CO₂ flux into its gross fluxes photosynthesis and day time respiration (Yakir & Wang, 1996). Thereby, day time respiration is the combined flux of autotrophic respiration (photorespiration and metabolic respiration from shoots and roots) and heterotrophic respiration (respiration of SOM and respiration of root exudates). The basic principle is that the two gross fluxes that are to be separated need to have a different ¹³C isotopic signature. This is given due to the isotopic disequilibrium introduced into the air-plant-soil system by the photosynthetic ¹³C discrimination. Many studies have been conducted since the

development of the method, but isotopic flux partitioning is still far from being a routine ecosystem analysis (Bowling *et al.*, 2001, Knohl *et al.*, 2005, Lai *et al.*, 2003).

Basically the same principle can be applied to the partitioning of water vapor fluxes within a plant canopy. Evapotranspiration (ET) as the net flux can be partitioned into plant transpiration (T) and soil evaporation (E) since the T and the E flux have a different oxygen isotopic signature. As water evaporates, the lighter H_2^{16}O molecules leave the water body more readily due to their smaller mass. The remaining (soil) water thus is progressively enriched in the relative amount of H_2^{18}O during the evaporation process (Craig & Gordon, 1965). Water transpired by the plants undergoes a different isotopic fractionation which is more complex since it also involves leaf water (Farquhar & Cernusak, 2005). Leaf water itself is highly enriched in H_2^{18}O during day time hours and its influence on the isotopic composition of the transpiration flux is still a topic of active research. Nevertheless, as for CO_2 , the two H_2O fluxes with their different isotopic oxygen signature can be identified and partitioned. This has been successfully applied by Yakir *et al.*, 1996 and Yopez *et al.*, 2003.

Since these methods require a high sampling frequency of air and water vapor samples to have a sufficient accuracy, there is a need for appropriate tools to further facilitate the applicability of the methods. The stable isotope methods have the advantage of being non-destructive and have the potential to provide information on gross fluxes within an ecosystem scale.

1.4 Objectives of this study

- Applying the isotopic partitioning methods for CO_2 and H_2O on a grassland site and identifying possibilities for further progress of the methods
- The development of tools to further facilitate trace gas sampling as a prerequisite for the isotopic CO_2 partitioning method
- Investigating the effect of ten years of elevated CO_2 on the soil carbon pool. Does elevated CO_2 cause an increase of SOM?
- Deploying the ^{13}C label of SOM after 10 years of FACE to quantify soil processes: soil carbon turnover and soil respiration (in relation to rhizosphere respiration)

A better understanding of the responses to changes in meteorological and climatic conditions within grasslands could provide important information for an improved assessment of the impact of possible future climatic changes on the carbon and water cycles of these ecosystems.

Chapter 2

2 A portable automated system for trace gas sampling in the field and stable isotope analysis in the laboratory

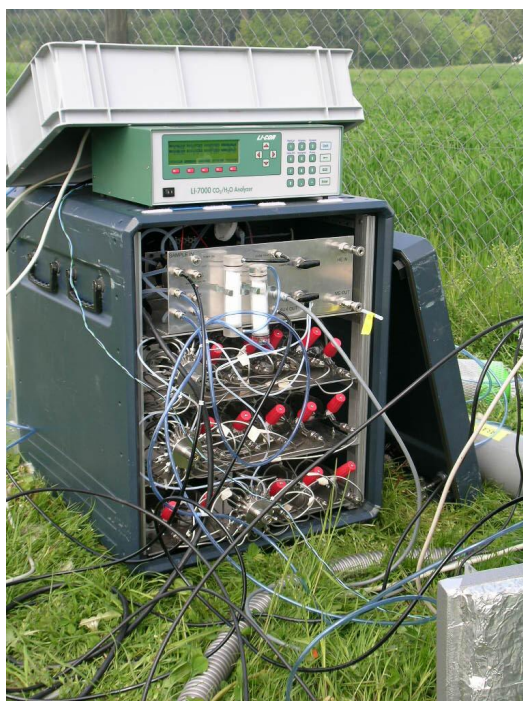


photo: W. Eugster

2.1 Summary

A computer controllable mobile system is presented which enables the automatic collection of 33 air samples in the field and the subsequent analysis for $\delta^{13}\text{C}$ and $\delta^{18}\text{O}$ stable isotope ratios of a carbon containing trace gas in the laboratory, e.g. CO_2 , CO or CH_4 . The system includes a manifold gas source input for profile sampling and an infrared gas analyzer for *in situ* CO_2 concentration measurements. Measurements of $\delta^{13}\text{C}$ and $\delta^{18}\text{O}$ of all 33 samples can run unattended and take less than six hours for CO_2 . Laboratory tests with three gases – compressed air with different $p\text{CO}_2$ and stable isotope compositions – showed a measurement precision of 0.03‰ for $\delta^{13}\text{C}$ and 0.02‰ for $\delta^{18}\text{O}$ of CO_2 (standard errors SE , $n=11$). A field test of our system, where 66 air samples were collected within a 24 hour period above a grassland, showed a correlation of 0.99 (r^2) between the inverse of $p\text{CO}_2$ and $\delta^{13}\text{C}$ of CO_2 . Storage of samples until analysis is possible for about one week, this can be an important factor for sampling in remote areas. A wider range of applications in the field is open with our system, since sampling and analysis of CO and CH_4 for stable isotope composition is also possible. Samples of compressed air had a measurement precision (standard errors SE , $n=33$) of 0.03‰ for $\delta^{13}\text{C}$ and of 0.04‰ for $\delta^{18}\text{O}$ on CO and of 0.07‰ for $\delta^{13}\text{C}$ on CH_4 . Our system should therefore further facilitate research of trace gases in the context of the carbon cycle in the field and opens many other possible applications with carbon and possibly non-carbon containing trace gases.

2.2 Introduction

With rising $p\text{CO}_2$ in the atmosphere, characterization and quantification of carbon fluxes within and between ecosystem and atmosphere are increasingly important factors in understanding and modeling global carbon related processes. The terrestrial biosphere is known to play an important role in observed seasonal and interannual $p\text{CO}_2$ fluctuations (Schimel, 1995). The measurement of stable carbon and oxygen isotopes has become a powerful tool in the study of carbon cycles at the ecosystem and global level. Isotopic fluctuations and gradients of $\delta^{13}\text{C}$ and $\delta^{18}\text{O}$ in air, plant tissue, and soil organic matter result from isotope effects that occur during gas exchange between the atmosphere and the vegetation (Bowling *et al.*, 2001, Yakir & Sternberg, 2000). In order to quantify individual carbon fluxes, e.g. assimilation and respiration, isotopic ratios of $\delta^{13}\text{C}$ and $\delta^{18}\text{O}$ in CO_2 have to be determined in a large number of air samples to assess temporal and spatial variability within an ecosystem. Manual air sampling techniques require a considerable amount of time and personnel in the field, as well as for the isotope analysis in the laboratory. Furthermore reproducibility is poor. To estimate ecosystem isotopic fluxes, net ecosystem exchange (NEE) of CO_2 is measured with e.g. the eddy covariance (EC) or open-flow chamber method and combined with flask air sampling for $^{13}\text{CO}_2$ isotopic ratio determination (Bowling and Pataki *et al.*, 2003). These methods allow non-intrusive characterization of ecosystem-scale carbon exchange processes. Due to the necessity of night time measurements for Keeling plot applications and of prolonged sampling periods, considerable efforts were recently made in the development of automated sampling systems for CO_2 and other trace gases in air. Another important factor is optimizing the precision of stable isotope ratio determination, in particular of $\delta^{13}\text{C}$ and $\delta^{18}\text{O}$ (McNamara *et al.*, 2002, Mortazavi & Chanton, 2002, Ribas-Carbo *et al.*, 2002, Schauer *et al.*, 2003). Our goal was to develop an automated, easy to use, portable system which guarantees high precision stable isotope ratio determination of atmospheric trace gases. Emphasis was placed on automation of air sampling, as well as automation of stable isotope ratio determination in the laboratory. We used large glass flasks (300 mL) in our system to account for difficulties reported with small sampling vials regarding changes in CO_2 isotopic composition (Nelson, 2000). The large flask volume also enables the isotopic analysis of other atmospheric trace gases such as CO and CH_4 which have a much smaller atmospheric partial pressure than CO_2 .

2.3 System design

2.3.1 Overview

The air sampler (ASA) is enclosed in a 60 cm x 55 cm x 75 cm portable weatherproof aluminium case equipped with small wheels (Incas, Knörr AG, Germany) and weighs 55 kg with the case. For sampling and storage of air, cylindric glass flasks (Keller Glas, Switzerland) with a diameter of 6 cm, reducing to a 6 mm connection tube with manual regulating valves on both ends, were used. The flasks have a volume of 300 mL each, in order to obtain a sufficiently large air sample for trace gas analysis. Eleven of these flasks are connected to a twelve position multiport valve (Valco multiport ST valve, VICI, USA) using 1/8" stainless steel tubes (VICI, USA). The twelfth position on the valve was connected to a small loop. The rotor material used in the multiport valves was Valcon M (VICI, USA), which is the most inert available in regard to isotopic exchange effects for ^{13}C and ^{18}O (Schauer *et al.*, 2003). Transition between glass flasks and stainless steel tubes was made with 6 mm to 1/8" connectors (Swagelok, USA) containing Teflon (PTFE) seals at the glass side. Three identical multiport valves with eleven flasks each are set up in serial connection through their inlets and outlets with flexible Teflon (PTFE) tubes, yielding a total of 33 sampling flasks (Figure 1). The system is built on four levels inside the aluminium case, three levels each hold one multiport valve connected to eleven glass flasks. The fourth level holds the pump, the electronic devices, and a front panel with the gas in- and outlets (Trigrass, Switzerland), control switches for power and the manual three way valves and a socket for the electronic control cable. Positions of the multiport valves are fully computer controllable making automated and unattended sampling and analysis possible. In the laboratory the ASA is directly connected to the mass spectrometer and is computer controlled, like an autosampler.

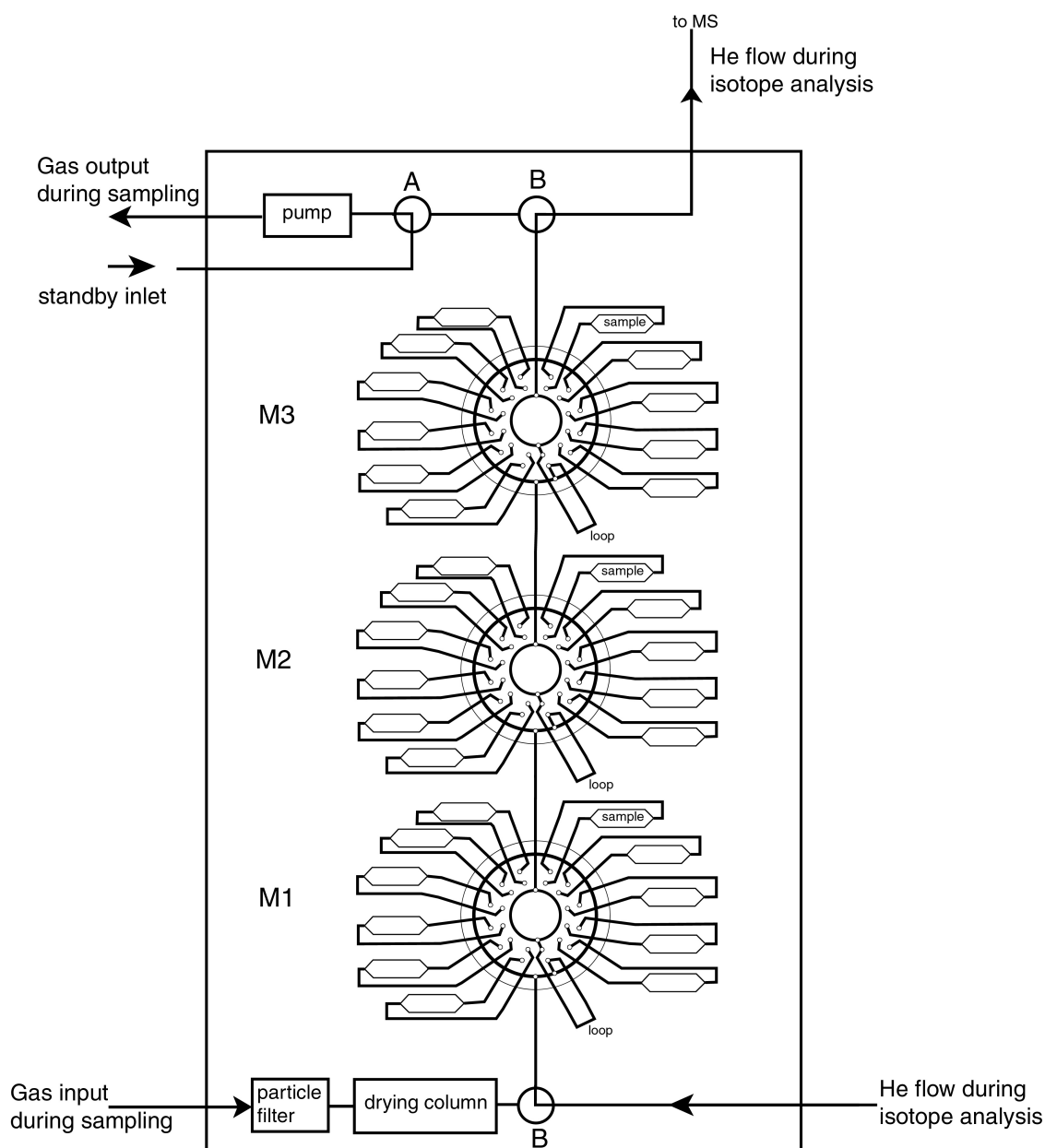


Figure 1 Diagram of the air sampler (ASA). A) magnet valve, controlling whether the pump draws air through the ASA (sampling state) or from the standby inlet (standby and release state). B) 3-way manually switchable valves to change between sampling mode or analysis mode. M1-3) multiport rotary valves connected to eleven sampling flasks each. The loop position serves as a bypass

2.3.2 Operation

A teflon membrane pump (811KNE, KNF, Germany) which is installed downstream of the flowline pulls the air through the ASA resulting in a flow of 2 L min^{-1} (flow rate of the pump without resistance is 11.5 L min^{-1}). After passing a particle filter (Hepa-Vent, Whatman, UK) and a MgCl_2O_8 drying column the air stream is subsequently directed to the desired sampling flask according to the momentary positions of the three multiport valves M1-M3. Between the last multiport valve M3 and before the pump, a magnet valve (EVT307-5T0-02F-Q, SMC,

Switzerland) switches between the flask line and a standby inlet (Figure 1). Between sampling intervals, when no flask is to be filled, the air flows through the standby inlet and not the flask line, preventing an early exhaustion of the desiccant. This is also thought to prolong the lifespan of the pump since switching it on and off many times during sampling sessions would most likely increase the risk of a breakdown. There are three states of the system: *standby state* where the magnet valve opens the standby inlet while all multiport valves are on the loop position, *sampling state* with the magnet valve switched to the flask line to fill the selected flask. To fill e.g. flask number 14 on the second level, the multiport valves M1 and M3 are set to the loop position, while multiport M2 is set to the appropriate flask position. Finally the *release state*: the magnet valve is switched to the standby inlet while the multiport valves remain in their position. This allows the equilibration of the pressure difference between the flasks and the ambient pressure, which is a result of the pump operating in downstream position. The system then goes back to the *standby state*.

The main outlet -after the three multiport valves- can be connected to an external infrared gas analyzer (IRGA) for in situ measurements of the CO₂ concentration of the individual samples. With an additional computer controlled manifold connected to the input of the system, automated sampling of several gas sources is possible, e.g. to sample height profiles in and above a plant canopy (Figure 2). The current construction of the system allows sampling of six gas sources. More inputs are possible, depending only on the construction of the peripheral input manifold.

2.3.3 Computer control

2.3.3.1 Sampling

For gas sampling in the field, the ASA and its peripheral components (IRGA, gas input manifold) are controlled with a LabView (National Instruments, USA) program running on a portable computer. The main elements of this program include control over sampling intervals and times, duration of the above mentioned system states, settings of the external gas input manifold and logging of the IRGA data. The different devices require individual communication protocols: the multiports M1-M3 are controlled with a modified RS485 protocol (semiduplex), the IRGA requires the RS232 protocol and finally the gas input manifold is controlled with +12V pulses. An interface was developed to provide two-way communication between the mentioned devices and the computer via one single RS232 or

USB port. The two-way communication enables the control program to verify the position of the multiports M1-M3.

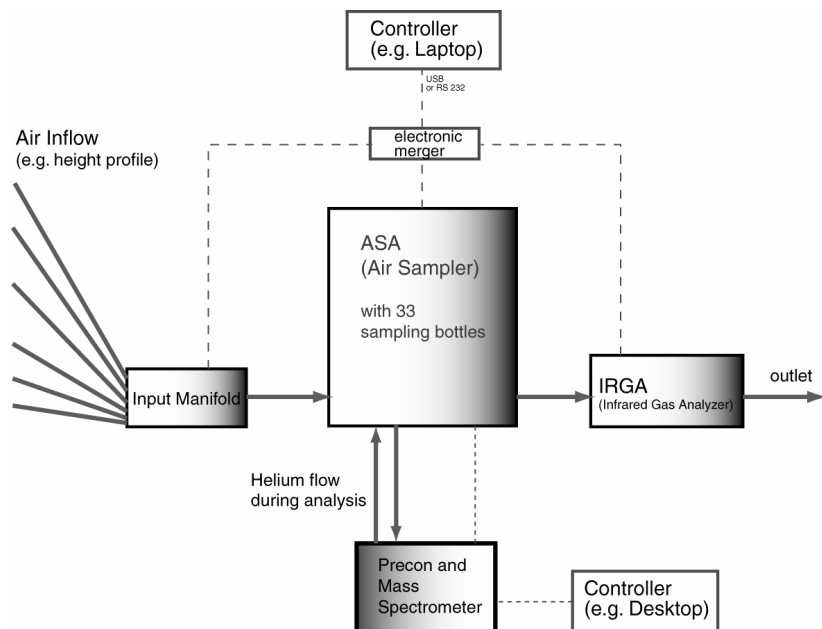


Figure 2 Schematic of the ASA and its peripheral components. Field situation with manifold and IRGA, and laboratory situation with precon and mass spectrometer.

2.3.3.2 Analysis

For laboratory use as an autosampler the three multiport valves are controlled by electric impulse signals coming from the Gasbench II (Finnigan, Germany), a peripheral of the Delta Plus XL mass spectrometer (Finnigan, Germany). Each multiport M1-M3 is switched via pulse relays built into the Gasbench II, thus the ASA can be controlled from within the Isodat Software (Version 2.0, Finnigan, Germany) used to control the mass spectrometer. This allows integration into the specific analysis protocol within the Isodat Software. Two interconnected but independent gas circuits on the used Precon-Device (Finnigan, Germany) were deployed to program a nested analysis mode, cutting down analysis time significantly (see below). A given sample is flushed from its flask by the Helium carrier gas at 50 mL min^{-1} for 380 seconds with the multiport of the Precon device in “load” position (Figure 3). For cryofocussing with liquid nitrogen the multiport is switched to the “inject” position for 10 seconds and then back to “load”. Gas chromatographic separation and mass spectrometric analysis take another 640 seconds, but instead of waiting for the sample to finish analysis

completely, 380 seconds before the end the next sample can already be flushed from its flask. With this nested protocol 33 samples can be automatically analyzed for $\delta^{13}\text{C}$ and $\delta^{18}\text{O}$ isotopic ratios of CO_2 in 5 hours and 52 minutes, corresponding to 10 minutes and 40 seconds per individual sample.

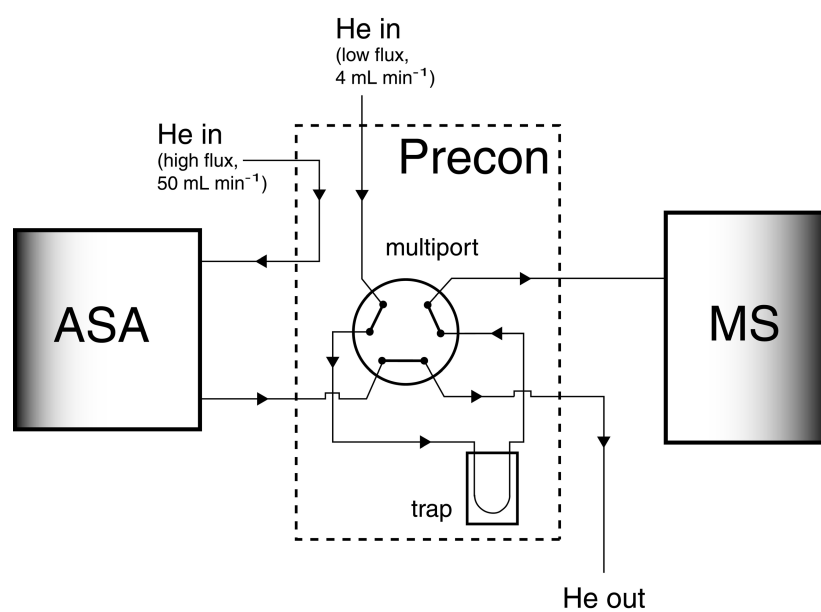


Figure 3 Schematic of the precon device with the gas flowpaths shown. The multiport has two switchable positions (load, inject) to control the carrier gas during analysis. The “load” position, as shown in the schematic, is used to flush the samples from the glass flasks in the ASA.

2.4 System performance

2.4.1 Calibration of the Mass Spectrometer

Calibration of the analysis system (mass spectrometer and used peripherals) for system related offsets is done by injecting calibrated reference gas with every sample (one reference peak per sample). Reference gas is 100% CO_2 (Air Liquide, Switzerland) which itself was calibrated with dual inlet analysis against a CO_2 standard gas (Oztech, USA). To rule out possible effects of the peripheral precon device during analysis the reference gas was tested against itself. Results for $\delta^{13}\text{C}$ and $\delta^{18}\text{O}$ were consistent against the reference peak when injecting the reference gas with a single glass flask through the precon device. The ASA itself was tested against single glass flask analysis (see Table 2) to exclude the possibility of a system related offset. Signal strength at mass 44 is 6 to 8 Volts for ambient CO_2 concentrations.

2.4.2 Laboratory performance

The performance of the ASA for $\delta^{13}\text{C}_{\text{VPDB}}$ and $\delta^{18}\text{O}_{\text{VSMOW}}$ of CO_2 in air was tested in the laboratory. Compressed air (Carbagas AG, Switzerland) and compressed mixtures of synthetic air (80% N_2 , 20% O_2 , Carbagas AG, Switzerland) with CO_2 of different isotopic ratios was used (Table 1). Sampling required a gas overflow which was maintained at $>1 \text{ L min}^{-1}$ at the input of the ASA. The internal pump in the ASA generated a through flow of 2 L min^{-1} and sampling flasks each were flushed with at least six-fold their volume. The difference to ambient pressure in the flasks after flushing was immediately equilibrated thereafter, as described above.

Table 1 Gas 1 is compressed air, gas 2 is a mixture of synthetic air (80% N_2 , 20% O_2) with CO_2 and gas 3 is a CO_2 calibration gas (Carbagas, Switzerland). CO_2 concentrations were measured with an IRGA (LI-COR 6262 $\text{CO}_2/\text{H}_2\text{O}$ analyzer). Isotopic ratios are expressed in the δ notation with \pm standard deviation (σ). Typical atmospheric values are given for comparison.

	Gas 1	Gas 2	Gas 3	Air
CO_2 (ppmv)	398.2	404.3	340.4	~380
$\delta^{13}\text{C}$ (‰)	-9.42 ± 0.08	-45.57 ± 0.06	-29.16 ± 0.07	~-9
$\delta^{18}\text{O}$ (‰)	33.15 ± 0.08	8.33 ± 0.07	9.20 ± 0.04	~-33

The three different gases with CO_2 concentrations in the range of ambient CO_2 (Table 1) were filled into the ASA in sequence (gas 1 in flask 1, gas 2 in flask 2, gas 3 in flask 3, gas 1 in flask 4 and so forth) so that every flask had two neighboring flasks with different gases. Isotope ratio determination was done within 6 hours after filling and showed good consistency within the individual gases (Figure 4). Observed standard deviations (σ) were between 0.06‰ and 0.08‰ for $\delta^{13}\text{C}_{\text{VPDB}}$ and between 0.04‰ and 0.08‰ for $\delta^{18}\text{O}_{\text{VSMOW}}$. The standard error (*SE*) representing the measurement precision was between 0.02‰ and 0.03‰ for $\delta^{13}\text{C}_{\text{VPDB}}$ and between 0.01‰ and 0.02‰ for $\delta^{18}\text{O}_{\text{VSMOW}}$ ($n=11$). These results lie within the range of the instrument precision using the cryofocussing technique and show that effects of possible leaks and mixing processes within the ASA are negligible on short term analysis, thus offering the potential for high precision measurements of field samples.

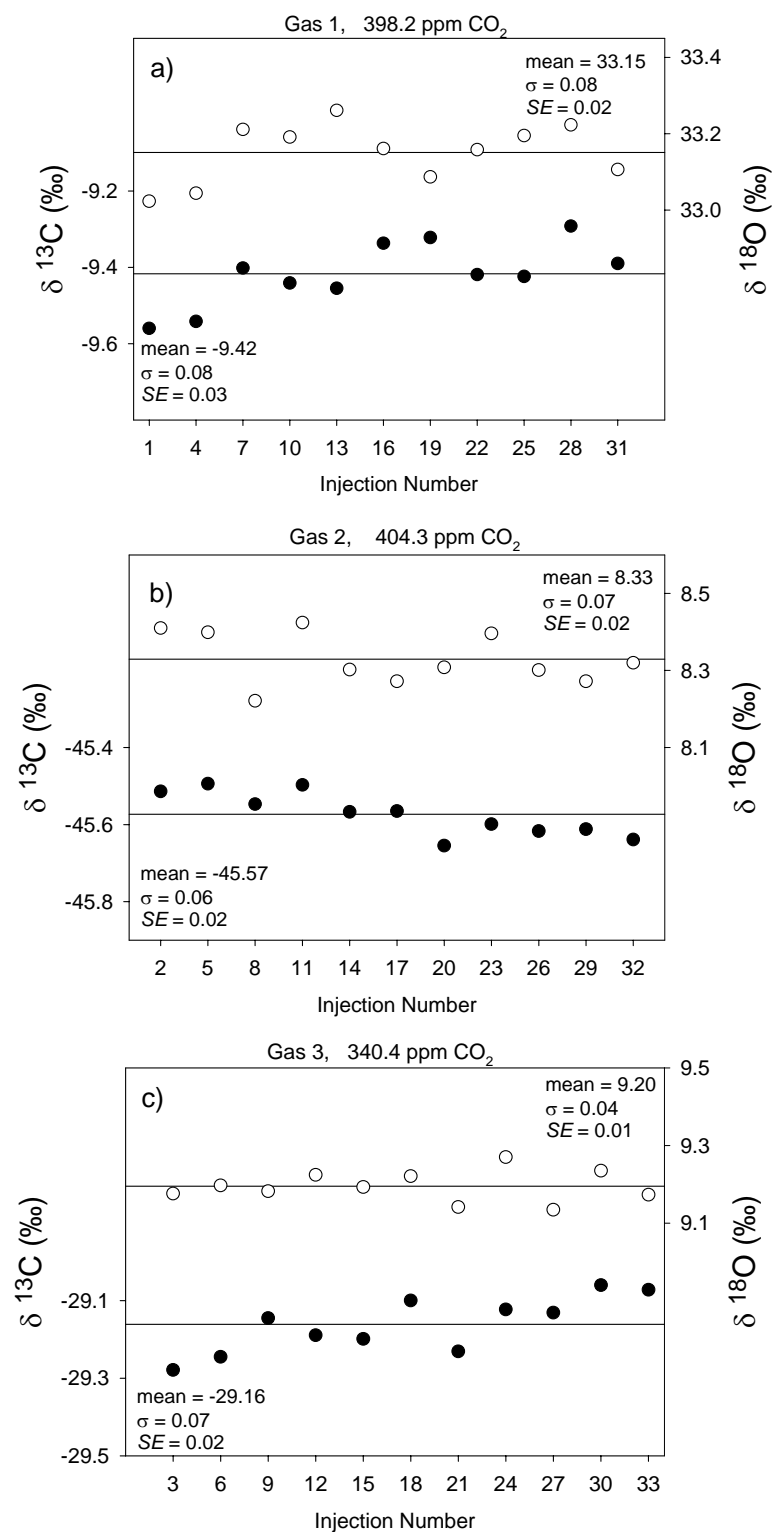


Figure 4, a-c Carbon and oxygen isotope ratios of CO₂ in a) compressed air, b) and c) synthetic air. The samples were collected with the ASA in sequence 1,2,3 1,2,3 and so forth. Standard deviation (σ) was between 0.04‰ and 0.08‰ and standard error ($SE, n=11$) between 0.01‰ and 0.03‰ for all samples.

2.4.2.1 Storage effects

Long time storage tests to evaluate for possible internal mixing, leakage or exchange effects have been done with the same experimental setup as described above, using the gases 1-3. The stopcocks of the glass flasks were left open during the experiments but for long time storage of samples they can be closed if desired. Isotope ratio determination for $\delta^{13}\text{C}$ and $\delta^{18}\text{O}$ of CO_2 was done 8 days after sampling and in a second experiment 27 days after sampling (Figure 5). Gas 1 proved to be relatively stable and showed changes of $0.07\text{‰} \pm 0.05\text{‰}$ for $\delta^{13}\text{C}$ and $0.51\text{‰} \pm 0.03\text{‰}$ for $\delta^{18}\text{O}$ within 27 days. Compared to the initial measurements on day zero gas 2 showed the largest variation regarding total drift as well as variation between individual samples, being expressed by the standard deviation (σ) of 0.43‰ for $\delta^{13}\text{C}$ and 0.34‰ for $\delta^{18}\text{O}$.

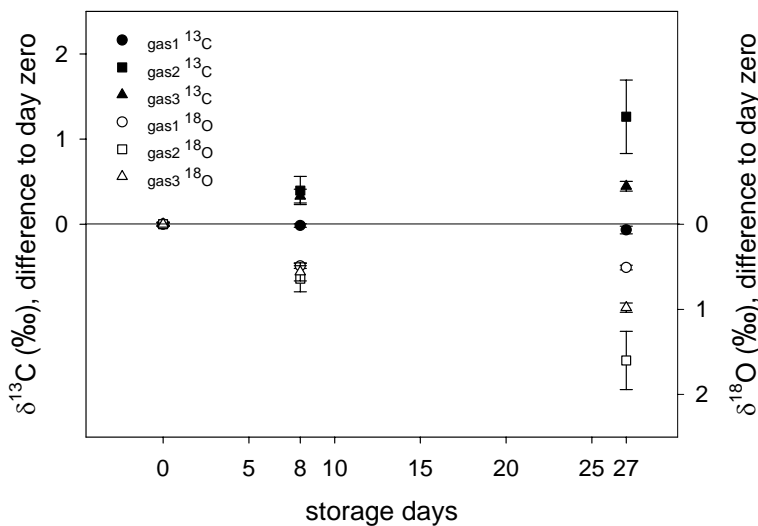


Figure 5 Storage effects on CO_2 stable isotopic composition. Horizontal line represents values at day zero for both $\delta^{13}\text{C}$ and $\delta^{18}\text{O}$ and error bars indicate \pm standard deviations (σ , $n=11$).

The three gases behave quite differently regarding magnitude and scatter of the observed drift. The largest variation was measured in gas 2, which is also the gas with the greatest isotopic differences to atmospheric CO_2 isotopic composition (Table 1). Gas 3 shows the second largest variations and gas 1, which has a similar CO_2 isotopic composition as the surrounding air, is relatively stable over 27 days, in particular for $\delta^{13}\text{C}$. Therefore it can be assumed that the cause of the drift is not internal mixing of gases inside the ASA, but exchange with outside air through very small leaks. This most likely occurs at the transitions from the glass

flasks to the steel tubes which are sealed by Teflon (PTFE) ferrules. But since gas 1 and 2 have similar CO₂ concentration gradients to ambient air, leakage can not fully account for the observed difference over time between the two gases. Other factors such as surface exchange effects with the used materials (glass, Teflon, stainless steel, valco rotor material) and exchange effects with water inside the system could have influenced the experiments. The magnitude of influence of each individual factor is unknown.

The data show that storage of samples is possible for about one week without the risk of strong drifts or isotopic exchange effects during that time. Air samples from the field which will usually have smaller differences to atmospheric isotopic composition than our test gases should therefore be even much less affected during storage.

2.4.2.2 Automated compared to manual gas sampling and analysis

To compare for stability and consistence of the ASA analysis, $\delta^{13}\text{C}$ and $\delta^{18}\text{O}$ of CO₂ was determined with manual sampling and analysis technique, using the same type glass flask as in the ASA. The same glass flask was used eleven times in sequence and was filled with gas 2 (Table 1) during two minutes at a flow rate of 1 L min⁻¹ each time. For analysis the glass flasks were connected to the Helium carrier gas flow of the Precon peripheral from the mass spectrometer.

The results for both $\delta^{13}\text{C}$ and $\delta^{18}\text{O}$ show a good consistency for each of the methods (Table 2). Standard deviations were 2 to 6-fold larger with the manual analysis than with the ASA. Peak areas also showed a much larger variation in the manual analysis, this exemplifies that the automation of the ASA helps to provide more stable results (Figure 6). The offset of the injection peak area between the two methods is due to a different analysis protocol for manual and automated analysis (flushing times, freezing times).

Table 2 Comparison of ASA and single flask analysis

	ASA		single flask	
	$\delta^{13}\text{C}$ (‰)	$\delta^{18}\text{O}$ (‰)	$\delta^{13}\text{C}$ (‰)	$\delta^{18}\text{O}$ (‰)
mean	-45.57	8.33	-45.84	8.17
σ	0.06	0.07	0.13	0.42
SE (n=11)	0.02	0.02	0.04	0.13

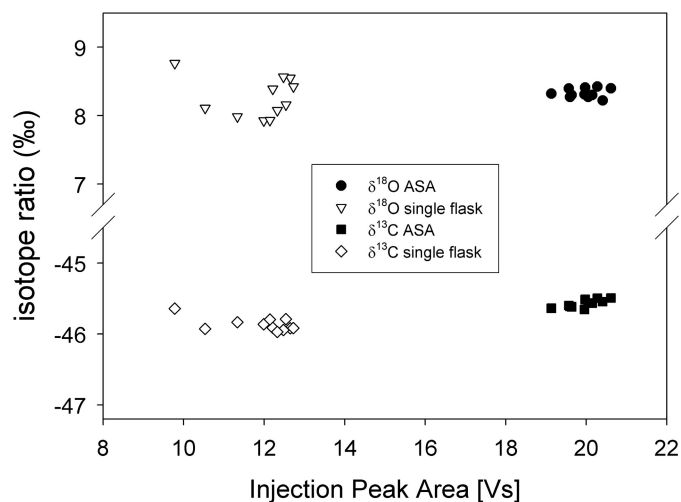


Figure 6 Comparison of manual single flask to automated ASA analysis of gas 2. Black symbols are ASA measurements of $\delta^{13}\text{C}$ (squares) and $\delta^{18}\text{O}$ (circles) of CO_2 ($n=11$). White symbols are single flask analysis of $\delta^{13}\text{C}$ (diamonds) and $\delta^{18}\text{O}$ (triangles) of CO_2 ($n=11$).

2.4.2.3 CO and CH_4 isotope analysis

To show a wider range of possible applications for the ASA in the field, performance was tested with other carbon containing trace gases such as CO and CH_4 with samples of compressed air. These trace gases have lower atmospheric concentrations than CO_2 (CO: $\sim 100\text{-}500$ ppbv, CH_4 : ~ 1.7 ppmv) and therefore require longer freezing times in the pre-concentration step of the isotope analysis. CO was separated from other carbonic trace gases using a Precon peripheral with a carbosorb (Hekatech, Germany) CO_2 removal tube and subsequent cryofixation of potentially not adsorbed CO_2 and other condensable gases such as H_2O . CO is passing the liquid nitrogen trap and is then oxidized to CO_2 with Schütze reagent (Mak & Yang, 1998) contained in a downstream glass tube. The CO $\delta^{13}\text{C}$ and $\delta^{18}\text{O}$ isotopic ratio could then be determined following CO_2 analysis protocols. Standard deviation (σ) for 33 samples of compressed air was 0.17‰ for $\delta^{13}\text{C}_{\text{VPDB}}$ and the standard error (SE) 0.03‰ ($n=33$) showing a measurement precision within the detection limit (Figure 7). Since Schütze reagent does not alter $\delta^{18}\text{O}$ isotopic composition of the original CO it can also be quantified after correction for O added by the reagent (Mak *et al.*, 1998). $\delta^{18}\text{O}$ of CO (data not shown) had a standard deviation (σ) of $\pm 0.20\text{‰}$ and a standard error (SE) of 0.04‰ ($n=33$), again exemplifying a good measurement precision.

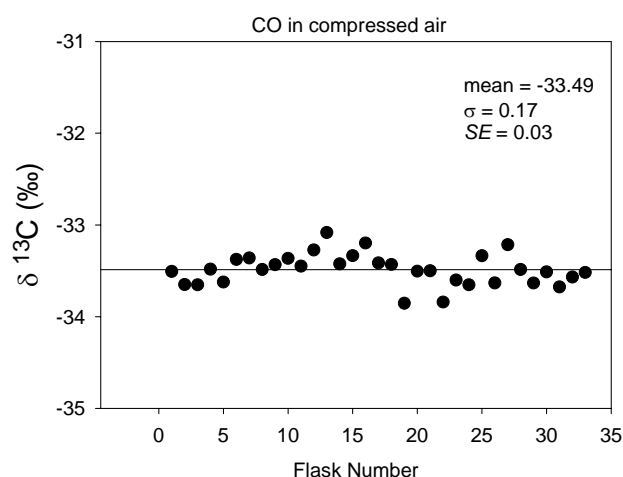


Figure 7 Carbon $\delta^{13}\text{C}$ isotopic ratios of CO (370 ppbv) in compressed air.

Similarly as for CO, CH_4 from compressed air samples needed to be separated from CO_2 during analysis using a Precon peripheral. After oxidation of CH_4 to CO_2 at 1050°C standard CO_2 analysis protocols were followed for $\delta^{13}\text{C}$ isotopic ratio determination. Results of CH_4 $\delta^{13}\text{C}$ showed a linear drift with an r^2 of 0.85, enabling calibration with the use of appropriate standards. Variation around the calculated drift had a standard deviation (σ) of 0.39‰ and a standard error (SE) of 0.07‰ ($n=33$) (Figure 8). The drift in $\delta^{13}\text{C}$ does not seem to be directly related to the ASA as a sampling device since this has been observed on other occasions in our laboratory using manual single flask analysis for CH_4 $\delta^{13}\text{C}$ (data not shown).

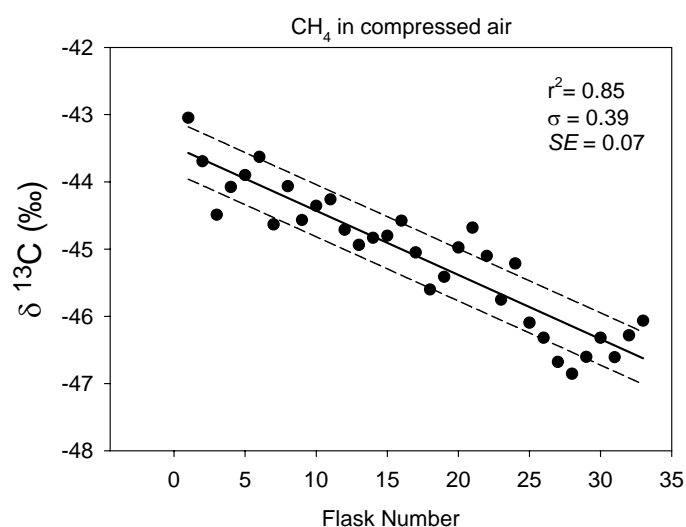


Figure 8 Carbon $\delta^{13}\text{C}$ isotopic ratios of CH_4 in compressed air (1.7 ppmv). A linear drift ($r^2 = 0.85$) of $\delta^{13}\text{C}$ during analysis was observed. Solid line is linear regression and dashed lines are \pm standard deviation ($\sigma = 0.39\text{‰}$).

2.4.3 Field performance

Air samples were collected at the grassland experimental site of the Federal Institute of Technology (ETHZ) in Eschikon near Zurich (8°41'E, 47°27'N). Monocultures of *Lolium perenne* are used to investigate carbon fluxes in a fertile grassland ecosystem under field conditions. An open-flow chamber system is used to measure net ecosystem CO₂ exchange and collect air samples for carbon δ¹³C isotopic ratios of CO₂. The chamber which is 0.6 m high and covers a square area of 0.49 m² consists of an aluminium framework covered with transparent Teflon (PTFE) film except for the side for the inlet and outlet which is made of Plexiglas (see Aeschlimann, 2003 for further description). Air samples were collected from the in- and outlet of the chamber during a 24 hour period on May 18th 2003 using two ASA devices, yielding a total of 66 samples. CO₂ concentration was measured in situ by connecting an IRGA at the outlet of the ASA. Calibration grade gas (Messer-Griesheim) was used to calibrate the IRGA before sampling and synthetic air (Carbagas AG, Switzerland) served as zero-calibration and as reference gas during the CO₂ concentration measurements. Air samples were analyzed for δ¹³C isotopic ratios of CO₂ in the laboratory within 24 hours. A Keeling Type plot where the carbon δ¹³C isotopic ratios of CO₂ are plotted against the inverse of the CO₂ concentration showed a correlation of 0.99 (r²) between the individual samples (Figure 9).

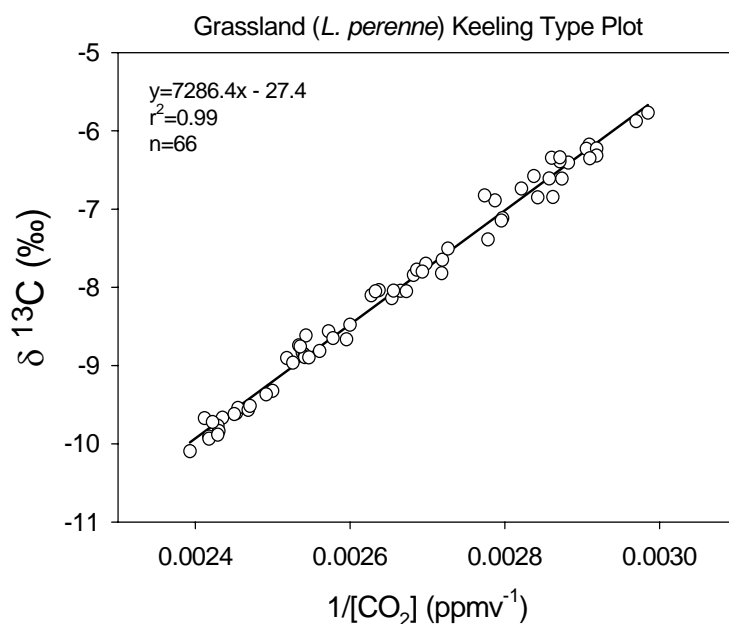


Figure 9 Keeling type plot analysis of the carbon δ¹³C isotopic ratios of CO₂ with linear regression line (r² = 0.99, n = 66). Samples represent a 24 hour period.

2.5 Conclusions

The ASA and its peripheral components offer the possibility to collect a large number of air samples with a mobile and automated device. High precision analysis for stable isotopes of various carbon containing trace gases can be carried out in a fast, reproducible and reliable manner. Furthermore the sampling unit can be directly connected to the mass spectrometer with two carrier gas lines leading to the Precon peripheral and a hardware plug for the electronic control of the ASA.

Since no glass flasks need to be removed from the sampler, a reproducible and fast analysis of the air samples in the flasks is possible. Furthermore, the potential contamination of the air samples is avoided by leaving the glass flasks in place. This saves much time and reduces the potential for errors during handling. The relatively high costs for the automated multiport valves are soon compensated for by reduced costs for personnel during field and lab work.

The system will be a useful tool to further investigate ecosystem carbon fluxes with a high sampling frequency thus making the results more reliable. The necessary measurements of the net ecosystem exchange (NEE) can either be carried out by means of a chamber system as described above or by applying the eddy covariance technique. It could be shown that the ASA is also a useful tool for trace gas sampling and analysis for gases with concentrations up to 1000 times less than that of CO₂. Applications for non-carbon containing trace gases, such as nitrous or sulphurous oxides, also seem possible – limited only by preparation peripherals and the analyzing capabilities of the involved mass spectrometer.

2.6 Acknowledgements

This study is supported by the COST 627 initiative “Carbon storage in European Grasslands” (Grant No. C01.0056), Federal office for education and Science. Thanks for technical help and advice to Robert Widmer. Thanks to Eva Bantelmann for help with the assembly of the ASA. Thanks also to April Siegwolf for proofreading the manuscript.

Chapter 3

3 Dynamics of soil organic matter turnover and soil respired CO₂ in a temperate grassland labelled with carbon-13



3.1 Summary

The fate of carbon in grassland soils is of particular interest since 98% of the carbon in grassland ecosystems is stored belowground and respiratory carbon release from soils is a major component of the global carbon balance. The use of ^{13}C depleted CO_2 in a ten year free air carbon dioxide enrichment (FACE) experiment, gave a unique opportunity to study the turnover of the carbon sequestered during the FACE experiment and also allowed an estimate of the proportional contribution of rhizosphere respiration to total soil respiration. SOM, soil air and plant material were analysed for $\delta^{13}\text{C}$ and carbon content in the last year of the FACE experiment (2002) and in the two following growing seasons. After ten years of CO_2 enrichment conditions to 600 ppm no significant differences in SOM carbon content could be detected between fumigated and non fumigated plots. A ^{13}C depletion of 3.4‰ was found in SOM (0-12 cm) of the fumigated soils in comparison to the control soils and a rapid decrease of this difference was observed after the end of fumigation. After two years a calculated 45% of the carbon in SOM (0-12 cm) had been replaced by fresh carbon and annual input was estimated to $9.8 \pm 3.7 \text{ Mg ha}^{-1}$. Rhizosphere respiration was calculated to 61% of total soil respiration, this is similar to recent findings in forest soils. Consideration of ecophysiological factors which drive plant activity is therefore important when soil respiration is to be investigated or modelled.

3.2 Introduction

Temperate grasslands cover about 20% of the land area in Europe (Soussana *et al.*, 2004). In these ecosystems up to 98% of the total carbon can be found belowground (Hungate *et al.*, 1997). In general, soil organic matter (SOM) contains twice the amount of carbon found in the atmosphere (Post *et al.*, 1982). Within the context of the expected future changes of climatic conditions and rising atmospheric CO₂ content it is still uncertain if the soil carbon pools will be a future source or sink.

Newly introduced carbon into soils is predominantly be found in coarse fractions (Balesdent *et al.*, 1987, Van Kessel *et al.*, 2000, Xie *et al.*, 2005). Non-hydrolysable soil fractions which mainly consist of stable humus are soil carbon pools with a very slow turnover rate and are therefore conservative in regard to new carbon input (Pelz *et al.*, 2005). Freshly introduced carbon, for instance after land use has changed from arable to grassland, is mainly sequestered into labile carbon pools. If land use is changed back to arable again, the previously accumulated carbon is released readily (Soussana *et al.*, 2004).

Balesdent calculated the introduction of new carbon into a soil where newly grown C₄ plants caused a gradual change in ¹³C isotopic composition of SOM on a field that previously was in isotopic equilibrium with C₃ plants (Balesdent *et al.*, 1987). In our study, the use of ¹³C depleted CO₂ of fossil origin in a ten year “free air carbon dioxide enrichment” (FACE) experiment, caused a strong ¹³C label within the soil (see Jones *et al.*, 2004). The ¹³C disequilibrium of SOM and plants after the end of the CO₂ enrichment gave a unique opportunity to calculate annual inputs of new carbon and to study soil processes like rhizosphere respiration, which are driven by the aboveground plants.

A large proportion of carbon that enters the soil is returned to the atmosphere by soil respiration (Jones *et al.*, 2004) and it is therefore considered a key factor for soil carbon turnover. Soil respiration has two major sources: heterotrophic microbial respiration of SOM and rhizosphere respiration. For the latter, the definition of Ekblad & Högberg, 2001 is used: rhizosphere respiration is regarded as the sum of respiration by living roots, their associated mycorrhizal fungi and heterotrophic respiratory transformation of root exudates. The proportions of the individual contributions to soil respiration are still uncertain; only few studies have been done. For grassland, rhizosphere respiration was reported to account for 16 to 95% of total soil respiration (Jones *et al.*, 2004). In forest ecosystems, rhizosphere respiration was recently found to be the dominating factor in soil respiration (Ekblad *et al.*,

2001, Högberg *et al.*, 2001). Measurements by Soe in a sugar beet field under FACE conditions showed the fraction of rhizosphere respiration to be 70% (Soe *et al.*, 2004). In contrast, Buchmann concluded microbial SOM respiration to be the dominating factor in stands of *Picea abies* (Buchmann, 2000). No standard method has yet been established, currently several techniques are being used (soil CO₂ evolution, soil air, tree girdling) based on ¹³C measurements. The question also remains how similar grassland and forest soils are regarding the individual proportions (rhizosphere and SOM respiration) within total soil respiration.

Photosynthetic activity of aboveground plant components, and therefore also micrometeorological conditions, seems to be a driving force for soil respiration. Numerous studies showed that the $\delta^{13}\text{C}$ of soil respired CO₂ is subject to seasonal changes (Ekblad *et al.*, 2005, Flanagan *et al.*, 1996, Steinmann *et al.*, 2004) and a close link to short term weather conditions was found (Bowling *et al.*, 2002, Ekblad *et al.*, 2001). High air temperatures and a large vapour pressure deficit (VPD) cause plant drought stress and stomatal closure (Scheidegger *et al.*, 2000). This decreases the proportion of root respiration within total soil respiration, leading to an increase in $\delta^{13}\text{C}$ of soil respired CO₂ (Ekblad *et al.*, 2001). In our study, the monitoring of soil respired CO₂ over three growing seasons gave the opportunity to analyse the impact of a drought period (summer 2003) on the soil CO₂ system and to calculate the proportional contribution of rhizosphere respiration to total soil respiration.

The goals of this study are

- to determine how fast the carbon which was sequestered during the CO₂ exposure has been replaced with fresh carbon after the FACE experiment, without a change in land use
- to evaluate the proportional contributions of rhizosphere respiration to total soil respiration
- to track seasonal changes in $\delta^{13}\text{C}$ of soil CO₂ and to assign the driving environmental factors

3.3 Materials and methods

3.3.1 Experimental site

The Swiss FACE site in Eschikon (8°41'E, 47°27'N) is located near Zurich at an altitude of 550 m above sea level. To study the impact of elevated CO₂ on a managed grassland ecosystem, monocultures of *Lolium perenne* have been fumigated to an average of 600 ppm CO₂ (± 10% over 92% of the fumigation time) during ten growing seasons using Free Air Carbon dioxide Enrichment (FACE) technology (Hendrey, 1992). The experiment was set up in three replicates of fumigated and non-fumigated control plots (diameter per plot: 18 m). CO₂-fumigation was started in May 1993 and maintained from March to November at daylight hours until discontinuation in November 2002 (see Zanetti *et al.*, 1996 and Hebeisen *et al.*, 1997 for further description). The added CO₂ from the fumigation tank was ¹³C depleted since it originated from the combustion of fossil C-sources (-28.8‰ δ¹³C of CO₂ in 2002). This resulted in a calculated average value in 2002 of -16‰ for δ¹³C in the CO₂ enriched air of the fumigated plots as compared to -8‰ in the control plots, according to the mass balance (see also equation 4):

$$\delta_{face} = \frac{c_a \delta_a + (c_{face} - c_a) \delta_{tank}}{c_{face}} \quad (1)$$

with c_a being ambient and c_{face} being the CO₂ concentration in the FACE rings. δ_a is the isotopic value of ambient, δ_{tank} of the ¹³CO₂ from the fumigation tank and δ_{face} the calculated isotopic value within a FACE ring during fumigation.

The isotopic composition of the stable isotope ¹³C is expressed in the δ unit (‰), relative to the standard Vienna Pee Dee Belemnite (VPDB):

$$\delta^{13}\text{C} = \left[\frac{R(\text{sample})}{R(\text{standard})} - 1 \right] * 1000 \quad \text{with} \quad R = \frac{{}^{13}\text{CO}_2}{{}^{12}\text{CO}_2} \quad (2)$$

In addition to the elevated CO₂ application, and maintained until 2004, all plots were fertilized each year with 55 kg P ha⁻¹ and 241 kg K ha⁻¹ to compensate for harvest losses. Two treatments of nitrogen (N) fertilization were applied (140 and 560 kg ha⁻¹ a⁻¹, as NH₄NO₃). *L.*

perenne swards were cut five times a year and all sampling was done shortly before harvest to avoid any effects of cutting, in particular on soil air CO₂. The soil is classified as an eutric Cambisol, containing 390 g kg⁻¹ silt, 310 g kg⁻¹ sand and 300 g kg⁻¹ clay in the top 0-10 cm with a pH of 7.1. Bulk density for 0-10 cm soil depth is 1.2 ± 0.2 g cm⁻³ (Van Kessel *et al.*, 2000).

3.3.2 Sampling and analysis

Soil, soil air and plant tissue samples were collected on six occasions from September 2002 to October 2004. A single field campaign lasted for 10-15 days during which all three FACE replicates were sampled. The N treatments were two subplots in the six plots; this gave a total of twelve sampling areas in each field campaign. Exceptions were May 2004 for soil air and September 2002 plus May 2004 for bulk soil samples when only the subplots (high and low N treatments) of one fumigated and the corresponding control plot were sampled.

3.3.2.1 Bulk Soil

Soil cores 2 cm in diameter and 12 cm in length were sampled and immediately split into three sections (0-3 cm, 3-6 cm and 6-12 cm). The samples were kept in airtight glass tubes (L18, Schott, Germany) and frozen at -20 °C within 24 hours. Further processing was done within three months after sampling. Samples were dried at 80 °C and 10⁻² mbar, sieved to remove roots (mesh size: 630 µm) and ground to powder with a ball mill (Retsol MM2000, Retsch, Germany). An exception were the soil samples from 2002 which did not undergo the sieving process but only had visible plant material such as fine roots removed manually. This resulted in higher carbon concentrations within some of the 2002 samples as compared to the sieved ones from 2003 and 2004. To remove any traces of carbonate (Ca₂CO₃) an aliquot of 20 mg of each sample was weighed in silver capsules and mixed with 40 µl 2.5 M HCl. After 24 hours the aliquots were washed twice with 40µl H₂O to remove remaining HCl. Analysis for carbon (C) and nitrogen (N) content and δ¹³C value of C was done by combusting the samples to N₂ and CO₂ in an Elemental Analyzer (Carlo Erba 1108, Italy) coupled to a Delta S mass spectrometer via the CONFLOII interface (both Thermo Electron, former Finnigan MAT, Germany) in continuous-flow mode. Since the soil was (unevenly) labelled with ¹⁵N from a previous experiment, analysis for δ¹⁵N was not performed. The achieved precision for repeated analysis of a standard material was ±0.1‰ for δ¹³C (standard deviation, σ). The relative precision for C and N content was ±2% (σ).

All samples from the control plots and the 0-3 cm samples from the fumigated plots from 2002 were corrected for carbon content and $\delta^{13}\text{C}$ due to the additional carbon they contained (see above). The new carbon content was the calculated mean of the interval defined by the lowest and highest values of the respective depths from 2003 and 2004, including the standard errors. This interval, defined by the lowest and highest boundaries of the standard errors, was subsequently used as error bar for the calculated values. Correction of $\delta^{13}\text{C}$ was done along the characteristic curves from Figure 10, using the same interval and thus calculating a new lower and upper boundary for $\delta^{13}\text{C}$ (used as error bar subsequently) and the mean thereof. Control plot samples were corrected according to $\delta^{13}\text{C} = -1.39 \cdot \text{C}\% - 26.67$ and the topsoil fumigated samples according to $\delta^{13}\text{C} = -5.53 \cdot \text{C}\% - 26.14$ (see Figure 10).

3.3.2.2 Soil air

At the beginning of the growing season and at least seven days prior to sampling brass tubes (15 cm long, 3 cm diameter) were inserted vertically into the soil (depth: 12 cm), leaving a hollow space inside the tubes. The top was closed airtight with a rubber plug covered with Teflon (PTFE) foil. The tubes had two opposing slits of 6 cm length to integrate soil air from 6 to 12 cm below the surface and were open at the bottom. Sampling was done by inserting a needle through the rubber plug and pulling 15 ml of air from the tubes into the syringe. The air samples were immediately transferred into evacuated 12.5 ml Vacutainers (LABCO Exutainers, Medical Instruments Corporation, Switzerland) and analyzed within 24 hours using a Gasbench II periphery connected to a Delta Plus XL mass spectrometer (both Thermo Electron, former Finnigan MAT, Germany). Samples with a CO_2 concentration of less than 850 ppm were discarded (4 of 235). Repeated measurements of a standard gas using the cryofocussing technique for CO_2 have a precision of $\pm 0.1\%$ (σ) on $\delta^{13}\text{C}$ of CO_2 and a relative precision of $\pm 1\%$ for CO_2 concentration.

Samples of soil air can have a CO_2 concentration ranging from almost ambient to several 10 000 ppm. To calculate the $\delta^{13}\text{C}$ of soil respired CO_2 (source value) a two component mixing model was applied (Keeling, 1958), where the $\delta^{13}\text{C}$ value (y -axis) is plotted against the inverse of the CO_2 concentration. The y -intercept is the isotopic value of the source CO_2 with a diffusional enrichment of 4.4‰ (Amundson *et al.*, 1998). The offset of 4.4‰ between the mean $\delta^{13}\text{C}$ value of the respired carbon sources and the calculated source (from the mixing model) arises from the more rapid diffusion of the lighter ^{12}C , leaving a ^{13}C enriched air mass behind.

3.3.2.3 Plant tissue

Swards of *L. perenne* were collected and immediately transferred to glass tubes (L18, Schott, Germany) and frozen at -20 °C within 24 hours. Drying and grinding was performed in the same manner as for soil samples (see above). Aliquots of 4 mg were then weighed into tin capsules and analysed for $\delta^{13}\text{C}$ and C and N content with the same mass spectrometer setup as for the soil samples and with the same precision.

3.3.2.4 Calculation of remaining labelled carbon

The bulk soil material in the FACE plots is labelled with ^{13}C after ten years of tracer application. The CO_2 depleted in ^{13}C , which was used for fumigation, was sequestered into the soil via humification of plant material. After the fumigation was stopped (autumn 2002) a sudden change in $\delta^{13}\text{C}$ of plant material (*L. perenne*) was observed. The following input of now differently labelled carbon into the soil caused a gradual change of $\delta^{13}\text{C}$ of SOM from 2002 to 2004. The fraction of new carbon with respect to total carbon of the soil can be calculated with a two component mixing model basing on the isotopic differences of old and new carbon (Balesdent *et al.*, 1987, Balesdent *et al.*, 1988).

At a given time t after the $\delta^{13}\text{C}$ change in the plant material, the soil will consist of the remaining part of the initial carbon stock (C_{old}) and the newly introduced carbon (C_{new}):

$$C_t = C_{old} + C_{new} \quad (3)$$

By approximating $C \approx {}^{12}\text{C}$ (introducing an error of about 1%) the quantities of ^{13}C in the respective carbon pools can be written as:

$$C_t R_t = C_{old} R_{old} + C_{new} R_{new} \quad \text{with} \quad R = \frac{{}^{13}\text{C}}{{}^{12}\text{C}} \quad (4)$$

Since the isotopic ratio R relates linearly to $\delta^{13}\text{C}$ (equation 2) and combining equation (4) with (3) gives:

$$x = \frac{\delta_t - \delta_{old}}{\delta_{new} - \delta_{old}} \quad \text{with} \quad x = \frac{C_{new}}{C_{old} + C_{new}} \quad (5)$$

where x is the fraction of new introduced carbon by the plants, δ_t the $\delta^{13}\text{C}$ value of SOM at time t , δ_{old} the $\delta^{13}\text{C}$ value of SOM at the starting point and δ_{new} the $\delta^{13}\text{C}$ of the plant material introducing the new label.

3.3.2.5 Calculation of rhizosphere respiration

Since equation (5) basically describes the mixing of two differently labelled substances it may also be used to separate CO_2 derived from SOM respiration and CO_2 derived from plant root and rhizosphere respiration if the plant material has a strong enough ^{13}C label. For this case equation (5) is rewritten to:

$$x' = \frac{\delta_{soilair} - \delta_{SOM}}{\delta_{plants} - \delta_{SOM}} \quad (7)$$

with x' as the fraction of plant derived CO_2 within the soil. $\delta_{soilair}$ is the $\delta^{13}\text{C}$ value of soil respired CO_2 minus the 4.4‰ offset (see above), δ_{SOM} the $\delta^{13}\text{C}$ value of SOM in 6-12 cm depth (since soil respired CO_2 is measured in this depth). δ_{plants} denotes the $\delta^{13}\text{C}$ value of the plant material.

3.3.2.6 Statistical analysis

Nonlinear regressions using an exponential decay function ($\delta(t) = \delta_0 e^{-kt}$) were done using Sigma Plot version 8 (SPSS Inc.). The sum of the residuals was < 0.004 in all cases. Treatment effects of the FACE experiment were analysed using ANOVA of the statistical software R (R 2.0.1, GNU public license). Soil samples from the year 2003 were analysed including the three replicates of fumigated and the corresponding control plots as described above. Samples from 2002 and 2004 did not have all replicates at all times, so replication was not considered as a factor in the ANOVA for these years.

3.4 Results

3.4.1 Plant material

$\delta^{13}\text{C}$ values of plant tissue represent an integrated isotopic signature of the CO_2 being incorporated during growth. A natural offset in $\delta^{13}\text{C}$, which is species and carbon fixation

pathway dependent (C_3 or C_4), has its origin in the photosynthetic ^{13}C discrimination, which is mainly caused by the enzyme RUBISCO (Farquhar *et al.*, 1989). Fumigation resulted in a $\delta^{13}\text{C}$ value of CO_2 (-16‰), which was 8‰ more negative than average values of the free troposphere (-8‰). This difference is reflected in the $\delta^{13}\text{C}$ of the plant material: during fumigation $\delta^{13}\text{C}$ of plants was $-37.4 \pm 0.1\text{‰}$ and with no fumigation $-28.3 \pm 0.1\text{‰}$. ANOVA revealed no significant effects of either N fertilisation or the former fumigation on $\delta^{13}\text{C}$ of *L. perenne* in 2003 and 2004.

3.4.2 Soil organic matter (SOM)

The carbon contents of the sieved soil fractions (<630 μm , 0-12 cm soil depth) varied between 38 and 46 Mg C ha^{-1} (Table 3). Nitrogen was found in amounts of 4 to 5 Mg N ha^{-1} . Differences between treatments and years were not significant (ANOVA) due to the scattering of the individual samples. C:N ratio was calculated to 8.8 ± 0.1 as an average for all samples.

Table 3 Carbon and nitrogen content of the <630 μm soil fraction, 0-12 cm soil depth

		C / Mg ha^{-1}	N / Mg ha^{-1}
2003	fumigated	41.0 ± 12.8	4.6 ± 1.2
	control	38.0 ± 11.1	4.4 ± 1.0
2004	fumigated	46.4 ± 10.1	5.3 ± 1.0
	control	40.6 ± 6.8	4.6 ± 0.6

The effect of the former CO_2 fumigation on $\delta^{13}\text{C}$ of SOM was still highly significant in all soil depths ($p < 0.01$) in 2003. The interaction between soil depth and CO_2 fumigation (as co-factor) was also significant ($p < 0.05$), showing that in each depth CO_2 fumigation had a different effect (see also Figure 11). Nitrogen fertilisation (140 and 560 $\text{kg ha}^{-1} \text{ a}^{-1}$) had no significant effect on $\delta^{13}\text{C}$ of SOM. No significant differences were measured between the three field campaigns from May 2003, August 2003 and September 2003.

Carbon content of SOM decreased with depth while at the same time $\delta^{13}\text{C}$ showed an increase (Figure 10, Figure 11). Soil depth profiles from fumigated plots increased stronger (1.8‰ maximum) compared to the control plots, where change with depth was three-fold smaller (0.6‰ maximum). The slope of a linear regression of $\delta^{13}\text{C}$ versus $\ln(\%C)$ (Figure 10) denotes the isotopic fractionation factor (O'Leary, 1981) which is a characteristic for a soil (Bundt *et al.*, 2001, Nadelhoffer & Fry, 1988). In undisturbed soils an increase of $\delta^{13}\text{C}$ with depth is

observed (Nadelhoffer *et al.*, 1988). Older SOM, on which only more specialised soil microorganisms can feed, is slightly enriched in ^{13}C (Figure 11). The soils that have been fumigated with fossil CO_2 show a much steeper gradient (Figure 10) for the reason that the newly introduced organic matter is strongly depleted in ^{13}C . In this case, the fractionation factor is a measure of the isotopic disequilibrium within the soil profile.

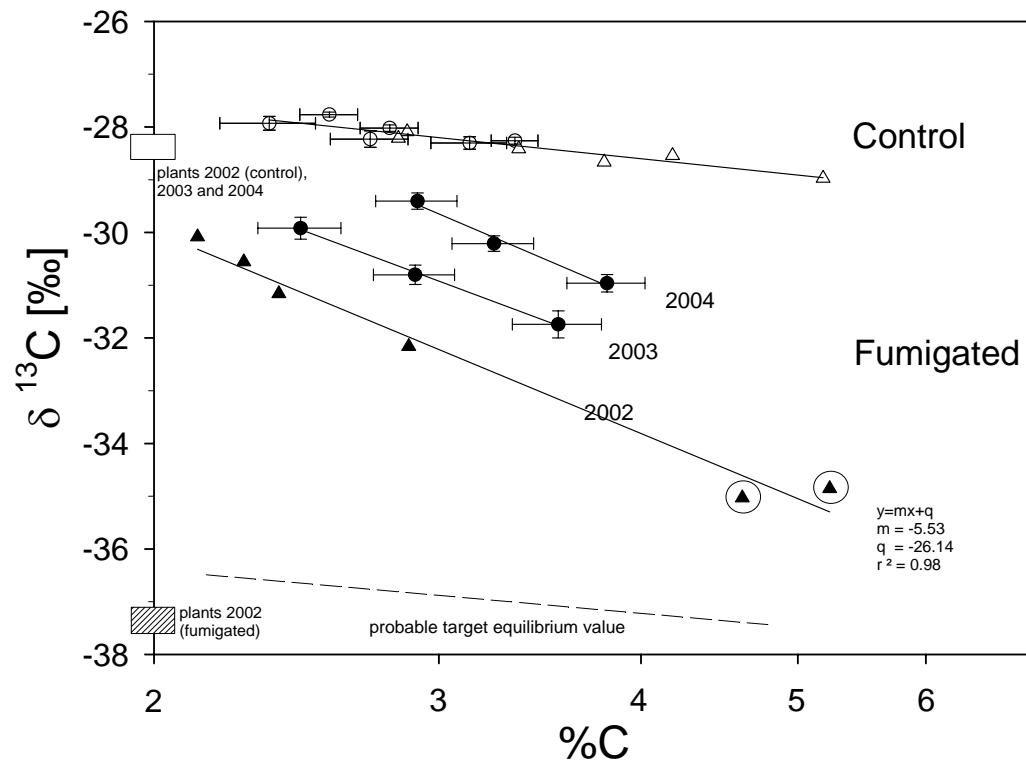


Figure 10 Relationship of $\delta^{13}\text{C}$ and carbon content of SOM with linear regressions (isotopic fractionation factors). Means of each year, separated into three depths (0-3 cm, 3-6 cm, 6-12 cm) are shown, data points from 2002 are single observations. Encircled data points and all control data from 2002 samples show higher C contents than data from other years (see below). Black symbols are fumigated (2002) or formerly fumigated plots (2003 and 2004), white symbols are control plots. Plant $\delta^{13}\text{C}$ values of fumigated (2002) and non-fumigated plots are depicted on the y-axis, box is mean \pm standard error (SE, $n=24$ for 2002 fumigated and $n=172$ for 2002 control and 2003, 2004). Error bars for soil data are SE (2003 $n=20$, 2004 $n=11$).

The control soils are expected to be in isotopic equilibrium with the respective plant material and all data pooled resulted in a linear relationship for $\delta^{13}\text{C}$ and $\ln(\%C)$ with an r^2 of 0.88 and $p < 0.001$. Soils from fumigated plots were in isotopic disequilibrium since it is assumed that no new isotopic equilibrium has been reached after ten years of fumigation (2002), or within the two years after the fumigation was stopped (2003, 2004). The probable target equilibrium value for the fumigated soils (if fumigation would have continued until a new equilibrium is reached) is proposed in Figure 10 and Figure 11. The line represents an estimate based on the

regression line (or depth profile) of the control plots in relation to the $\delta^{13}\text{C}$ value of the respective plant material.

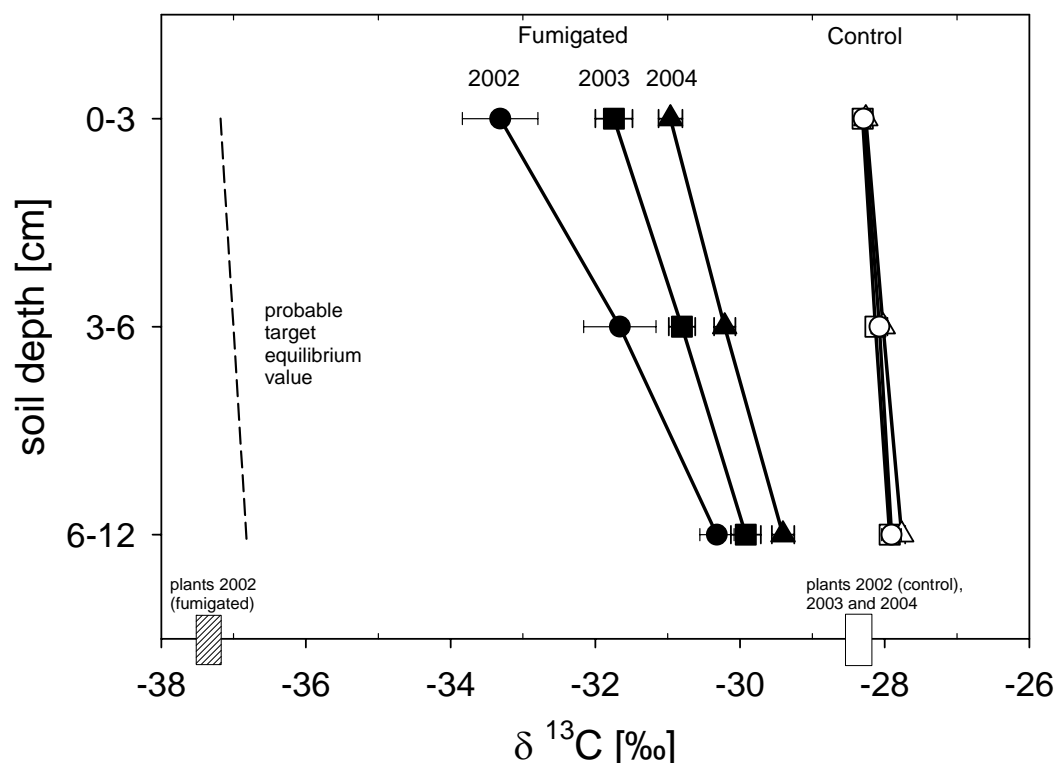


Figure 11 Soil depth profiles of $\delta^{13}\text{C}$ of SOM with yearly means from 2002 to 2004 in both fumigated (or formerly fumigated) and control plots. Topsoil values of fumigated 2002 and all control 2002 samples are calculated (see above). Black symbols are fumigated or formerly fumigated plots, white symbols are control plots. Boxes on x-axis are $\delta^{13}\text{C}$ values of plant material with SE. Error bars are SE (2002: n=2, 2003: n=20, 2004: n=11), except for control 2002 and topsoil 2002, where error bars are calculation intervals (see above).

Samples from 2002 showed a linear relationship for $\delta^{13}\text{C}$ and $\ln(\%C)$ with an r^2 of 0.98 and $p < 0.001$. All samples from the control plots and the topsoil (0-3cm) of the fumigated plots in 2002 had a higher carbon content compared to samples of the two following years. This is most likely due to the fact that in 2002 the samples did not undergo a sieving process ($< 650 \mu\text{m}$) like the samples collected thereafter; only visible root material was removed manually. This additional carbon source has a more negative $\delta^{13}\text{C}$ value, probably influenced by the isotopic signature of the fumigated plant material. Therefore, the 2002 samples were corrected for their carbon content and $\delta^{13}\text{C}$ values along the characteristic curves (see materials and methods and Figure 10).

The effect on $\delta^{13}\text{C}$ of SOM from the 10-year fumigation and also from the reverse process, after the end of fumigation, was invariably strongest in the topsoil 0-3 cm. These effects became weaker with increasing depth. This is expressed in more negative slopes of the

regression lines from fumigated plots (-5.7 to -5.0) as compared to control plots (-1.4) in Figure 10.

The sudden change in $\delta^{13}\text{C}$ of the plant material after the fumigation had significant effects on $\delta^{13}\text{C}$ of SOM ($p < 0.05$) in all investigated depths already in the first year after fumigation (Figure 11). The change in $\delta^{13}\text{C}$ from 2002 to 2003 was strongest in the topsoil level (+ 1.6‰) and diminished with increasing depth. The same, yet less pronounced pattern could be seen in the second year (2003 to 2004) where $\delta^{13}\text{C}$ of the topsoil level increased by 0.7‰. The $\delta^{13}\text{C}$ values in the control plots stayed within $\pm 0.1\text{‰}$ (SE) for a given depth in all three years and showed a consistent increase of 0.4‰ from topsoil to the 6-12 cm layer in all three years.

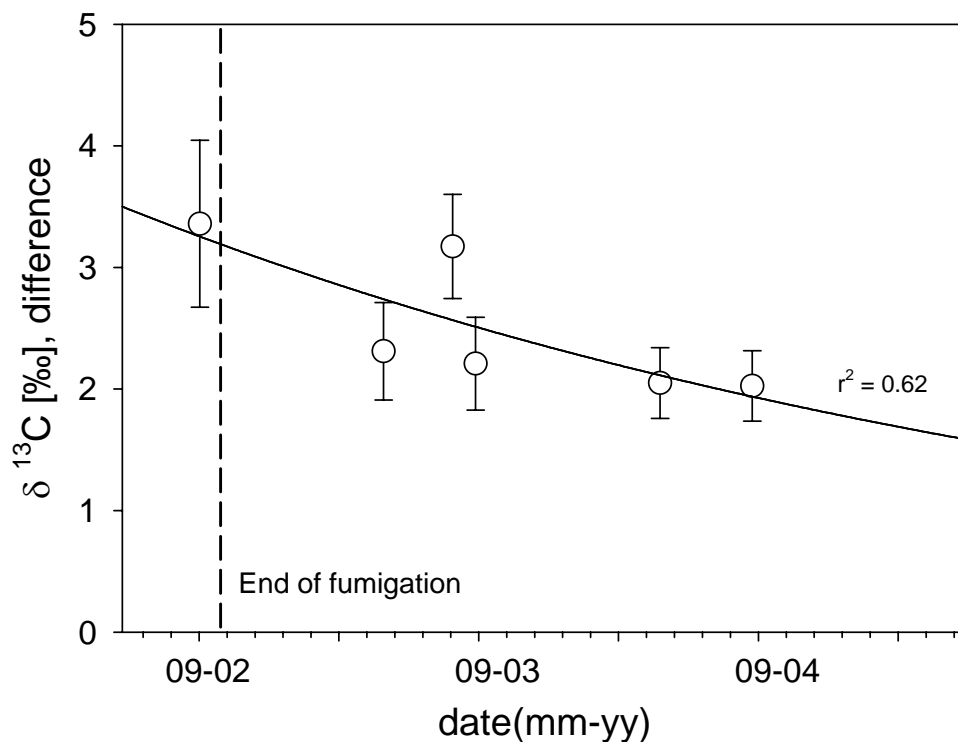


Figure 12 Differences in $\delta^{13}\text{C}$ of SOM between fumigated and control plots (means) from integrated values over 0-12cm soil depth. The curve is the best fit of an exponential decay function. Error bars are derived by error propagation based on the SE of the mean values.

The difference in $\delta^{13}\text{C}$ of SOM between the fumigated and the control plots changed over time and with depth (Figure 11). An exponential decay function fitted to the $\delta^{13}\text{C}$ differences in 0-12 cm soil depth over time yielded an r^2 of 0.62 with $p = 0.06$ (Figure 12). The time, after which the difference in the $\delta^{13}\text{C}$ signal is halved, was calculated to 960 days (with 690 to 1570 days as 95% confidence interval). This means that in a little less than three years the

difference in $\delta^{13}\text{C}$ between the fumigated and the control plots in 0-12 cm depth is calculated to be half the signal we found at the end of the ten year fumigation period.

Samples from the August 2003 field campaign tended to show a larger difference than expected from the model. Control samples from August 2003 were $1.0 \pm 0.2\text{‰}$ less negative than the other samples from 2003, resulting in larger differences for August 2003. These are the samples taken during the exceptionally hot and dry summer experienced throughout Europe (Figure 13).

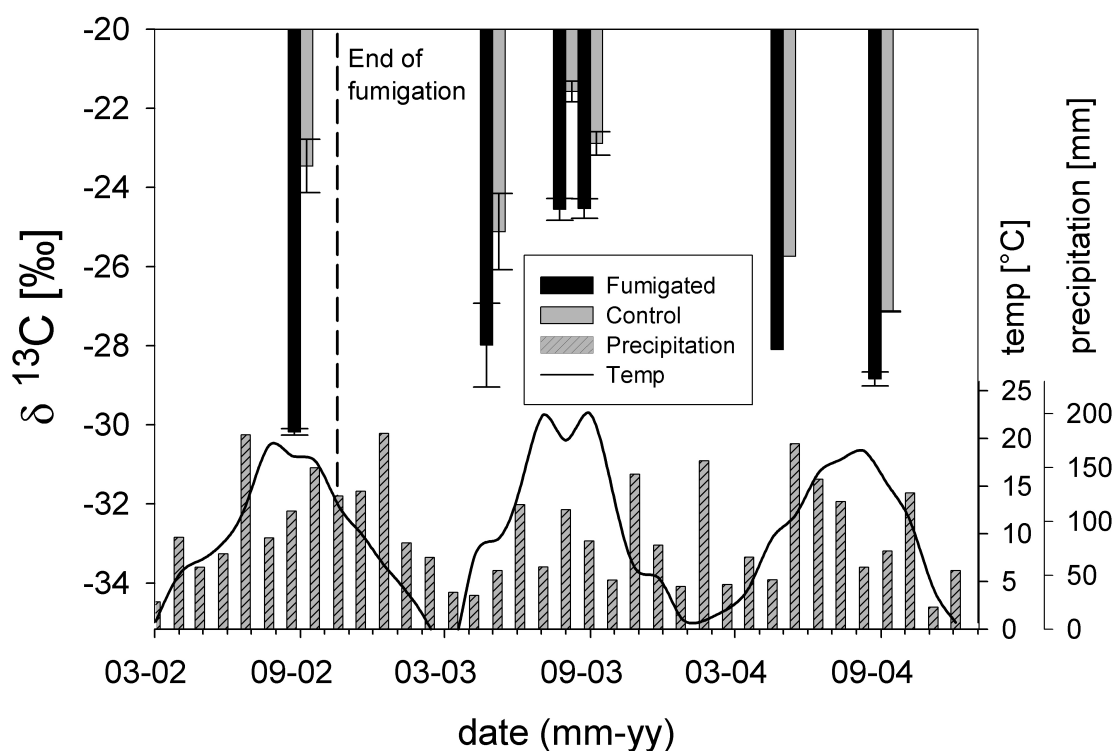


Figure 13 $\delta^{13}\text{C}$ of soil air, means of Keeling plot intercepts from the three FACE-plot replicates. Shaded bars are monthly means of precipitation and the curve is the temperature from a nearby station (Zürich, MeteoSchweiz). Error bars are SE from means; no error bars where not all three replicates were sampled (0504).

3.4.3 Calculation of new carbon after fumigation

Introduction of new carbon into the soil was calculated for the two years after fumigation according to equation (5). In all three analysed soil depths the fractions were similar with an associated error of 10-15% (Table 4). In the first year a maximum of 31% of new carbon was found and in the second year the (cumulative) amount of new carbon was 47% at maximum. Annual new carbon input was estimated to $9.9 \pm 3.1 \text{ Mg ha}^{-1}$ in the top 12cm for the first year and to $9.6 \pm 2.1 \text{ Mg ha}^{-1}$ for the second year after fumigation.

Table 4 Cumulative fractions of new carbon sequestered after 2002 for three soil depths

depth	2003	2004
0-3 cm	0.31 ± 0.10	0.47 ± 0.10
3-6 cm	0.26 ± 0.15	0.43 ± 0.15
6-12 cm	0.20 ± 0.12	0.45 ± 0.12

3.4.4 Soil respired CO₂

Soil respired CO₂ showed a strong seasonal pattern in $\delta^{13}\text{C}$ values (Figure 13), with a maximum variation in $\delta^{13}\text{C}$ between -25.1 to -21.6‰ (May to August 2003). Dry and hot conditions tend to lead to more positive $\delta^{13}\text{C}$ values (Steinmann *et al.*, 2004); this is reflected in the samples of August 2003. The summer period in 2003 showed monthly mean temperatures of 23°C for June and August with at the same time very little precipitation of 58 and 82 mm respectively (Figure 13). Thirty year means for June are 15°, 124 mm and for August 17°, 133 mm (MeteoSchweiz). As also seen in the SOM samples, the difference in $\delta^{13}\text{C}$ values between the control and the fumigated plots in August 2003 was larger compared to the findings in the preceding campaign in May 2003 (Figure 14).

To eliminate seasonal effects, the differences between control and fumigated plots were calculated and showed a general decrease over time (Figure 14). An exponential decay function was fitted to the data and the rate constant k was 2.5-fold higher than the one calculated for SOM in the topsoil level. This is mainly due to the sharp decrease in soil respired CO₂ $\delta^{13}\text{C}$ differences after the first year, from 6.7 to 2.9‰. Such a strong change could not be found in the SOM samples. The effect of fumigation (2002) on soil respired CO₂ was much stronger than the effect on SOM (Figure 15). There is a 3.3‰ offset from the 1:1 line which must have been caused by a direct or indirect effect of fumigation since it was only observed in 2002. During fumigation (2002) the difference in $\delta^{13}\text{C}$ of the plant material from fumigated and control plots was 9.1‰ and the difference for 0-12cm depth SOM 3.4‰. Soil respired CO₂ showed a difference of 6.7‰ between fumigated and control plots, this implies a substantial influence of rhizosphere respiration on $\delta^{13}\text{C}$ of soil respired CO₂. This effect was most clearly visible in 2002, since the isotopic disequilibrium was most expressed in the last year of fumigation (Figure 11). In 2003 and 2004 $\delta^{13}\text{C}$ of plant material was again much closer to $\delta^{13}\text{C}$ of SOM and the detectable effect of root respiration on $\delta^{13}\text{C}$ thus became smaller and is masked by the scattering of the samples (Figure 15).

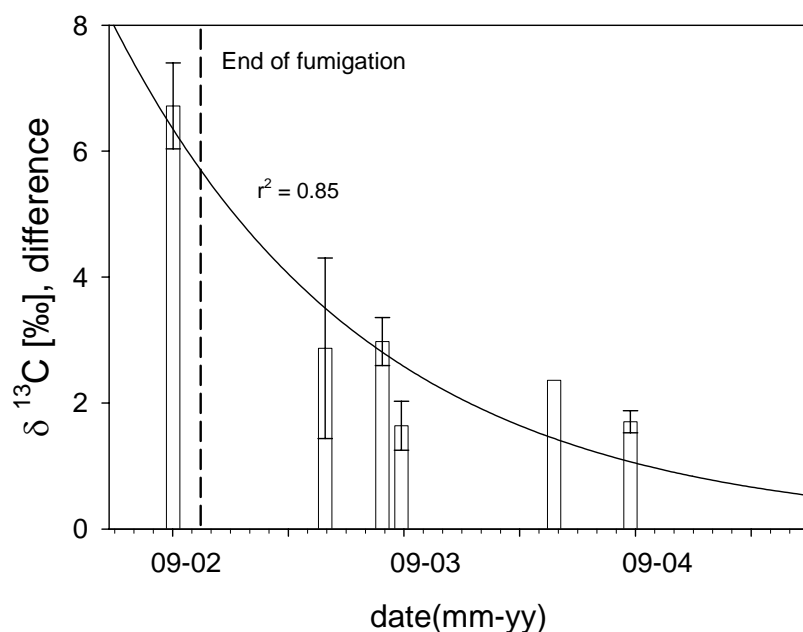


Figure 14 differences in $\delta^{13}\text{C}$ of soil air between fumigated and control plots. Curve is the best fit of an exponential decay function. Error bars are derived by error propagation based on the SE of the mean values.

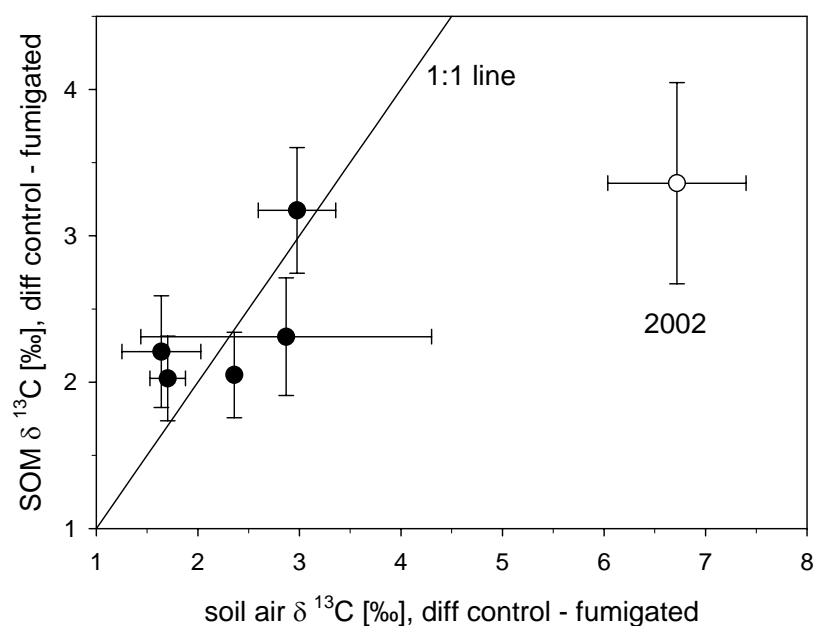


Figure 15 Differences between fumigated and control plots of soil air $\delta^{13}\text{C}$ against differences of SOM $\delta^{13}\text{C}$ (0-12cm depth). White point is from 2002, black points are from 2003 and 2004. Error bars are SE.

The proportion of rhizosphere respiration within total soil respiration in the year 2002 (fumigated plots) was calculated to $61 \pm 10\%$ according to equation (7). For this calculation a -4.4% offset in soil respired CO_2 was included (Amundson *et al.*, 1998) and the isotopic values for SOM were taken from 6-12 cm depth; the same depth where the soil CO_2 was sampled from.

3.5 Discussion

3.5.1 SOM carbon content and isotopic disequilibrium

No significant difference in soil total organic carbon content between fumigated and control plots was observed. This is in agreement with previous findings after six and nine years of fumigation by Six *et al.*, 2001, Van Kessel *et al.*, 2000, Xie *et al.*, 2005. The carbon content of the soil in our study was similar to that observed by the above authors after six years of fumigation although a direct comparison of the soil carbon content cannot be made, since different pre-treatments were applied in each study plus the analysed depths were slightly different (0-12 cm as opposed to 0-10 cm).

Soils from fumigated plots were found to be in strong isotopic disequilibrium with respect to the plant canopy. Compared to a 2.2‰ difference in $\delta^{13}\text{C}$ between SOM of fumigated and control plots (0-10 cm depth) observed after six years of fumigation (Six *et al.*, 2001) we measured a 3.4‰ difference (0-12 cm depth) after ten years of fumigation in 2002. This shows that with increasing time of fumigation the difference in $\delta^{13}\text{C}$ became stronger. After ten years, the fumigated soils were still far from a new estimated isotopic equilibrium (Figure 10, Figure 11) when considering the respective isotopic differences between plant material and SOM from the control soils as an equilibrium situation. Ten years of fumigation therefore caused a strong ^{13}C label in SOM, which was expected to increase if fumigation had been continued.

3.5.2 Soil carbon exchange after fumigation

SOM showed a fast response as soon as the fumigation had been stopped in 2002. After two years, in 2004, 45% of the total carbon in the 0-12 cm soil already consisted of carbon introduced after the end of fumigation. Annual input of new carbon was estimated to 9.8 ± 3.7 Mg ha⁻¹ for the first two years after fumigation in the 0-12 cm soil depth. This suggests that the carbon, previously introduced under FACE conditions, had been predominantly sequestered into labile soil carbon pools, which exchanged readily with new carbon after the end of fumigation. Similarly, Van Kessel *et al.*, 2000 reported that in the same soil after six years of FACE 64% of the sequestered new carbon was found in the sand fraction and predominantly in the top 0-10 cm soil depth.

A steep gradient in $\delta^{13}\text{C}$ of SOM was found within the 0-12 cm soil layer, with the most negative values in the topsoil 0-3 cm. Input of new carbon from plants is therefore strongest

close to the soil surface. Nevertheless, calculating the fraction of new carbon according to equation (5) shows little variation between the three analysed depths, in particular for the second year (Table 4). This reflects that the total carbon pool gets smaller with increasing depth, even within 0-12 cm (Figure 10) but turnover rates of the affected pools do not seem to differ substantially. Assessing the change in $\delta^{13}\text{C}$ over time by comparing the $\delta^{13}\text{C}$ between the fumigated and the control plots (Figure 12) gave a calculated 960 days for a 50% decrease of the differences between the plots. This is in accordance to the calculation with the fraction model (equation 5), after which 45% of the carbon is exchanged in 730 days.

The low C:N ratio of 8.8 found in the soil indicates a high microbial activity. This ratio was found to be quite stable over the years (De Graaf *et al.*, 2004, Van Groenigen *et al.*, 2003) and supports the findings of the rapid turnover of the carbon introduced under FACE conditions.

3.5.3 Effects of the dry summer 2003 on SOM and soil respiration

During the unusually dry summer of August 2003, $\delta^{13}\text{C}$ values of respired soil CO_2 and SOM were less negative than expected, compared to May and September 2003. For both, soil CO_2 and SOM, this was particularly apparent in the control plots and is thus reflected in larger differences between the plots, as seen in Figure 12 and Figure 14.

In August 2003 there was practically no plant growth in all plots, the canopies consisted mainly of dry and presumably dead or biologically inactive *Lolium perenne*. Estimated from photographs, the surface area covered with brown, dry plants was 60-90%. The flow of photoassimilates from the plants to the soil and thus the influence of the plants on soil CO_2 and SOM must therefore have been much smaller at that time in comparison to a situation when 100% of the soil surface area is covered with green and photosynthesising *L. perenne*. Three primary mechanistic effects caused by the drought are thought to occur simultaneously and impact on the carbon flow of the plant-soil system:

i. Declined plant activity. In the fumigated plots $\delta^{13}\text{C}$ of the plants was less negative than $\delta^{13}\text{C}$ of SOM (Figure 11). With decreasing activity of the plants the $\delta^{13}\text{C}$ of soil respired CO_2 and SOM would therefore become more negative. The control plots were in the opposite situation, with plant material being more negative than SOM; so minimizing plant influence would cause a general rise in $\delta^{13}\text{C}$ for the control plots. This would explain the larger than expected differences in $\delta^{13}\text{C}$ of soil respired CO_2 and SOM, since minimizing plant influence causes opposite effects on $\delta^{13}\text{C}$ in fumigated and control plots.

ii. Decreased photosynthetic discrimination. Plant ^{13}C discrimination during photosynthesis decreases in hot and dry conditions (high VPD) due to stomatal closure (Scheidegger *et al.*, 2000). This leads to more positive $\delta^{13}\text{C}$ values in the plant material, which is then reflected by more positive root respiration and exudates. Living and photosynthesising plants are therefore a possible cause for the observed increase in $\delta^{13}\text{C}$ differences during the drought period.

iii. SOM respiration shifting to greater depths. Aerobic microbial respiration of SOM is strongly driven by soil moisture and soil temperature (Wardle & Parkinson, 1990). Dry conditions cause microbial soil respiration to minimise or cease (Wang *et al.*, 2003). The main source of microbial SOM respiration will therefore shift to greater soil depths where still enough moisture might be available. This would lead to more positive $\delta^{13}\text{C}$ values of soil respired CO_2 , since $\delta^{13}\text{C}$ of SOM increased with soil depth.

The influence on $\delta^{13}\text{C}$ of soil CO_2 of effect (iii) depends on the $\delta^{13}\text{C}$ gradient of SOM within the soil depth profile. But since this gradient was much stronger in the fumigated than in the control plots (Figure 11), the increase in $\delta^{13}\text{C}$ of the soil air should have been more pronounced in the fumigated plots. This, however, was not the case, since the observed general decrease from May to August 2003 was by 0.1‰ stronger in the control plots (Figure 13). Effect (ii), the decreased discrimination of plants, should affect all plots in the same manner, shifting $\delta^{13}\text{C}$ to more positive values. Possible differences between plots could arise due to unequal distribution of still living plants, but this would only randomize the causes of the effect if it was the dominating factor. Since effect (i) is thought to cause opposite changes in $\delta^{13}\text{C}$ of soil respired CO_2 and SOM, it seems to have been the dominating factor resulting in the August 2003 changes in soil $\delta^{13}\text{C}$. Root respiration and the carbon flow from the plants to the soil were most likely strongly reduced during that time. This substantial influence of plants on $\delta^{13}\text{C}$ of soil respired CO_2 indicates that rhizosphere respiration is the dominating factor in soil respiration.

3.5.4 Soil respired CO_2

The strong isotopic disequilibrium in the fumigated soils in 2002 allowed an estimate of the proportional contribution of rhizosphere respiration to total soil respiration. In September 2002, 61% of soil respiration was calculated to be from rhizosphere respiration. This is an integrated value over the three fumigated plots and has an associated error of 10% (derived by error propagation) since it was calculated from SOM and soil CO_2 data which already have

their individual errors. Nevertheless the results show that a major part of soil respiration in grassland is in fact plant-driven. The analysis of the effects of the dry summer 2003 (see above) supports this conclusion even though the evidence is indirect and, in this case, only allows a qualitative estimation of the proportional contributions to soil respiration.

Only little is known about the proportional contributions to soil respiration, particularly for grassland ecosystems. In forest soils Ekblad reported 50 to 65% of soil respiration to be plant-driven in recent studies (Ekblad *et al.*, 2005, Ekblad *et al.*, 2001). Our findings here suggest that there is a similarity in proportional contributions to soil respiration between forest and grassland soils.

Since the influence of plants seems to be substantial for soil respiration, it is important to consider ecophysiological factors such as photosynthetic active radiation (PAR), VPD and temperature which drive plant photosynthesis and respiration. A strong coupling of soil respiration to plant activity and thus to ecophysiological factors was also found by Craine (Craine *et al.*, 1999). The close connection of plant activity and soil respiration found in this study should be considered when investigating soil respiration.

3.6 Conclusions

The shutdown of the CO₂ exposure provided the opportunity to study the turnover of carbon which was freshly introduced into the soil by the plants. There is no significant evidence that ten years of elevated CO₂ changed the size of the carbon pool in SOM. New carbon introduced into the soil was predominantly found in labile pools; within two growing seasons up to 50% of the previously sequestered carbon was exchanged. Within the soil depth profile (0-12 cm) the turnover rates of the SOM carbon pools were fairly constant, indicating that physical, chemical and biological soil properties are homogeneous within this soil layer.

The isotopic disequilibrium in the fumigated soils gave a unique opportunity to estimate proportional contributions within soil respiration with practically no disturbance of the system. Rhizosphere respiration was calculated to 61% of total soil respiration for September 2002. The individual proportions of responsible components for soil respiration in grassland seem to be similarly distributed as found in forest soils; with rhizosphere respiration as the dominating influence. It is therefore important to consider ecophysiological factors which drive plant activity when soil respiration is to be investigated or modelled.

3.7 Acknowledgements

This study is supported by the COST 627 initiative “Carbon storage in European Grasslands” (Grant No. C01.0056), Federal office for education and Science. Meteorological data with thanks from MeteoSchweiz.

Chapter 4

4 Partitioning of CO₂ and H₂O-vapor fluxes in a temperate grassland using stable isotopes



4.1 Summary

In a temperate grassland site in central Europe (Switzerland), CO₂ and H₂O was sampled for stable isotope analysis using an open-flow chamber system (0.3 m³ volume) on five days in May 2004 with the goal to partition net CO₂ and H₂O fluxes.

Transpiration (T) was assessed with the H₂¹⁸O water vapor partitioning method which is based on isotopic differences of the transpiration and evaporation fluxes (Keeling plot approach using water vapor concentrations). We did not find satisfactory results with the assumption of isotopic steady state (ISS) for the transpiration water flux on our temperate grassland site (98% contribution of transpiration to evapotranspiration, shortly after rainfall). As a basis for further discussions, we tested the hypothesis that the H₂¹⁸O composition of the transpiration flux follows the day time course of leaf water δ¹⁸O enrichment. This yielded more realistic results for the relative amounts of the transpiration flux (63% of ET was transpiration, shortly after rainfall). Independent of the model used, results for Δ_{canopy} showed a close link to VPD (c_i / c_a vs. VPD, $r^2 = 0.82$), consistent with isotope fractionation models. Furthermore, on two days with fluctuating global radiation due to clouds, a negative correlation between Δ_{canopy} and NEE of CO₂ was found ($r^2 = 0.69$).

For the CO₂ data set a close link between Keeling-plot-calculated δ¹³C signature of assimilation and respiration during the following night was found. Differences of day time (δ_N) to the following night time (δ_R) δ¹³C signatures were between 4.1 and 6.7‰. Additionally, night time δ_R correlated to meteorological conditions (VPD) 3-4 days prior to sampling. Our data clearly showed preferable time slots for ¹³CO₂ sampling in an investigated ecosystem. Both night time and day time Keeling plots showed a good stability when excluding the transition times around sunset and early morning (intercept errors between 0.4 and 0.9‰). All day sampling periods (excluding transition times), were found to be representative also for the mid day 12.00 to 14.00 hour time period within ± 0.2‰, and in addition showed smaller errors of the intercept values (0.1 to 0.6‰ smaller).

We found that the calculation of Δ_{canopy} remains a crucial point in CO₂ flux partitioning studies. As an alternative to the widely used Penman-Monteith equation at eddy covariance study sites, we applied an equation to calculate Δ_{canopy} using stomatal conductance inferred from transpiration measurements. The needed parameters were net ecosystem exchange (NEE) of CO₂, vapor pressure deficit (VPD), ambient CO₂ concentration and transpiration. A sensitivity analysis of the equation used in the partitioning of CO₂ fluxes showed only little

influence from variations of day and night time Keeling plot intercepts (δ_N and δ_R) if isotopic disequilibrium between assimilation and respiration flux was strong (δ_A and δ_R). A high sensitivity to ambient $^{13}\text{CO}_2$ values was found, showing that locations for sampling of ambient CO_2 at flux sites should be carefully chosen.

4.2 Introduction

Grasslands cover an estimated 24% of the global land surface (Sims *et al.*, 2000) and 20% of the land area in Europe (Soussana *et al.*, 2004). A better understanding of the responses to changes in meteorological and climatic conditions within grasslands could provide important information for the assessment of the impact of future climatic changes on these ecosystems.

Net ecosystem exchange (NEE) of CO₂ is being measured on many sites around the world, but net fluxes provide only marginal information on the underlying processes of photosynthesis and (day time) respiration. The same applies for H₂O, where in evapotranspiration (ET) studies the underlying gross fluxes transpiration and evaporation are not routinely measured. These gross fluxes, assimilation and transpiration, can be measured with a high precision at the leaf level (Percy *et al.*, 1989), but at the cost of poor spatial representation. Stable isotopes of carbon and oxygen could provide useful means to quantify gross sub-fluxes for both CO₂ and H₂O ecosystem exchange (Bowling *et al.*, 2001, Lai *et al.*, 2003, Yakir *et al.*, 1996, Yopez *et al.*, 2003). The stable isotope methods are non-destructive and potentially provide information on ecosystem scales.

An important parameter when calculating assimilation and respiration fluxes is the mean discrimination of the entire plant canopy (Δ_{canopy}) against ¹³CO₂ during the photosynthetic process (Farquhar *et al.*, 1989). This is predominantly done (at eddy-covariance flux sites) using latent and storage heat fluxes along with micrometeorological parameters. This approach, using the “Penman-Monteith” equation does not always yield satisfactory results (Ogee *et al.*, 2003). Our intention was to test a different approach by calculating canopy conductance from the transpiration rate and VPD and together with NEE of CO₂ and ambient CO₂ concentrations calculate Δ_{canopy} . This requires an accurate determination of the transpiration flux, which has been successfully applied before in the study of Yopez *et al.*, 2003.

Nevertheless, there are still a few uncertainties involving the assessment of the relative contribution of the transpiration flux to the ET flux on the canopy scale using ¹⁸O. The isotopic composition of both the evaporation (E) and the transpiration flux (T) must be determined accurately. $\delta^{18}\text{O}$ of the E flux is determined from soil water measurements and the H₂¹⁸O fractionation during evaporation is calculated in an isotope fractionation model using relative humidity of the air and its H₂¹⁸O composition (Gat, 1996, Moreira *et al.*, 1997). Since $\delta^{18}\text{O}$ tends to decrease with increasing soil depth (Ogee *et al.*, 2004) due to enrichment in the

evaporative layer, it is not yet certain which soil depth is most representative for the momentary E flux. The T flux is generally derived from plant stem water ^{18}O measurements, with the assumption that the stem water evaporates through the leaves with unchanged isotopic composition. This approach assumes isotopic steady-state (ISS) conditions within the transpiring plant organs (Wang & Yakir, 2000). However, leaves get enriched in $\delta^{18}\text{O}$ up to 20‰ during transpiration and deviations from ISS often occur (Farquhar *et al.*, 2005, Harwood *et al.*, 1999). It is still uncertain how and to what extent this affects the isotopic composition of the T flux.

We applied the ET partitioning approach using stem water for the T flux, and, alternatively, tested a hypothesis using $\delta^{18}\text{O}$ of leaf water for the T flux, with an intermediate, temperature dependent equilibrium fractionation factor after Majoube, 1971. The resulting calculated values of Δ_{canopy} from both approaches were then applied to a $^{13}\text{CO}_2$ dataset and a sensitivity analysis was done for the calculation of the assimilation (F_A) and respiration (F_R) fluxes. The main aim of the study was to assess the applicability of CO_2 and H_2O partitioning methods in an open-flow chamber system on a grassland site.

4.3 Materials and Methods

4.3.1 Experimental site

Our study was conducted on a managed grassland ecosystem with *Lolium perenne* monocultures on the former “free air carbon dioxide enrichment” site (FACE, discontinued in 2002) in Eschikon (8°41'E, 47°27'N) near Zurich, Switzerland, see Zanetti *et al.*, 1996 for a further description of the FACE site. An intensive measurement campaign of fluxes and stable isotopes was carried out in May 2004 on five sunny days: on May 11, 14, 18, 29 and 30 (see Figure 18 and Figure 16 for meteorological data). May 11 and 14 were partly cloudy (see Figure 20).

Due to the fumigation with ^{13}C depleted CO_2 during the ten years of the FACE experiment a ^{13}C label in the soil could still be found in 2004 ($2.0 \pm 0.3\text{‰}$ difference between control and fumigated plots in 0-12 cm soil depth, see chapter 3). A formerly fumigated and a control plot (diameter per plot: 18 m) were investigated in our study, with each plot being divided into two subplots with different nitrogen fertilizer treatments (140 and 560 kg ha $^{-1}$ a $^{-1}$, as NH_4NO_3). In addition, all plots were fertilized with 55 kg P ha $^{-1}$ and 241 kg K ha $^{-1}$ at the beginning of the growing season to compensate for harvest losses.

4.3.2 Sampling and analysis

4.3.2.1 Net ecosystem exchange (NEE)

NEE of CO₂ and H₂O was measured using a computer-controlled open-flow chamber system. The system consisted of two identical but independent units, each including two chambers, so that simultaneous measurements could be made of both N treatments on the formerly CO₂ enriched and the control plot. The chambers were 0.6 m high and covered a square area of 0.49 m². They consisted of an aluminum framework covered with transparent Teflon (PTFE) film except for the side with the inlet and outlet, which was made of Plexiglas. The air in the chambers was exchanged up to two times per minute during day-time and once every two minutes during night-time. Overpressure due to the airflow was < 0.1 mbar, measured with a pitot tube. CO₂ exchange within the chambers was measured by sampling air at the in and outlet of the chambers. This air was pumped through flexible PE-tubes to an infra-red gas analyzer (Binos 100 4P, Fisher-Rosemount, Germany) where the difference in CO₂ concentration between the two sampling points (inlet and outlet) was measured. In order to determine air humidity, the air was pumped through heated PTFE tubes to a dew point sensor (MTR 2.0, IL Metronic, Germany). Temperature inside the chambers was measured by thermistors with bead shaped sensors (Fenwal, USA, R₂₅ = 10kΩ) placed in a shaded position in the outlets of the chambers. For a further description of the system see Aeschlimann *et al.*, 2005.

NEE was calculated from the differences in CO₂ (and H₂O) fluxes between the inlet and outlet of the chambers: $NEE = ([CO_2]_{out} - [CO_2]_{in}) * J_{chamber} / SA$, where NEE is in μmol m⁻² s⁻¹, CO₂ the concentration in μmol mol⁻¹, J_{chamber} the air flow through the chamber in mol s⁻¹ and SA the surface area enclosed by the chamber in m². Measurements were made every nine minutes on average which corresponds to a frequency of 0.002 Hz. Mid-day means of the fluxes were calculated from 12.00 to 14.00 hours for day time data. Night time averages were from 20.00 to 05.00 hours, the boundaries being the times when net photosynthesis reached zero and photon flux density (PFD) was at or below light compensation (< 30 μmol m⁻² s⁻¹), all times are daylight savings time. Measurements from all four treatments were pooled since no significant differences were observed between treatments (t test of mid day means).

4.3.2.2 Air samples

From the inlets and outlets of the chambers, air was sampled for ^{13}C and ^{18}O analysis of CO_2 and CO_2 concentration was measured *in situ* with an infrared gas analyzer (IRGA, LI-6262, LICOR, USA). PVC tubing was connected to a custom-built air sampler (ASA), which is a computer controlled mobile system for air sampling. The ASA contains 33 glass flasks of 300 mL volume, which are interconnected with multiport valves (Valco ST, VICI, USA) using stainless steel tubes (VICI, USA). A Teflon membrane pump (811KNE, KNF, Germany) pumped the air through the ASA at a flow rate of 2 L min^{-1} , while a MgCl_2O_8 drying column assured that no water vapor entered the system. Compressed air (Carbagas AG, Switzerland) was used as a standard gas (3 samples of 33), which was filled into the ASA *in situ* in the same manner as the other samples. Standards from one field campaign were stable within 0.02‰ for $\delta^{13}\text{C}$ and 0.05‰ for $\delta^{18}\text{O}$ (standard errors, $n=50$).

Sampling time was three minutes for an individual sample and CO_2 concentration was measured at the outlet of the ASA. Calibration grade gas (Messer-Griesheim, Germany) was used to calibrate the IRGA before sampling and synthetic air (Carbagas AG, Switzerland) served as zero-calibration and as reference gas during the CO_2 concentration measurements. In the laboratory the ASA was connected to the mass spectrometer and was computer controlled, like an autosampler (see Theis *et al.*, 2004 for a further description of the ASA). Air samples were analyzed within 24 hours using a Gasbench II periphery connected to a Delta Plus XL mass spectrometer (both Thermo Electron, former Finnigan MAT, Germany). The achieved precision with the ASA system was $< \pm 0.1\text{‰}$ for $\delta^{13}\text{C}$ and $\delta^{18}\text{O}$ (standard deviations, σ). See equation (1) below for the definition of δ .

Samples from all four treatments (former fumigation and nitrogen levels) were pooled since no significant differences were found between treatments (Student's *t* test of Keeling plot intercepts). The data was divided into day (10.00 to 19.00 hours) and nighttime periods (22.00 to 01.00 hours).

4.3.2.3 Water vapor

Water vapor was sampled hourly between 11.00 and 17.00 from the inlet and outlets of the chambers on the control plot on May 29 and 30, 2004. The air was aspirated through Teflon (PTFE) tubing by electromagnetic piston pumps (Reciprotor A/S, Copenhagen, Denmark) at a flowrate of 5 mL s^{-1} . Water vapor was cryo-trapped in glass U-tubes of 12 mm inner diameter

and 200 mm length cooled to -80°C by a dry-ice (CO_2) ethanol slush. Sampling time was 30 minutes, after which the frozen vapor was thawed and transferred to 2 ml crimp vials (Infochroma, Switzerland). The water samples were analyzed for $\delta^{18}\text{O}$ by pyrolytic conversion to CO in a high temperature furnace (TC/EA), which was linked via Conflo III to a Delta Plus XL mass spectrometer (all Thermo Electron, former Finnigan MAT, Germany), with a precision of $\pm 0.1\text{‰}$. Dew point temperature was measured using separate flow lines with dewpoint sensors (Walz, Effeltrich, Germany).

4.3.2.4 Soil water

Soil cores 2 cm in diameter and 12 cm in length were sampled and immediately split into three sections (0-3 cm, 3-6 cm and 6-12 cm). The samples were kept in airtight glass tubes (L18, Schott, Germany) and frozen at -20°C within 24 hours. Further processing was done within three months after sampling.

Soil water was extracted by cryo distillation. The glass tubes were connected to a vacuum line ($5 \cdot 10^{-2}$ mbar) and warmed to 80°C in a water bath. To freeze the evaporating water an intermediate $\text{N}_2(l)$ cold trap was used. Analysis for $\delta^{18}\text{O}$ was done as for the water vapor samples (see above).

4.3.2.5 Plant water and carbon

Leaves of *L. perenne* were collected without the main middle vein to monitor the accumulation of ^{18}O during transpiration. Samples were immediately transferred to glass tubes (L18, Schott, Germany) and frozen at -20°C within 24 hours. Water extraction was performed in the same manner as for soil samples (see above). The dried samples were ground to powder with a ball mill (Retsol MM2000, Rentsch, Germany). Analysis for carbon (C) content and $\delta^{13}\text{C}$ value of C was done by combusting the samples to CO_2 in an Elemental Analyzer (Carlo Erba 1108, Italy) coupled to a Delta S mass spectrometer via the CONFLOII interface in continuous-flow mode (both Thermo Electron, former Finnigan MAT, Germany). The achieved precision for repeated analysis of a standard material was $\pm 0.1\text{‰}$ for $\delta^{13}\text{C}$ (standard deviation, σ) and the relative precision for C content was $\pm 2\%$ (σ).

Analysis of $\delta^{18}\text{O}$ in plant water was the same as for water vapor samples (see above).

4.3.2.6 Meteorological data

Micrometeorological parameters from two stations nearby the field site were used. Data retrieved from the Lindau station (~800 m distance) were air temperature, relative humidity and precipitation. Global radiation data was obtained from the Zürich-Kloten station (~7 km distance).

VPD, temperature, CO₂ concentration (c_a) and $\delta^{13}\text{C}$ of CO₂ (δ_a) inside the chambers as used in the following equations were mean values from all four chamber outlets during the sampling times (9 minutes). This was done assuming that the chambers are a fully turbulent and mixed environment. An additional fan inside the chambers assured proper mixing.

4.3.3 Calculations

The abundance of the stable isotope ^{13}C in CO₂ is expressed in the δ notation (‰), relative to the standard “Vienna Pee Dee Belemnite” (VPDB):

$$\delta^{13}\text{C} = \left[\frac{R(\text{sample})}{R(\text{standard})} - 1 \right] * 1000 \quad \text{with} \quad R = \frac{^{13}\text{C}}{^{12}\text{C}} \quad (1)$$

The stable isotope ^{18}O in H₂¹⁸O is expressed in analogy to $\delta^{13}\text{C}$, but is referred to the standard “Vienna standard mean ocean water” (VSMOW).

4.3.3.1 Partitioning of CO₂ fluxes

Measurements of the stable isotope $^{13}\text{CO}_2$ together with CO₂ NEE was used to partition the net flux of CO₂ into its corresponding one-way gross fluxes, assimilation (F_A) and respiration (F_R), after Yakir *et al.*, 1996 and Bowling *et al.*, 2001.

$$F_N = F_A + F_R \quad (2)$$

with F_N being the net flux of the chamber system. By writing a mass balance for ^{13}C and approximating total C in the respective fluxes with ^{12}C , we introduce an error of about 1.1%. We also substitute ^{13}R with $^{13}\delta$, since they relate linearly according to equation (1) and receive:

$$F_N \delta_N = F_A \delta_A + F_R \delta_R \quad (3)$$

with the subscripts of δ corresponding to “net flux” (N), “assimilation” (A) and “respiration” (R) respectively. $F_N \delta_N$ is called isoflux and is the total net ^{13}C flux within the system. δ_R is the isotopic signature of the respiration flux, which is comprised of soil and plant respiration. For an estimate of δ_R a two-component mixing model is applied on nighttime data (Keeling plot, after Keeling, 1958). This is the most promising method to assess the isotopic signal of the daytime respiration flux, with the assumption that isotopic signal of day and nighttime respiration do not differ substantially (Pataki *et al.*, 2003). δ_N is derived from daytime Keeling plots (Ogee *et al.*, 2004), which give an integrated value for δ_N .

The isotopic signature of the photosynthetic CO_2 flux, δ_A is not easily measured, but can be calculated using the following equation after Bowling *et al.*, 2001:

$$\delta_A = \delta_a - \Delta_{canopy} \quad (4)$$

with δ_a as the isotopic composition of background CO_2 (taking the means from the chamber outlets, representing the “ambient” air in the canopy; see above) and Δ_{canopy} as the photosynthetic ^{13}C discrimination of the canopy. We calculated Δ_{canopy} as shown below, from transpiration data and micrometeorological parameters.

It should be noted at this point that we considered the canopy as a “big leaf” (Ogee *et al.*, 2003) and the values for the parameters were chosen accordingly, in particular to calculate Δ_{canopy} . In the context of this study the term Δ_{canopy} -as commonly found in literature- was used to signify discrimination against ^{13}C . However in our case Δ_{canopy} is not only the discrimination of the plant canopy against ^{13}C but the discrimination of the whole system; thus including soil derived ^{13}C . For better understanding we refrained from naming the system discrimination Δ_{system} but reverted to the common name Δ_{canopy} . In analogy to a leaf, the soil derived CO_2 was regarded as an additional mitochondrial CO_2 source within the “big leaf” model. The same consideration was applied further below concerning c_i (leaf internal CO_2 concentration) and leaf conductance g_c (for H_2O and CO_2). These two terms were also used with their common names and should be understood as “big leaf” internal CO_2 concentration and “big leaf” conductance, as stated above. Combining equations (2), (3) and (4) we get the following equation for the assimilation flux F_A :

$$F_A = F_N \left[\frac{\delta_N - \delta_R}{\delta_a - \delta_R - \Delta_{canopy}} \right] \quad (5a)$$

and substituting Δ_{canopy} according to equation (12) we get

$$F_A = F_N \left[\frac{\delta_N - \delta_R}{\delta_a - \delta_R - a - (b-a) \left[1 - \frac{|NEE| \times VPD}{T \times c_a \times 1.6} \right]} \right] \quad (5b)$$

this is in analogy to Yakir *et al.*, 1996 but with the calculation of Δ_{canopy} included. The respiration flux F_R : can then easily be calculated from equation (2).

4.3.3.2 Partitioning of water vapor into evaporation and transpiration

By approximating $H_2O \approx {}^1H_2{}^{16}O$ the mass balance for ${}^{18}O$ in the evapotranspiration flux can be written as:

$$F_{ET} R_{ET} = F_T R_T + F_E R_E \quad \text{with} \quad R = \frac{{}^1H_2{}^{18}O}{{}^1H_2{}^{16}O} \quad (6)$$

with the subscripts ET indicating evapotranspiration, T transpiration and E evaporation respectively. The isotopic ratio R relates linearly to $\delta^{18}O$ (equation 1) and by substituting F_E with $(F_{ET} - F_T)$ equation (6) can be rewritten as:

$$T(\%) = \frac{\delta_{ET} - \delta_E}{\delta_T - \delta_E} \times 100 \quad \text{with} \quad T(\%) = \frac{F_T}{F_{ET}} \times 100 \quad (7)$$

$R^{18}O$ in water vapor from soil evaporation was calculated using soil water $R_{soil}{}^{18}O$ values from 0-3 cm depth (n=14). Evaporated water is depleted in heavy isotopes relative to the remaining water body. Evaporated soil water $R_e{}^{18}O$ is a function of the isotopic composition of vapor in the atmosphere (R_a), the relative humidity (h , expressed as fraction) and

equilibrium and kinetic fractionation factors (α^* and α_k respectively). After Gat, 1996 and Moreira *et al.*, 1997 we write:

$$R_e = \frac{(R_{soil} / \alpha^*) - R_a h}{1-h} \frac{1}{\alpha_k} \quad (8)$$

with R_e being the $R^{18}O$ of evaporated water and R_{soil} the $R^{18}O$ value of soil water. The fractionation factors α^* and α_k were inserted as 1.0104 (15°C, average measured soil temperature, Majoube, 1971) and 1.0189 for a turbulent boundary layer (Flanagan & Ehleringer, 1991). R_e was converted to δ_e using equation (1). It should be noted at this point, that equation (8) is very sensitive to changes in α_k , the kinetic fractionation factor. We decided to use the fractionation factor for a turbulent boundary layer, since at the soil surface, despite the dense plant canopy, we presumed turbulent conditions within the well ventilated chambers. The influence of the relative humidity of air (h) on the fractionation is minor up to a relative humidity of 0.7 (1‰ change for $h=0.7$, as compared to $h=0$) and increases to infinite values for $h \rightarrow 1$. Humidity in our case was $h=0.43$ as a highest value; this deviates from the fractionation calculated with $h=0$ by 0.3‰, indicating that relative humidity had only a minor influence on fractionation during evaporation.

Assuming steady-state leaf water enrichment, the transpired water vapor isotope signal equals the source water signal, according to (Wang *et al.*, 2000). For $\delta^{18}O$ in water vapor from transpiration (δ_T), soil water $\delta^{18}O$ from 3-12 cm depth was used since this was the depth where *L. perenne* derived its source water from. This was separately assessed by stem water measurements, which were compared to soil water in different depths (data not shown). Leaf water isotopic steady state (ISS) is a topic of current research and therefore the values of (δ_T) are not firmly established for this study (see discussion). We therefore applied a second approach where we included leaf water $\delta^{18}O$, which was enriched during the day up to values of 16.4‰. Since vapor pressure is around saturation at the site of evaporation within the leaves, equation (8) cannot be applied and the influence of the kinetic fractionation factor α_k (Cappa *et al.*, 2003) is negligible. We used a simple model with an equilibrium fractionation factor (α^*) of 1.0093 for temperatures at 25°C (Majoube, 1971), which was the average temperature during the afternoons of the samplings:

$$R_T = \frac{R_{leaf}}{\alpha^*} \quad (8b)$$

with R_T the $R^{18}O$ of transpired water from the leaf, R_{leaf} as the $R^{18}O$ value of leaf water. Leaf water $\delta^{18}O$ was determined hourly from 11.00 to 17.00 hours (the water vapor sampling time) and the calculated means from each day were inserted in equation (8b).

For the value of δ_{ET} , the isotopic signal of evapotranspiration, the intercept with the ordinate of Keeling plots from air water vapor data was used (see below for explanation of Keeling plots).

4.3.3.3 Calculating canopy discrimination

According to Farquhar *et al.*, 1989 discrimination (Δ) of a plant canopy against $^{13}CO_2$ during photosynthesis can be expressed by equation (9):

$$\Delta_{canopy} = \bar{a} + (b - \bar{a}) \frac{c_i}{c_a} \quad (9)$$

with \bar{a} (~4.4‰) as the kinetic fractionation by CO_2 diffusing from the canopy air space to the site of carboxylation (see equation 9a) and b (~27.5‰) the enzymatic fractionation by the CO_2 -fixing enzyme ribulose-1-5-biphosphate-carboxylase (RUBISCO). The ratio c_i / c_a is the ratio of the CO_2 concentration in the leaf (“big leaf”) intercellular space and ambient air. In analogy to the explanatory note above concerning Δ_{canopy} , we refer to c_i as the theoretical value of the entire system (plant canopy and soil). This is similar to the “big leaf” model where an entire plant canopy is regarded as a single, large leaf (Ogee *et al.*, 2003). The “big leaf” model itself does not include the CO_2 efflux from the soil. When, as in our study, measurements are made within a whole system, soil derived CO_2 is an additional source of CO_2 . In our “whole system” model this efflux can be regarded as additional mitochondrial respiration within the “big leaf”, thus making the link back to the “big leaf” model. The same principle applies for the stomatal conductance g_c .

The kinetic fractionation \bar{a} is expressed as follows within the big leaf model (Ogee *et al.*, 2003):

$$\frac{-}{a} = \frac{a_b g_c + a g_a + (a_s(T) + a_1) g_c g_a g_m^{-1}}{g_c + g_a + g_c g_a g_m^{-1}} \quad (9a)$$

where a_b is the fractionation of CO₂ diffusing through the laminar boundary layer to the stomata (2.9‰), a denotes diffusional fractionation from the leaf surface to the substomatal cavity (4.4‰), $a_s(T)$ is the fractionation when CO₂ enters solution (1.1‰ at 25°C) and a_1 the fractionation of dissolved CO₂ diffusing through water (0.7‰). The canopy conductance g_c for CO₂ is calculated from equation (11, g_{cCO_2}) and g_m is the conductance for CO₂ within the mesophyll, estimated with 0.6 mol m⁻² s⁻¹, according to Evans & von Caemmerer, 1996. The aerodynamic conductance for CO₂ (g_a) is calculated by the following relation of g_a to g_t and g_b (in m s⁻¹, converted to mmol m⁻² s⁻¹ with a conversion factor of 37.5 after Nobel, 1983):

$$\frac{1}{g_a} = \frac{1}{g_t} + \frac{1}{g_b} \quad (9b)$$

where $1/g_a$ is the sum of a turbulent resistance ($1/g_t$) and a boundary layer resistance ($1/g_b$), after Lamaud *et al.*, 1994. Taking medium values for the turbulent and the boundary layer resistance, since the chamber system was a turbulent environment, we receive values of 4.4‰ which are insensitive to changes in canopy conductance g_c .

The CO₂ concentration of ambient air (c_a) can easily be measured (the mean concentration at the outlets of the chambers, see above), but not the intercellular CO₂ concentration c_i . However, c_i , assuming the system as a “big leaf”, can be derived from equation (10), once the assimilation rate A (in our case the absolute value of day time NEE) and the stomatal conductance (g_{cCO_2}) are known.

$$A = g_{cCO_2}(c_a - c_i) \quad \text{therefore} \quad c_i = c_a - \frac{A}{g_{cCO_2}} \quad \text{with} \quad A = |\text{NEE}| \quad (10)$$

Stomatal conductance (in our case canopy conductance g_{cCO_2}) can be derived from equation (11) describing the transpiration as a function of the vapor pressure difference between the leaf intercellular spaces and the ambient air and g_{cH_2O} .

The transpiration rate is calculated from the measured NEE of H₂O and equation (7) and relates to stomatal conductance for water g_{cH_2O} as follows:

$$T = g_{cH_2O}(e_i - e_a) \quad \text{and since} \quad g_{cCO_2} = 1.6 \times g_{cH_2O} \quad \text{we get} \quad g_{cCO_2} = \frac{1.6 \times T}{e_i - e_a} \quad (11)$$

with T the transpiration in $\mu\text{mol m}^{-2} \text{s}^{-1}$ and g_{cCO_2} the stomatal conductance for CO₂. The term $(e_i - e_a)$ is the difference of water vapor partial pressure from the leaf intercellular space to ambient air. It is assumed that the relative humidity in the leaf intercellular spaces is 100%, e_i can therefore be calculated as the saturation vapor pressure (e_{sat}) for a given (leaf) temperature. Under non-turbulent conditions the leaf temperature is higher than the ambient air temperature. However, the air in our gas exchange chambers was well mixed based on the high turbulence within the chambers, so that the temperature difference between ambient air and the leaves was presumed to be negligible. This means that $(e_i - e_a)$ can be approximated with the vapor pressure deficit (VPD) of ambient air within the chambers, which is $(e_{sat} - e_a)$. Therefore, if the transpiration rate (calculated from equation (7) and multiplied with the NEE flux for H₂O from the chambers /100), the rate of net photosynthesis (NEE flux for CO₂ from the chambers), VPD and ambient CO₂ concentration is known, Δ_{canopy} can be calculated by combining equations (9) (10) and (11) and substituting $(e_i - e_a)$ with VPD. Equations (9) and (10) give:

$$\Delta_{canopy} = \bar{a} + (b - \bar{a}) \left[\frac{c_a - \frac{|NEE|}{g_{cCO_2}}}{c_a} \right] \quad (12a)$$

and by substituting g_{cCO_2} with equation (11) and $(e_i - e_a)$ with VPD we get:

$$\Delta_{canopy} = \bar{a} + (b - \bar{a}) \left[1 - \frac{|NEE| \times \text{VPD}}{T \times c_a \times 1.6} \right] \quad (12b)$$

4.3.4 Statistical analysis

For $\delta^{13}\text{CO}_2$ and $\delta\text{H}_2^{18}\text{O}^{16}\text{O}$ source determination a two component mixing model (Keeling Plot) was applied using geometric mean (GM) regression. Outliers were selected (and removed) by an iterative method described by Bowling *et al.*, 2002 using linear regression from statistics software R (Gnu public license) for residual calculation. Data points with an absolute value of the residual larger than twice the residual standard error were removed and this process was iteratively repeated. This resulted in removal of 10% of the data points (27 of 273) for CO_2 and in 8% (3 of 39) for H_2O . GM regression was calculated according to Webb *et al.*, 1981 using an application written by M. Sawada, University of Ottawa. For error estimation of the intercepts we followed the suggestions by Pataki *et al.*, 2003 and Sokal & Rohlf, 1995 using the standard error of the intercept from the linear and not the geometric regression model.

The four treatments (high N and low N with each former high and low CO_2 levels from the FACE experiment) were pooled since no significant differences were observed between different treatments. Mid day means of H_2O and CO_2 NEE were analyzed with a Student's *t* test, assuming normal distribution of the individual datasets. Night time Keeling plot intercepts from former high and low CO_2 levels were analyzed with a Student's *t* test, also presuming normal distribution of the underlying datasets.

4.4 Results

4.4.1 NEE and micrometeorology

The beginning of May 2004 was characterized by low temperatures of 5-10 °C maximum and cumulated precipitation of 53 L m⁻² from May 6 to May 9 (Figure 16a). The following days from May 10 to May 12 showed increasing temperatures with maxima up to 20 °C, a VPD of 10 to 14 hPa and a global radiation of over 800 W h m⁻². After another rain event with 12 L m⁻² during the night of May 12, temperature and VPD dropped to 12 °C and 5 hPa on May 13. Subsequently, temperature and VPD increased from day to day until reaching peak values of 26 °C and 24 hPa respectively on May 18 (Figure 16a).

All three CO_2 sampling days (May 11, 14 and 18) were mostly sunny (some clouds on May 11 and 14, see Figure 20) with peak temperatures of 17 to 26 °C and VPD between 11 and 24 hPa. The first two days had similar micrometeorological conditions and contrasted to the third day. May 11 and May 14 were characterized by peak temperatures between 17 and 20 °C and

VPD between 11 and 14 hPa. On May 18, the third sampling day, temperature reached 26 °C and VPD was 1.9 times higher than the mean of the other two days. VPD within the chambers differed even more between the two sets of meteorological conditions (Figure 18).

NEE of CO₂ was highest on day two (May 14), where the mid day average from 12.00 to 14.00 hours reached -27.2 $\mu\text{mol m}^{-2} \text{s}^{-1}$. Concurrently, the smallest night time respiration flux of 2.8 $\mu\text{mol m}^{-2} \text{s}^{-1}$ was observed in the night of May 14. The warm and dry day three showed the smallest day time NEE of -20.4 $\mu\text{mol m}^{-2} \text{s}^{-1}$, being 78% of the average of the other two days. Respiration during the following night was highest of all three sampling days and reached 3.8 $\mu\text{mol m}^{-2} \text{s}^{-1}$ (Figure 16b).

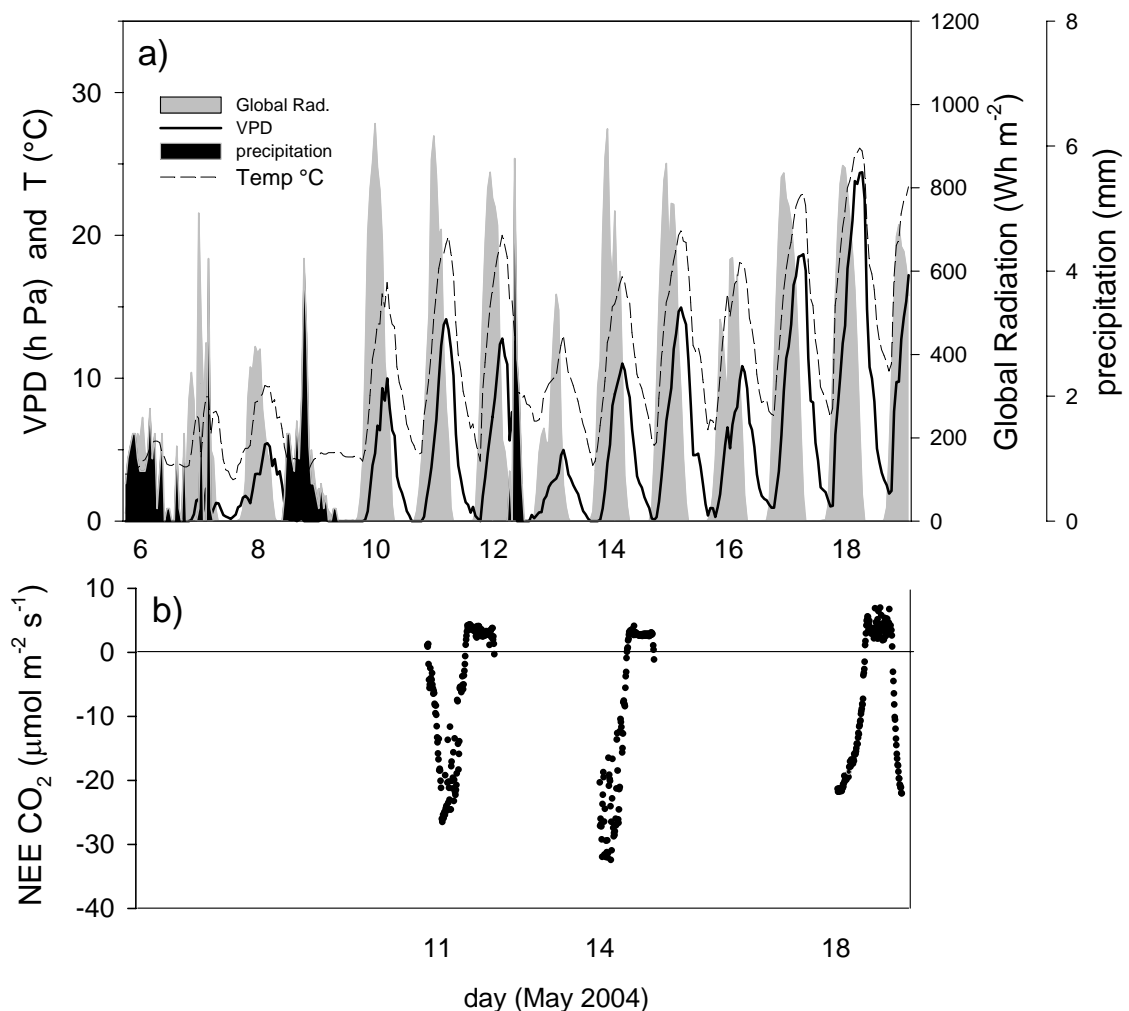


Figure 16 a) Micrometeorological data from May 6 to 19 from the Lindau station, except for global radiation from the Zürich-Kloten station. **b)** Measured net ecosystem exchange (NEE) for CO₂ from the chambers. Time periods are from 06.00 to 06.00 hours (May 11) and from 09.00 to 06.00 hours (May 14) and from 10.00 to 10.00 hours (May 18).

4.4.2 Water vapor flux partitioning

The isotopic signal of the evapotranspiration (ET) flux δ_{ET} as derived by the ordinate intercepts from Keeling plots were -11.0‰ on May 29 and -10.3‰ on May 30 (Figure 17, a and b). They differed by 0.7‰ between the two days and the associated errors were ± 0.5 and ± 0.4 ‰ respectively. Evaporation $\delta^{18}\text{O}$ as calculated by equation (8) showed a small difference of 0.2‰ between the two sampling days, which was mainly caused by the 0.3‰ difference in soil water between the two days. The change in relative humidity from 0.43 to 0.37 attenuated this difference to soil water by 0.1‰.

We applied two different models concerning the transpiration $\delta^{18}\text{O}$ for comparison. The first one (i) assuming isotopic steady state (ISS) during transpiration and $\delta^{18}\text{O}$ equaling stem water and the second one (ii) based on $\delta^{18}\text{O}$ of leaf water assuming non-ISS during our sampling times from 11.00 to 17.00 hours (Figure 17, a and b).

The values for δ_{ET} were close to the signal of pure transpiration using the stem-water model (i) and therefore high relative amounts of transpiration were calculated: $96.3 \pm 4\%$ for May 29 and $99.2 \pm 4\%$ for May 30, according to equation (7). The errors were derived by error propagation from the individual errors in equation (7). With the leaf-water model (ii) we calculated relative transpirations of $61.7 \pm 3\%$ for May 29 and $64.4 \pm 3\%$ for May 30. For both models the relative transpiration on the two days differed only within the calculated errors of each, giving mean values of 98% (i) and 63% (ii) respectively.

Both models showed a consistent increase in relative amounts of transpiration from May 29 to 30, by 2.9% (i) and 2.7% (ii) respectively. The driving variable for this increase was the rise in VPD by 9.5 hPa from May 29 to May 30 (Figure 18). The measured ET flux increased by 9% during the two days, this resulted in a calculated increase of the transpiration flux by 12% (i) and 14% (ii) between the two days, depending on the model used.

Model (i) seems to overestimate the relative amount of transpiration, since on the two days prior to sampling there was 15 mm of precipitation (Figure 18) and the soil was moist. Model (ii) seems to provide more realistic results and is therefore used in the following calculations. The implications of either model are further discussed in the following results.

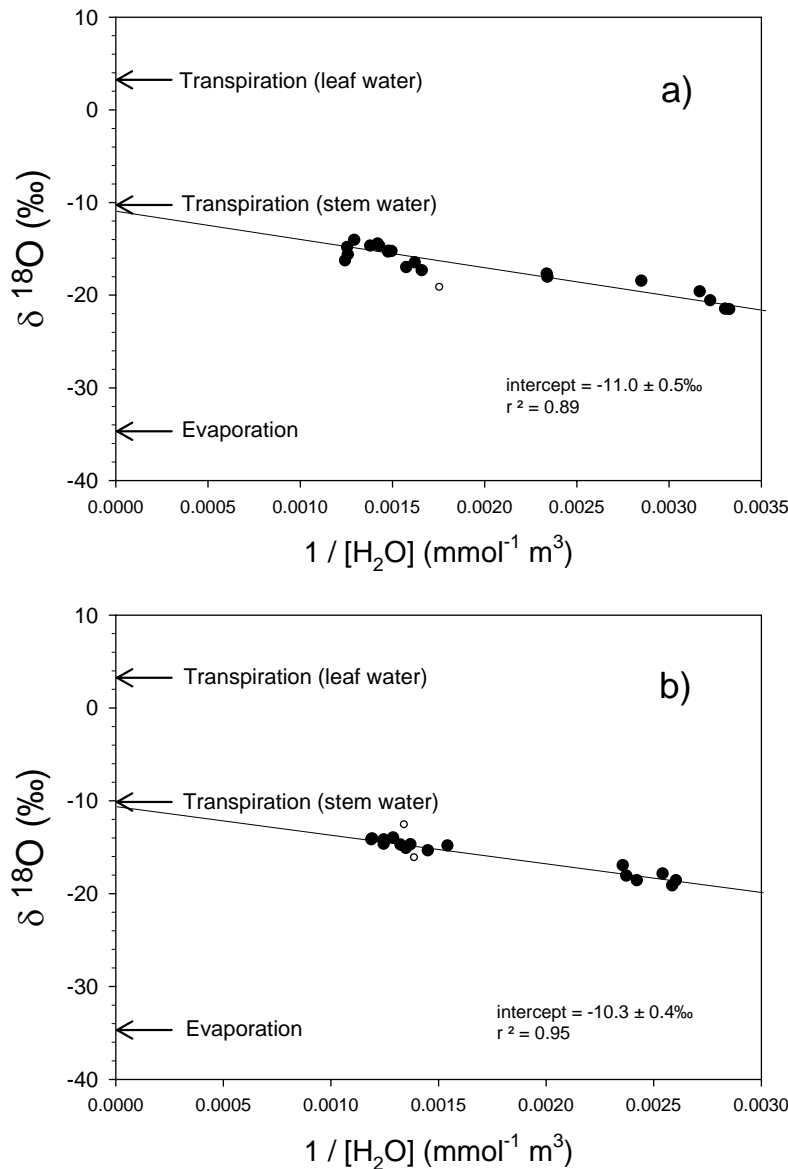


Figure 17 a) and b) Keeling plots of water vapor from May 29 (a) and 30 (b). The intercepts indicate the isotopic composition of the evapotranspiration flux. White dots are outliers not included in the regression and arrows mark the isotopic value of the evaporation flux and transpiration flux (stem water and leaf water model).

May 11 and 14 showed similar meteorological conditions to the H₂O sampling day May 29. Average 24 hour temperatures were between 11 and 12°C on May 11 and 14, and 13°C on May 29 and rain periods were observed 1-2 days before each sampling day. On May 30 temperature was higher (16°C), causing the observed increase in VPD (Figure 18). Nevertheless, and not depending on the model used for calculating transpiration, May 29 and 30 showed an increase of 3% in their relative transpiration rate. These were two consecutive

days without intermediate precipitation and our data shows that the relative amount of transpiration increased even with a totally increasing NEE of H₂O. The increase of the NEE was therefore caused by the increase of the absolute transpiration rates by 14% (with model ii), driven by the higher temperature and VPD. This makes the extrapolation of the measured relative transpiration rate to May 11, 14 and 18 difficult. May 11 had a preceding day with high temperature and VPD (Figure 16a), just after the rain event. This could mean that soil evaporation from the precipitation event would already have diminished again. Otherwise, May 14 was preceded by a day with low temperature and VPD, following the precipitation event. This has most likely caused the relative evaporation to be still high on May 14 and most likely comparable to May 29 (and 30). We address this issue further in the following sections.

In general, model (i), with stem water does not seem to fit well to the meteorological conditions, since a relative transpiration of 98% is not realistic in a temperate climatic area shortly after a rain event. We therefore used model (ii), with leaf water in the following calculations, but considered model (i) results for comparison.

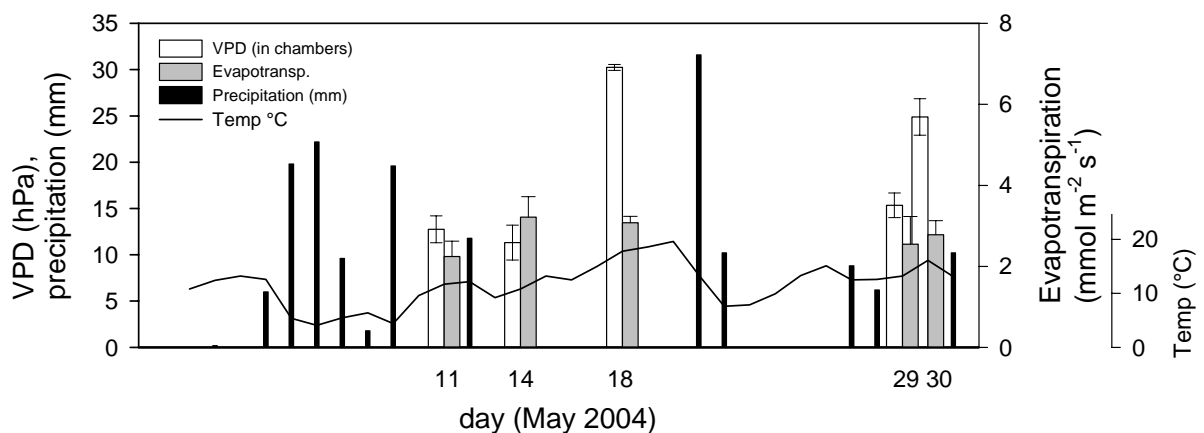


Figure 18 Mid day (12-14 h) vapor pressure deficit (VPD) in the chambers, and evapotranspiration at the five sampling days in May 2004. Black bars are precipitation in May 2004. Timescale is linear and error bars are the standard error of the means.

4.4.3 Canopy discrimination

The mean value of 63% transpiration (from model ii) of the two H₂O sampling days was taken as a basis to calculate the transpiration fluxes, which are one of the terms in equation (12b) that was used to calculate the canopy discrimination Δ_{canopy} . Implications of using model (i) or (ii) will be further discussed below.

Canopy discrimination was calculated for the three CO₂ sampling days May 11, 14 and 18 at an hourly time resolution from 12.00 to 18.00 hours. Using model (ii) with 63% transpiration, the calculated values were between 13.6 and 23.8‰. May 11 and 14 were close together and May 18, the day with dry conditions, showed consistently lower discrimination values. May 11 and 18 showed a gradual increase during the day, but May 14 varied up to 7‰ within two hours. The instability of May 11 and 14 was be directly related to meteorological conditions, see Figure 20 and Figure 21 and further below. The average canopy discrimination of the entire growth period (Figure 19) was calculated to 20.6‰, from mean plant $\delta^{13}\text{C}$ of -28.6‰ (δ_{plant}) and an estimated mean of -8‰ for atmospheric (δ_{atm}) CO₂. ($\Delta_{\text{canopy}} = \delta_{\text{atm}} - \delta_{\text{plant}}$).

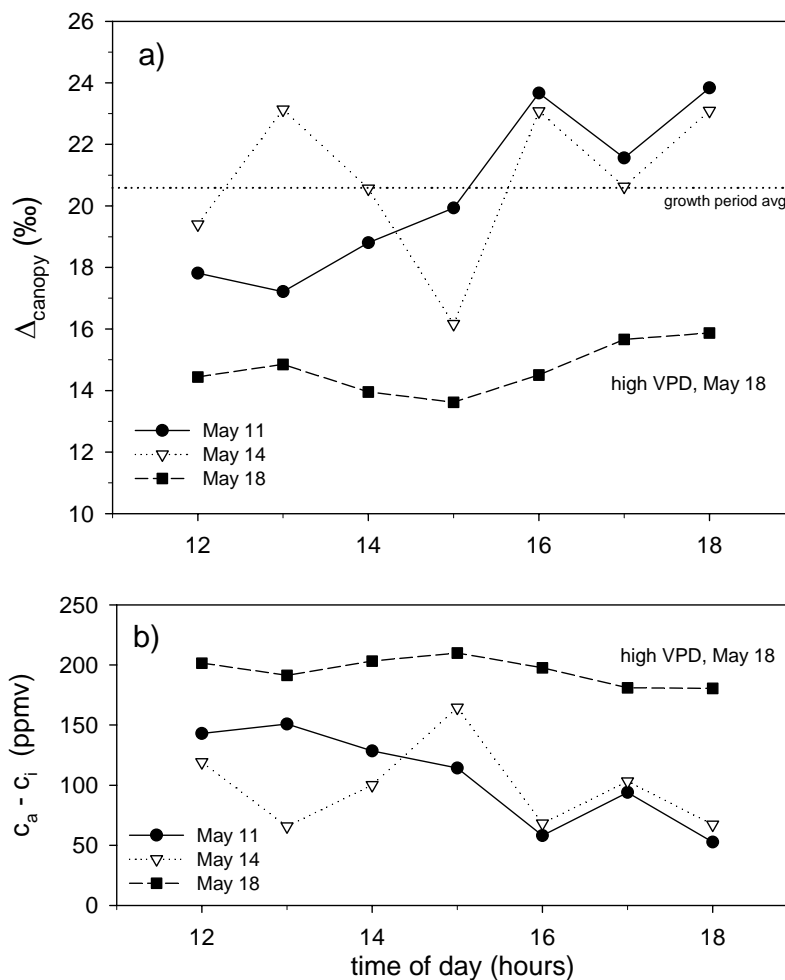


Figure 19 a) Canopy discrimination on May 11, 14 and 18 as calculated by equation (12). Dotted line is the mean Δ_{canopy} of the entire growth period. b) Differences between chamber ambient and canopy-scale intercellular CO₂ concentrations. May 18 was a dry day characterized by a VPD within the chambers 2.5 times higher than the average of the other two days (averages from 12-14 h).

Leaf-internal CO₂ concentration (c_i) was calculated from equation (9). Again, May 18, as the dry and warm day, showed a consistent and stable pattern from 12.00 to 18.00 hours, with an average value which was 195 ppm lower than the average ambient CO₂ concentration. On the other two days the differences were smaller, lying between 95 and 105 ppm on average, providing a higher availability carbon to the CO₂ fixing enzyme RUBISCO. This caused a higher discrimination, closer to the maximum value of 27.5‰ (equation 9, if $c_i / c_a = 1$ is assumed).

A close link between NEE of CO₂ and Δ_{canopy} was found on two days, but not for the dry day May 18 (Figure 20 and Figure 21a). With an increasing NEE flux, canopy discrimination was also increasing, but this was only found on the two days with moderate temperatures and VPD. All three days showed a close correlation to VPD, with an increase in VPD causing lower leaf internal CO₂ concentrations (Figure 21b).

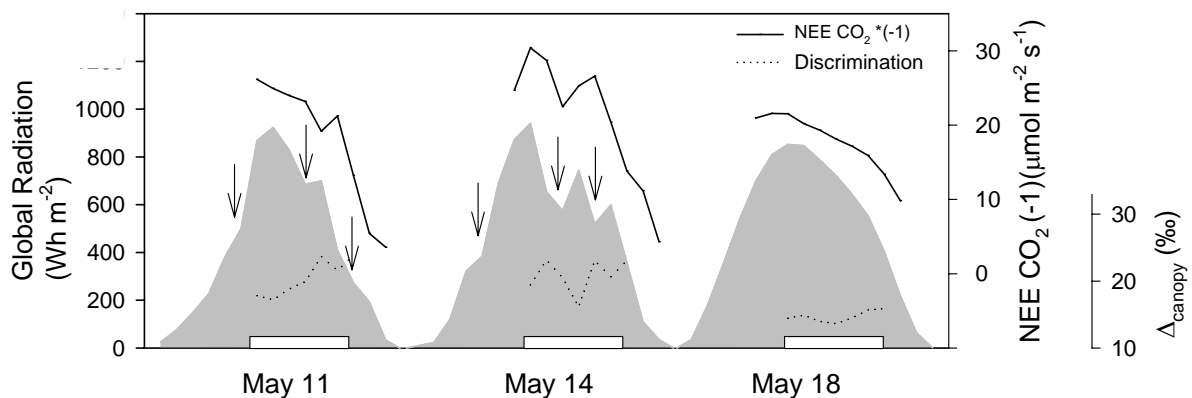


Figure 20 Global radiation, NEE of CO₂ (black line) and canopy discrimination (dotted line) on May 11, 14 and 18. Arrows point at events diminishing global radiation (clouds) and white bars are times from 12.00 to 18.00 hours.

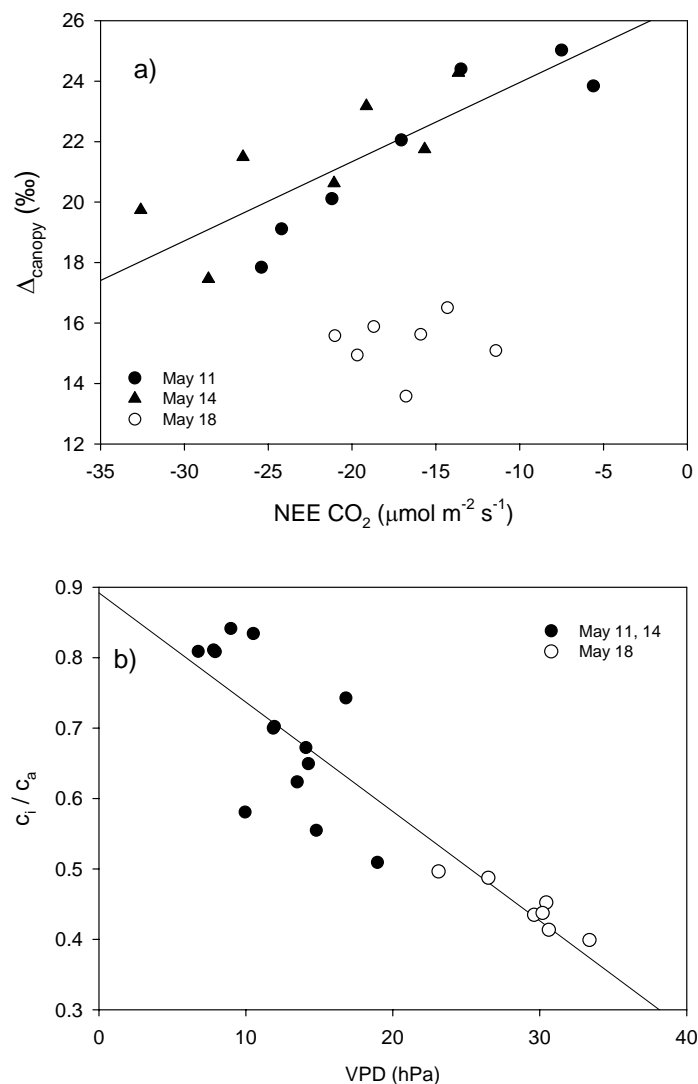


Figure 21 a) Delta canopy versus NEE of CO_2 on the three sampling days May 11, 14 and 18. White circles represent May 18 and regression line through the other dates is with $r^2 = 0.69$. b) Ratio of leaf internal $[\text{CO}_2]$ to ambient $[\text{CO}_2]$ versus VPD in the chambers on May 11, 14 and 18. White circles are the dry day May 18. Regression: $r^2 = 0.81$.

4.4.3.1 Influence of transpiration on canopy discrimination

As mentioned above, the relative amount of transpiration from evapotranspiration was calculated using two different approaches, model (i), with stem water and model (ii), with leaf water $\delta^{18}\text{O}$. To see how this affects the calculated Δ_{canopy} we tested several relative transpiration rates (Figure 22). Two distinct features were found: the closer Δ_{canopy} is to the

maximum value of 27.5‰ the smaller the effect of any change. Second, the magnitude of change becomes larger with decreasing transpiration rates.

This means, that an accurate quantification of transpiration becomes more important the dryer the environmental conditions (decrease of Δ_{canopy} with increasing VPD, see Figure 21b). Otherwise, dry conditions are generally characterized by a low soil evaporation and high relative transpiration. This attenuates the magnitude of the error since errors get smaller with a high transpiration. As an example, shifts in transpiration from 63 to 80% caused shifts between 0.8 and 3‰ within our dataset, with the largest changes occurring at low Δ_{canopy} values (calculated with equation 12b). This seems to be a realistic magnitude of possible changes, since our dataset covers a wide spectrum from 13.6 to 23.8‰ and changes from 63 to 80% could be realistic under field conditions in temperate areas.

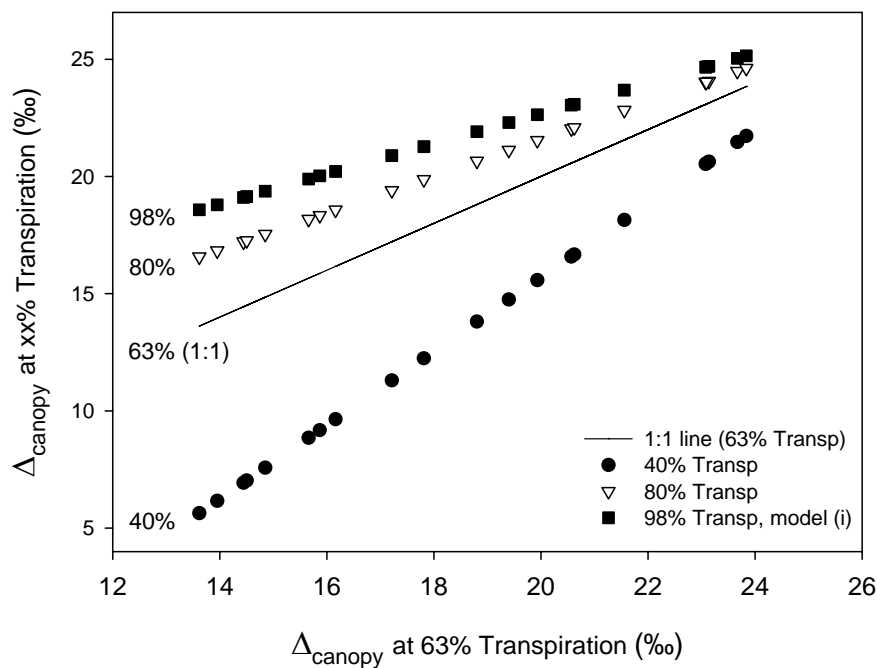


Figure 22 Δ_{canopy} from all three days calculated at 63% (model ii) versus Δ_{canopy} calculated at different relative transpiration rates, 98% corresponding to model (i).

4.4.4 CO₂ flux partitioning

4.4.4.1 Day – night course of CO₂ and $\delta^{13}\text{C}$

Chamber inlet and outlet differences directly show the influence of the enclosed vegetation and soil. During daytime the outlets showed CO₂ concentrations up to 40 ppm lower than the inlets, this at an average flow rate of 6 L s⁻¹. Simultaneously, CO₂ was relatively enriched in ¹³C compared to the inlets, up to a maximum of 2.2‰ (Figure 23). The enclosed grass ecosystem segment assimilated CO₂ and the relative enrichment of ¹³C in the remaining air was caused by the ¹³C discrimination of the photosynthetic process. A midday peak at 12.00 hours could be observed in these characteristics and a transition time towards night with increased scattering of individual measurements from 17.00 to 20.00 hours. After nightfall CO₂ concentrations were higher by 5.5 ppm at the outlets compared to the inlets and CO₂ was depleted in ¹³C by -0.3‰ on the average.

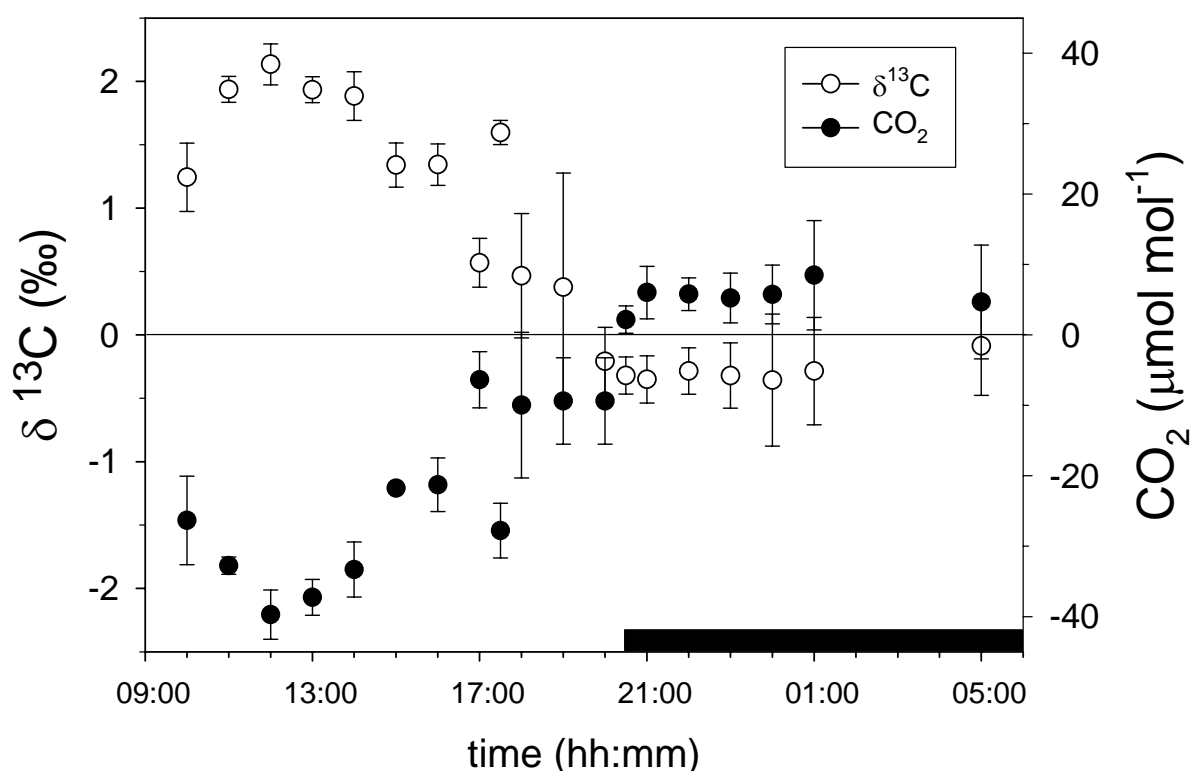


Figure 23 CO₂ and $\delta^{13}\text{C}$ differences from chamber outlets to inlets on May 11. Night time data was standardized to day time chamber airflow (6 L s⁻¹ average) to enable comparison. Dark bar indicates night time (sunset at 20:30h), error bars are standard error of the means.

Midday ecosystem CO₂ uptake was 7.3 times higher than respiratory release at night, the grassland was a strong CO₂ sink during our measurement days (see also Figure 16b). Integrated values for a 24 hour period on May 14 showed that the investigated grassland areas assimilated 7.4 times more carbon during the day than they respired in the night (data not shown). Midday peak values therefore seem to be a good measure for whole day ecosystem CO₂ uptake.

4.4.4.2 Keeling plots

Intercepts of CO₂ Keeling plots can differ during the course of a day or night, depending on the time period chosen and the number of samples as also shown by Knohl *et al.*, 2005. Both daytime (δ_N) and nighttime Keeling plot (δ_R) intercepts are crucial parameters in equation (5b) to calculate F_R and F_A .

Daytime intercepts on the three sampling days varied by 2.4 to 4.7‰ within one sampling day, when different sampling times were used for the calculation (Figure 24). One must note however, that a two-hour period only consisted of twelve data points. Keeling plots from 10.00 to 19.00 hours were based on a large dataset ($n = 66$, Figure 25a and b) and also showed the smallest associated error of all analyzed time intervals within a single day. Since the time period of interest for the flux partitioning is mid day 12.00 to 14.00 hours, Keeling plots from that time would be the choice to represent this time period. Nevertheless, whole-day Keeling plots lied within a range of 0.2‰ of mid day Keeling plots and showed a smaller associated error on the intercepts (0.1 to 0.6‰ smaller) and were therefore chosen to represent mid day δ_N (Table 5).

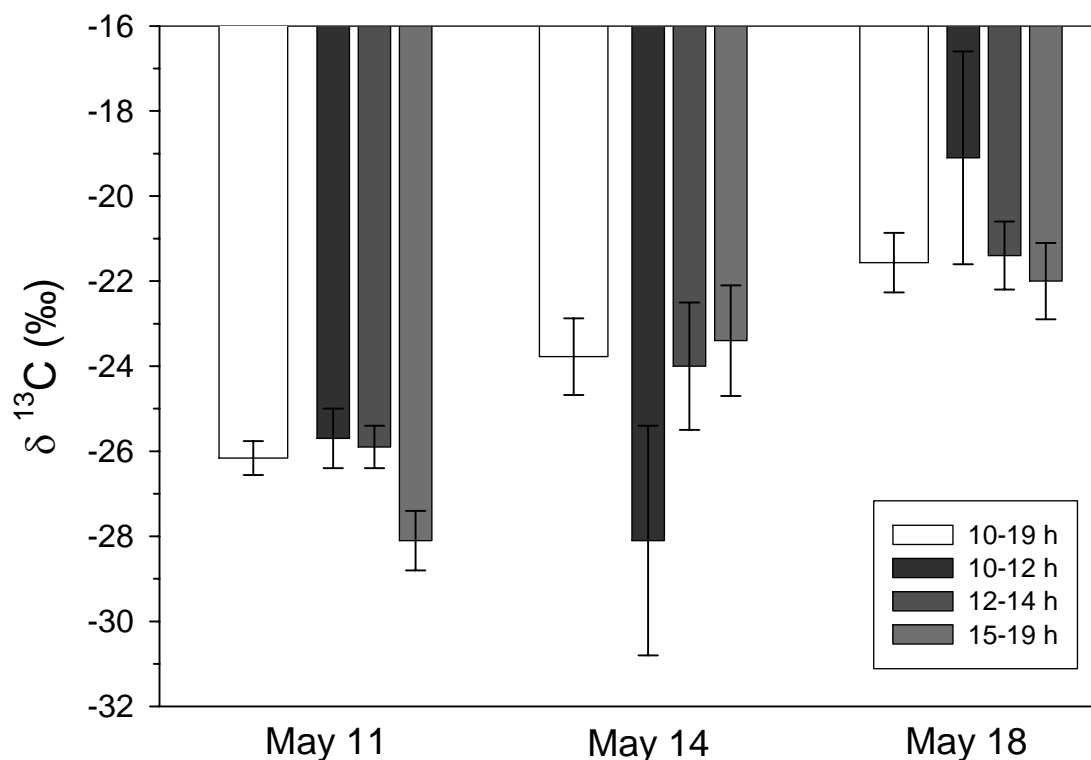


Figure 24 Daytime Keeling plot intercepts for different time spans on the three CO₂ sampling days in May 2004. Error bars are the standard error of the intercepts.

Time periods that deviated from the whole day and mid day intercepts were morning and late afternoon hours. No pattern regarding intercept values could be found for these transition times. Day one and three showed less negative values during morning hours and more negative values in late afternoon hours. On May 14 (day two) the opposite was observed. A common feature though for the transition times on all days was the generally larger standard error of the intercept (Figure 24).

The sensitivity of the intercept calculation becomes clear when studying the example of whole day data from May 11, as shown in Figure 25a and b. CO₂ concentrations (without outliers) covered a range of 64 ppm (329 to 393 ppm) and $\delta^{13}\text{C}$ values a range of 3.3‰ (Figure 25a). The source value of the Keeling plot two-component mixing model is found by plotting the inverse of the CO₂ concentrations against the corresponding $\delta^{13}\text{C}$ values and calculating the intercept of a linear regression model with the ordinate. Extrapolating $1/[\text{CO}_2]$ to zero actually means calculating the $\delta^{13}\text{C}$ value for $\lim_{n \rightarrow \infty} [\text{CO}_2]_n$ (Figure 25b). Since this is a

large extrapolation, the robustness of the fit of the linear model to the underlying data is crucial. In this example, after outlier removal (see statistical analysis), we calculated an r^2 of 0.97 (which was the least of all three days, see Table 5) and a probability of $p < 0.001$ that the model was wrong.

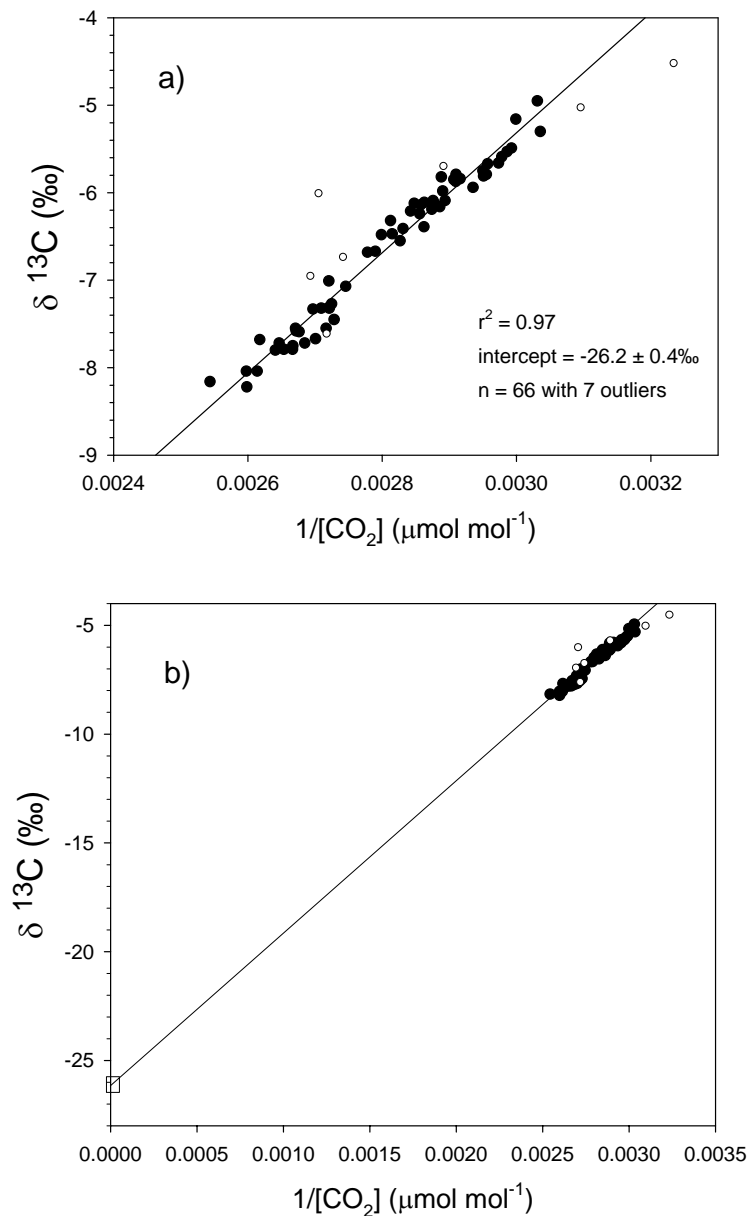


Figure 25 a) Day time Keeling plot with data from 10 - 19 h on May 11. White dots are outliers not included in the regression. **b)** shows the same data but with the abscissa going to zero and the white box on the ordinate being the standard error of the intercept.

Errors of the intercepts from H₂O and CO₂ Keeling plots were in the same range of 0.4 to 0.9‰ (Figure 17, Table 5). The larger scattering of the H₂O data points, being expressed as lower r^2 values, was compensated by a much smaller extrapolation when the intercept with the abscissa was calculated.

Night time Keeling plots varied within 2‰ between the three days (Table 5) and, like the day time Keeling plots, showed a trend towards less negative values in the time period from May 11 to May 18. The variation although was less than half as within day time Keeling plots (which varied by 4.6‰). Sample numbers at night were slightly less than half as during day time, nevertheless the correlations were consistently very robust with $r^2 = 0.99$ for all three nights and errors of the intercepts lied between 0.5 and 0.7‰.

Table 5 Intercepts of Keeling plots for night (δ_R , 22.00 to 01.00 hours) and day periods (δ_N , 10.00 to 19.00 hours). 10% of the data points were identified as outliers and not included in the regression analysis. All regressions were with $p < 0.001$.

date	δR (night) /‰	δN (day) /‰
May 11	-30.3 ±0.6 (n=24, $r^2=0.99$)	-26.2 ±0.4 (n=66, $r^2=0.97$)
May 14	-28.7 ±0.5 (n=24, $r^2=0.99$)	-23.8 ±0.9 (n=66, $r^2=0.99$)
May 18	-28.3 ±0.7 (n=30, $r^2=0.99$)	-21.6 ±0.7 (n=63, $r^2=0.99$)

Night time Keeling plots were also time sensitive, like day time plots. Particularly the data from 20.00 to 22.00 hours shifted the intercepts up to several permil. This period was a transition time from day to night that showed a much larger scatter of the data than the period from 22.00 to 01.00 hours (Figure 26). Late night samples from 05.00 hours also showed large scattering and in addition had the highest CO₂ concentrations. The confounding time periods from 20.00 to 22.00 hours and from late night 05.00 hours were therefore excluded from the calculation of δ_R , thus we obtained the most stable possible results (see Table 5).

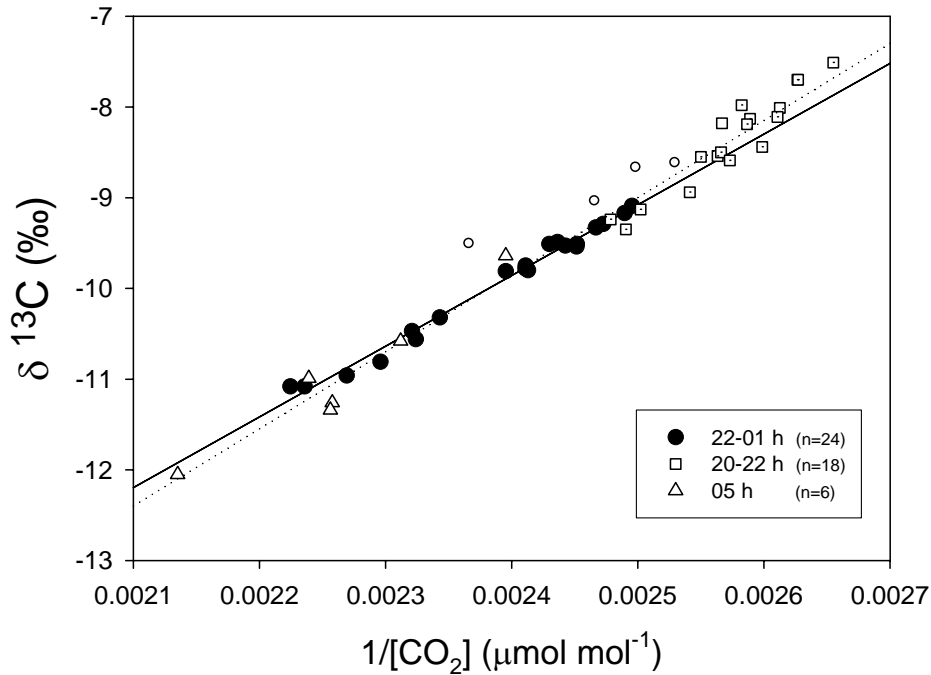


Figure 26 Night time Keeling plot from May 14. Data separated into time periods from 20.00 to 22.00 (white boxes), 22.00 to 01.00 (black circles) and 05.00 (white triangles). Solid regression line is from 22.00 to 01.00 data only, dotted regression line is from all time periods. White circles are outliers not included in the regressions. Note the increasing CO_2 concentration during the course of the night.

4.4.4.3 Assessment of CO_2 fluxes F_R and F_A

Equation (5a) followed a day time course mostly influenced by Δ_{canopy} values and to a lesser extent by δ_a (max. variation 1.7‰). The numerator and the denominator of equation (5a) were calculated on an hourly timescale from 12.00 to 18.00 hours on the three CO_2 sampling days. Three different relative transpiration rates were used; 63% from model (ii) the “leaf evaporation model”, 80% as an intermediate value and 98% from model (i) the “stem water model” (Figure 27 a, b and c). Also shown is the value of the denominator for the estimated mean growth period canopy discrimination of 20.6‰.

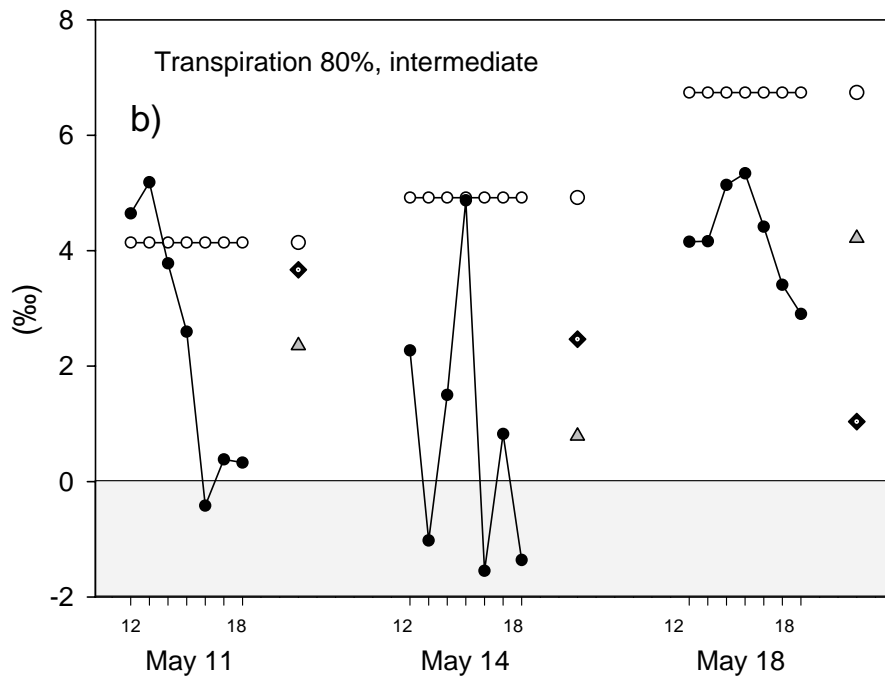
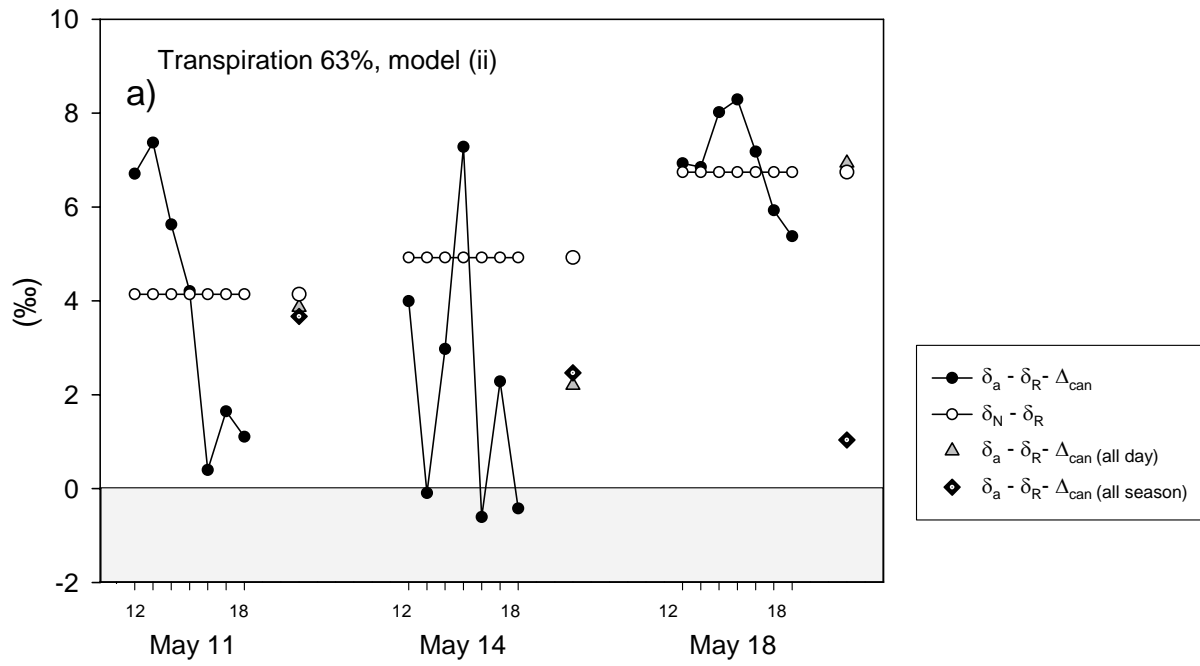
The factors in equation (5a) need to meet two conditions to calculate useful values for the assimilation flux F_A and consequently the respiration flux F_R . First, the numerator ($\delta_N - \delta_R$) should be larger than the denominator ($\delta_a - \delta_R - \Delta_{canopy}$) to yield a result ≥ 1 . If this fails, the result is an assimilation flux which is smaller than the NEE and consequently a negative respiration flux. We will refer to this situation as “error (a)”. The second meaningless result

occurs if one of the factors in the fraction becomes negative, resulting in positive calculated assimilation fluxes. We refer to this situation as “error (z)”, with “z” derived from zero.

All three tested relative transpiration rates showed an error (z) on at least 3 of 21 points of time (63% transpiration). The maximum was 7 of 21 data points including the all day mean of May 14 (98% transpiration). Error (a) occurred largely (10 of 21 points of time) at 63% transpiration, including the all day mean of May 18. The 80% transpiration simulation showed only two errors (a) and 98% showed none. This was since an increase in transpiration and thus canopy conductance caused an increase of Δ_{canopy} (see Figure 22).

The time period from 12.00 to 14.00 showed a higher tendency towards an error (a) on all three days (with May 14 fluctuating strongly), particularly at low transpiration rates of 63% as from model (ii). Later afternoon hours from 15.00 onwards and mean values generally fulfilled the requirements of equation (5a) but with increasing relative transpiration the risk of an error (z) increased, even for mean values. This was caused by the gradual increase of Δ_{canopy} during the afternoon hours (Figure 19a), except for May 14 which showed a very irregular pattern resulting in an error (z) also for the 13.00 hour sampling time and at all transpiration rates.

Values of the denominator with the growth period mean of Δ_{canopy} showed neither an error (a) nor an error (z) on any of the three days but yielded unrealistic high values for F_A on May 18, the dry day (Figure 28a).



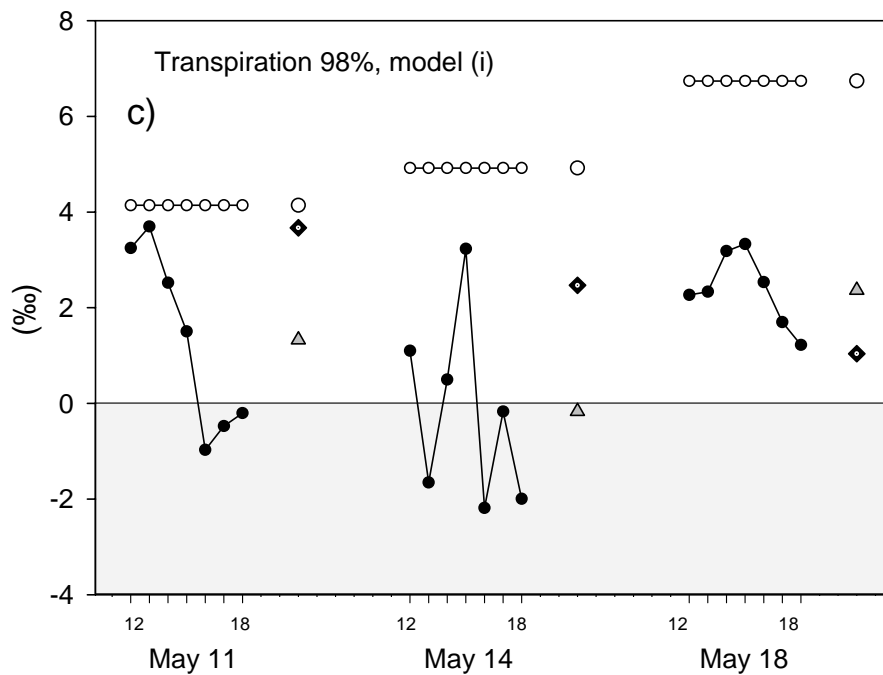


Figure 27 a) b) and c) Numerator and denominator of equation (5a) used for CO₂ flux partitioning on an hourly timescale (12.00 to 18.00 hours) on May 11, 14 and 18. Black symbols are the denominator ($\delta_a - \delta_R - \Delta_{canopy}$), grey triangles are the daily means of the denominator and white circles are the numerator ($\delta_N - \delta_R$). Black diamonds with white dots are the denominator ($\delta_a - \delta_R - \Delta_{canopy}$) calculated from growth period average Δ_{canopy} . Shaded areas indicate values of zero and below for which equation (5a) becomes meaningless, since positive values for the assimilation (F_A) would result. Ordinates are time of day (hours).

None of the three relative transpiration situations fitted all three days simultaneously, even when taking daily mean values. The mean Δ_{canopy} of the entire growth period gave values close to the calculation of Δ_{canopy} with 63% transpiration on two days, but not on the dry May 18. This shows that day to day changes in relative and absolute transpiration and thus canopy conductance exert an essential influence on canopy discrimination, which in term is reflected in the ¹³CO₂ signature. Choosing between the three relative transpiration rates, the independently gathered CO₂ isotopic data fits well when using 80% for May 11 and 18 and the 63% from model (ii) on May 14. This is an arbitrary selection (regarding the exact ratios) but shows and confirms the trend regarding meteorological conditions and relative transpiration as discussed in the first section “water vapor flux partitioning” (see above).

On this (presumed) basis of relative transpiration rates we can calculate F_R and F_A from the CO₂ isotopic data and the mean Δ_{canopy} values from 12.00 to 18.00 hours (Figure 28a) plus F_A for growth period means of Δ_{canopy} . The calculated values may not be compared between days,

since the relative amounts of transpiration rates are only estimates. A re-calculation of Δ_{canopy} (which was calculating using 63% transpiration for all days in Figure 19a) using the above stated transpiration rates is shown in (Figure 28b), confirming the trend already seen in Figure 19a, with May 18 showing lower discrimination values than the other two days, although lying closer together after the re-calculation.

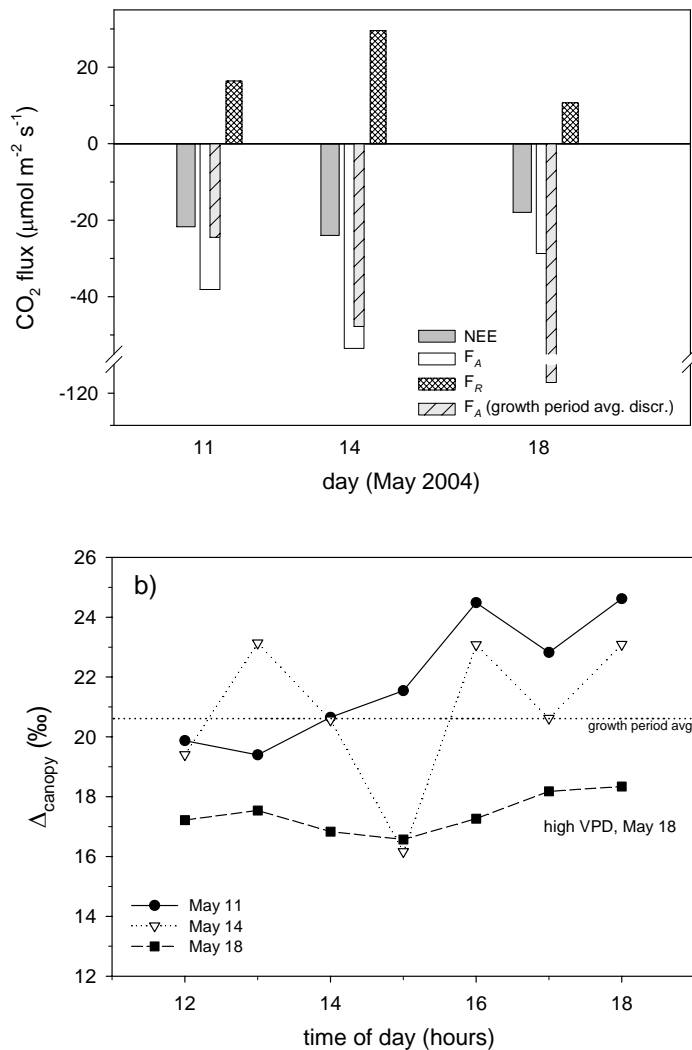


Figure 28 a) NEE, F_A and F_R as calculated by equation (5a) using 80% relative transpiration for May 11 and 18 and 63% for May 14. Grey structured bar is F_A calculated with growth period means for Δ_{canopy} . **b)** Calculated Δ_{canopy} with equation (12b) using the same amounts of relative transpiration (80, 63 and 80%) as in a). Dotted line is the mean Δ_{canopy} of the entire growth period.

4.5 Discussion

4.5.1 Water vapor flux partitioning

The isotopic approach to partition ecosystem water vapor fluxes into transpiration and evaporation bases on $\delta^{18}\text{O}$ differences of these individual fluxes. Both the transpiration and evaporation fluxes have their origin in soil water, but undergo different intermediate processes, which alter $\delta^{18}\text{O}$ composition individually (Wang *et al.*, 2000).

Evaporating water from soil is strongly depleted in the heavy ^{18}O isotope by the evaporation process itself, according to equation (8). Relative humidity, temperature and $\delta^{18}\text{O}$ of the liquid water body influence the magnitude of this depletion. In our case, we found depletions between -28.8 and -29.3‰. The basic question still remains, at which soil depth water for this calculation should be sampled. We decided to use $\delta^{18}\text{O}$ from 0-3 cm soil depth, since a difference of 5.3‰ to water from deeper layers was observed on May 29, after a period of warm and dry weather conditions (data not shown).

Water for transpiration is taken up by the roots of the plants and evaporates with unchanged $\delta^{18}\text{O}$ composition, assuming isotopic steady state (ISS) in plant leaves (Yakir *et al.*, 2000). Recent studies have shown that under field conditions there can be substantial deviations from ISS with a time lag of up to several hours (Farquhar *et al.*, 2005). An isotopic enrichment of leaf water can be observed during the day (Dongmann *et al.*, 1974, Flanagan & Ehleringer, 1991, Harwood *et al.*, 1999) and in our study we found enrichments of $\delta^{18}\text{O}$ up to +16.4‰ (data not shown). Using the model where the transpiration flux has the isotopic composition of stem water (model i), assuming isotopic steady state (ISS) as applied by Yepez *et al.*, 2003 in a semiarid environment, did not yield convincing results in our case. However, since the leaf water is the direct source of transpiration and shows a diurnal course in $\delta^{18}\text{O}$, with high enrichment during day time hours (which is also seen in the water vapor of the ambient air, Bantelmann *et al.*, 2005, unpublished data), we tested a different approach. Model (ii) is using the isotopic composition of leaf water and with the temperature dependent equilibrium fractionation the isotopic composition of the transpiration flux δ_T was calculated. The obtained results were acceptable in magnitude when compared to the few existing studies that relate T to ET. Sene, 1994 calculated a T/ET ratio of 0.65 in a sparse vine crop whereas a more recent study done by Kato *et al.*, 2004 found T/ET ratios between 0.7 and 0.82 in a sparse sorghum canopy. Both authors use models such as Shuttleworth-Walace (Shuttleworth

& Wallace, 1985) and Penman-Monteith to calculate T and ET from meteorological parameters.

For the model (ii) approach we presumed non-ISS conditions, which is supported by our data. We therefore introduced model (ii) to obtain an isotopic value for δ_T where the actual isotopic signature of leaf water is taken into account. From the newest literature it is obvious, that this is the current basis for in-depth discussions as to how δ_T should be determined.

4.5.1.1 Keeling plots of H₂O

Keeling plots of $\delta^{18}\text{O}$ from the sampled water vapor correlated not as well to the fitted linear regressions than ^{13}C CO₂ data did (Figure 17, Figure 25). This was most likely caused by the fact that $\delta^{18}\text{O}$ of water is altered by evaporation and condensation processes along its way to the atmosphere and that the water vapor sampling itself involves a freezing and a thawing process and represents an integration over 30 minutes sampling time. Scattering of water vapor samples was also observed by Yopez *et al.*, 2003 and Moreira *et al.*, 1997. Deviations from a linear Keeling plot may further be caused by changes in the relative contributions of E and T to ET during the course of the day. Nevertheless, the errors of the intercepts were in the same range (0.5‰) as for CO₂ data, since the extrapolation to zero was much smaller. In addition, the errors for δ_{ET} were smaller than the errors for δ_T (1.0‰), as derived from the means of leaf water measurements showing a daytime course, and can therefore be considered acceptable.

4.5.2 Discrimination

Discrimination during photosynthesis against ^{13}C CO₂ was calculated as Δ_{canopy} with equation (12b). The obtained values with 63% transpiration showed two distinct clusters, one with an average discrimination of $20.6\text{‰} \pm 0.7\text{‰}$ (SE, standard error) for May 11 and May 14, two days with moderate temperatures and VPD. The second one, on May 18, showed lower discrimination ranging from 13.6 to 15.8‰ and with a decrease during the course of the day. May 18 was characterized by warm temperatures above 25°C and high VPD, the lower values for Δ_{canopy} on this day were caused by the high VPD of 30.2 hPa within the chambers. The dry air lead to stomatal closure (decrease in stomatal conductance g_{cCO_2}), to a lower c_i / c_a and to a lower Δ_{canopy} . This was in analogy to the model developed by Farquhar *et al.*, 1989. These findings were independent of the model used for the underlying transpiration calculation

(Figure 19a and Figure 28b), even though the mean values were lower by 3.1‰ at 63% transpiration.

Mean values of the canopy discriminations from all three days were 18.8‰ for model (ii, leaf water) and 21.9‰ for model (i, stem water). The average $\delta^{13}\text{C}$ of leaf material was $-28.6 \pm 0.6\text{‰}$ in May 2004. An average value for discrimination during the growth period was calculated, presuming an average ambient $\delta^{13}\text{CO}_2$ value of -8‰ and taking the measured average leaf material $\delta^{13}\text{C}$ of -28.6‰ : $\Delta_{average} = -8\text{‰} - (-28.6\text{‰}) = 20.6\text{‰}$. The values we calculated with each model were either lower by 1.8‰ (model ii) or higher by 1.3‰ (model i). Since our calculated daily means did not include morning hours, where discrimination generally is higher (Baldocchi & Bowling, 2003) than from 12.00 to 18.00 hours, a lower mean value in respect to the growth period average value is not a contradiction. In addition, deviations between long-term and instantaneous Δ_{canopy} have been reported before by Lai *et al.*, 2003 and Flanagan *et al.*, 1996. Warm and dry days are not prevailing for the local temperate climate, where 725 mm of precipitation and average temperatures of 13.2 °C are measured between April and October (30 year means, MeteoSchweiz). It is therefore thought that a calculated average value, (originating from the two days with moderate temperatures and VPD, May 11 and 14), which is higher than the growth period Δ_{canopy} might not be representative. These are indications that in fact model (i) using stem water for δ_T , might not be applicable under these climatic conditions and favor model (ii).

A close link to environmental conditions of canopy discrimination was found, in particular to VPD (Figure 21b). On May 11 and 14, which were partly cloudy, we found a day time course of Δ_{canopy} , which inversely related to global radiation. This shows that mean values of entire sampling periods should be taken when calculating a partitioning of CO_2 fluxes, since the underlying $^{13}\text{CO}_2$ data is generally derived from means of at least several hours.

Combining calculated Δ_{canopy} with CO_2 isotopic data for flux partitioning showed, as a basic conclusion, that day to day variations in the relative amount of transpiration must have occurred (presuming accuracy of the CO_2 data) and results cannot be readily transferred from one day to the other. A second characteristic as revealed together with the CO_2 data set was that model (i) with stem water did not yield any results considered acceptable (or realistic) for all three days, since calculated assimilation fluxes would have been either three or more times higher than CO_2 NEE or returned an error (z), see Figure 27, a-c. Model (ii) with leaf water as calculated on May 29 and 30 was basically applicable for May 14. Intermediate values of 80%

transpiration yielded acceptable results for May 11 and 18, this in analogy to the first conclusion that variations between different days in relative transpiration may be substantial. Thus, using the transpiration values calculated for May 29 and 30 on for other days may cause a considerable error.

In conclusion, establishing and validating a new model to estimate proportional transpiration fluxes could provide the basis for a useful alternative to calculate Δ_{canopy} . Particularly on eddy-covariance sites Δ_{canopy} is generally calculated using the “Penman-Monteith” equation, which does not always yield satisfactory results (Ogee *et al.*, 2003).

4.5.3 Diurnal and inter-diurnal variations of Keeling plot intercepts

Keeling plots of CO₂ data were sensitive to the integrative time period used, this both for day and night time data. As also reported by Knohl *et al.*, 2005 we found strong diurnal variations of Keeling plot intercepts. During two of our three daytime courses the intercept values were becoming more negative towards late afternoon, but on the third day, May 14, the opposite was observed. May 14 was the day with the lowest VPD and temperature of all three days and the one with the highest NEE.

Strong inter-diurnal variations were observed within our eight-day sampling period both for δ_R and δ_N (up to 2 and 4.6‰ respectively). We noted an isotopic link between assimilation and respiration as also found by Knohl *et al.*, 2005. An increase of day time δ_N was consistently followed by an increase of δ_R during the next night. Increases of day time δ_N were more distinct than for night time δ_R on all three sampling days (see Table 5).

The magnitude of change was not the same within day and night time data. This is presumed to be a result of the different underlying processes that caused these changes. As discussed above, variations in δ_N are an expression of proportional changes within the sub-fluxes of δ_N . The photosynthetic flux is the most important since it is the dominating factor by magnitude.

4.5.3.1.1 Day time intercepts

Intercepts of daytime Keeling plots (δ_N) still represent a mix of two gross CO₂ fluxes, namely photosynthesis and day time respiration (which itself again is comprised of several sub-fluxes; plant metabolic respiration, photorespiration and soil respiration). Considering this, diurnal fluctuations of δ_N actually represent changes in the proportions of the respective gross fluxes. A proportional increase of the photosynthetic CO₂ flux over the respiration flux causes less

negative values for δ_N due to the photosynthetic ^{13}C discrimination (Farquhar *et al.*, 1989). This was the situation on May 14, meaning that the proportional respiration flux was higher during morning hours than later in the day. This seems feasible since the night following May 14 showed the smallest night time respiration of all three sampling days. The opposite situation, a diurnal course with more negative δ_N towards sunset, shows the proportional increase of the respiration sub-flux during the course of the day, as seen on May 11 and 18.

4.5.3.1.2 Night time intercepts

Variations in sub-fluxes are also thought to be the cause for night time δ_R changes. For δ_R , the division into sub-fluxes can be made as follows: i) plant respiration, ii) plant root respiration iii) respiration of soil organic matter (SOM) by heterotrophic microorganisms (see chapter 3 for further details). These respiration sources show differences in their $\delta^{13}\text{C}$ signatures. Plant respiration (i) is assumed to stay relatively constant with little or no isotopic fractionation occurring during respiration (Lin & Ehleringer, 1997, although Duranceau *et al.*, 1999 found different $\delta^{13}\text{C}$ values for respiration at different temperatures. Plant root respiration (ii) includes heterotrophic respiration of root exudates and different plant compounds are known to vary in $\delta^{13}\text{C}$ composition (Ghashghaie *et al.*, 2001). Finally, heterotrophic respiration of SOM (iii) can change in $\delta^{13}\text{C}$, depending on the soil depth from which it mainly originates (Nadelhoffer *et al.*, 1988 and chapter 3, this study) and by the involved group of microorganisms and their current physiological state (Boschker & Middelburg, 2002, Fontaine *et al.*, 2003). The driving variables for the factors ii) and iii) are still poorly understood and remain an active area of research.

A link of δ_R to environmental conditions such as VPD has been described by Högberg *et al.*, 2001 and Bowling *et al.*, 2002 in forest sites, involving time lags of 5-10 days. Our dataset showed a strong correlation with VPD 3-4 days earlier (data not shown). This seems feasible since in a grassland ecosystem responses are expected to be on a shorter time scale than within forest systems, due to the faster spreading of fresh assimilates within the plants. It should be noted however, that our dataset covered only three night time δ_R values.

4.5.3.1.3 Time slot for night time sampling

Night time δ_R was calculated from data between 22.00 to 01.00 hours, excluding the period from 20.00 to 22.00 and 05.00 hours. Even though net photosynthesis was zero after 20.00

hours and nightfall was at 20.30 hours, Keeling plot data from 20.00 to 22.00 hours confounded δ_R by yielding more negative results of up to 1.7‰. The same was the case for the late night data from 05.00 hours, but to a lesser extent. The data from transition times lied on the two far ends of night time data when producing Keeling plots (Figure 26). Given the fact that this data also showed a larger scatter than the mid night data from 22.00 to 01.00 hours, their over-proportional influence on the intercept and thus δ_R becomes clear. Unlike the daytime data, which showed a larger scatter during the whole day period due to the day time course of photosynthesis (Figure 25a), the night time data was relatively stable when transition times were not included in the mixing model.

Taking the larger scattering of day time data into account we concluded that the best results for day time Keeling plots are obtained with an all-day sampling strategy, excluding the transition times of early morning and early evening. In our case this was from 10.00 to 19.00 hours (day light savings time).

4.5.4 CO₂ flux partitioning

The $\delta^{13}\text{C}$ signature of the daytime respiration flux cannot be measured directly. The basic assumption has to be made that night time δ_R is representative for day time δ_R of the ecosystem. This assumption involves several independent underlying processes. Respiration of plants during the day possibly has a different $\delta^{13}\text{C}$ signature than during the night, depending on the isotopic composition of the respired substrate molecules (Ghashghaie *et al.*, 2001, Tcherkez *et al.*, 2003). $\delta^{13}\text{C}$ of soil respiration might differ from night to day due to substrate changes in plant root and heterotrophic root exudate respiration. Finally, heterotrophic respiration of SOM might be subject to change in isotopic composition. Considering that the main driving factors for heterotrophic soil respiration are soil temperature and moisture (Wardle *et al.*, 1990), which stay relatively constant within a 24 hour sampling period, changes in $\delta^{13}\text{C}$ from heterotrophic SOM respiration are not considered to be a major factor. It was recently shown by Ekblad *et al.*, 2005 that above ground meteorological conditions are the driving factor for the whole system by influencing plant photosynthesis. For a further discussion see Pataki *et al.*, 2003.

The values of F_A and F_R as shown in Figure 28 could not be further compared to each other since they were calculated based on assumptions made for the relative transpiration flux. Nevertheless, we could show that short-term changes in meteorological conditions (even

clouds) can cause large fluctuations of Δ_{canopy} , making CO₂ flux partitioning difficult, even when taking daily means (Figure 27). In the same figure, we demonstrated that the calculation of F_A and F_R are strongly influenced by Δ_{canopy} , which in our case was again depending on the accurate calculation of the transpiration flux. See below for a further discussion of the individual terms influencing the calculation of F_A according to equation (5a).

4.5.5 Sensitivity analysis

4.5.5.1 Calculation of Δ_{canopy}

The calculation of Δ_{canopy} with equation (12b) was relatively robust to variations of a single factor, since no term in equation (12b) was close to zero. But, as an example, a 20% increase in NEE of H₂O, and simultaneously in VPD, caused Δ_{canopy} to increase between 0.3 and 2.0‰, depending on time of day and sampling day. May 18 proved to be most sensitive to changes of input values. The most critical parameter in our case was the transpiration flux, since it could not be directly measured but was estimated via water vapor partitioning using H₂¹⁸O with uncertainties regarding the model that should be applied (stem or leaf water, model i and ii respectively).

When the relative value of 63% transpiration as calculated by model (ii) is changed to 98%, as calculated by model (i), we observed increases of Δ_{canopy} between 1.3 and 5.0‰. Again, May 18 was most sensitive to the variations (see Figure 22). The changes in relative transpiration presented here are massive, but not unrealistic in a temperate environment. The calculation of Δ_{canopy} is not hypersensitive to changes in input variables, but since substantial changes in transpiration may occur between different days this remains a crucial parameter. This is amplified by the uncertainties of the calculation method for the relative transpiration.

4.5.5.2 Calculation of F_R and F_A

The values we calculated for Δ_{canopy} brought the term $(\delta_a - \delta_R - \Delta_{canopy})$ in equation (5a) to values between -2.2 and +8.3‰ depending on time of day and the input model used (transpiration amount). With the exception of May 14, which showed large afternoon fluctuations due to changing sunlight, the times from 16.00 to 18.00 hours proved most critical for being close to zero or negative (Figure 27, a-c). Negative values return a “z-type” error from equation (5a) as discussed previously. Generally, small but positive values close to zero are critical in regard to slight changes of δ_a and δ_R , even by fractions of a permil, since

the risk of an error (z) is high. With the input values we used (Figure 28), all terms were well away from zero and close attention should be directed to this point when calculating the partitioning of CO₂ fluxes with equation (5a).

The $\delta^{13}\text{C}$ of ambient CO₂, δ_a , is a value that can be directly measured with a high precision and is therefore not considered to be an important source of error. δ_R and δ_N on the other hand are indirectly derived values from Keeling plots and are therefore subject to larger uncertainties than δ_a (but see below, *in situ* measurement of δ_a).

4.5.5.2.1 Varying δ_N and δ_R

We varied day time δ_N and night time δ_R in equation (5a) as used in the calculation (see Figure 28a) by the average error of 0.6‰ from the Keeling plot intercepts. We added 0.6‰ to δ_N and subtracted 0.6‰ from δ_R (case 1) or *vice versa* (case 2) to test the “extreme” positions. Case (1) caused the assimilation flux F_A to change within $\pm 3\%$, corresponding to a maximum change of $1.2 \mu\text{mol m}^{-2} \text{s}^{-1}$. Case (2) lead to changes of F_A within $\pm 5\%$, being the equivalent of $2.1 \mu\text{mol m}^{-2} \text{s}^{-1}$. The calculations were apparently not sensitive to changes in day and night time Keeling plot intercepts δ_N and δ_R since the fraction in equation (5a) was far from 1, namely between 1.6 and 2.2. Having a strong isotopic disequilibrium of several permil between the isotopic signature of the assimilation flux $\delta_A (= \delta_a - \Delta_{canopy})$ and the respiration flux δ_R is a prerequisite for not being close to 1 in the fraction of equation (5a).

4.5.5.2.2 c_a and δ_a

The values for c_a (ambient CO₂ concentration) and δ_a ($\delta^{13}\text{C}$ of ambient CO₂) are interconnected. Assuming conditions stay constant, an increase in c_a means more negative δ_a values (along a Keeling plot line). An increase of c_a by 15 ppm and a simultaneous decrease of δ_a by 1‰, corresponds to a shift on the Keeling plot line towards the intercept with the ordinate by one fourth of the data range covered by the samples. This resulted in differences for canopy discrimination of 0.4‰ maximum (for May 18, with a low discrimination). The effects on F_A and F_R were much more dramatic, since δ_a is a direct parameter in the denominator of equation (5a). Assimilation fluxes F_A increased by factors between 1.5 and 2.4, with May 14 being most sensitive. With the concurrent change in Δ_{canopy} the highest proportional decrease in the denominator was caused, since it was the smallest of all three days.

Nevertheless, c_a and δ_a are not considered to be critical parameters as such, since they can be directly measured with a high precision. But using an arbitrary “standard” value of -8‰ for c_a should be avoided by all means and replaced by elaborate *in situ* measurements.

These simple variations of the underlying data show that c_a and δ_a are highly sensitive parameters and a locally adapted system design has to ensure that the actual “ambient” values are being measured. This is the critical point, since the concentration and $\delta^{13}\text{C}$ of CO_2 can both be measured with a high precision and are not considered a problem as such. Taking samples of “ambient” air could be readily done in the chamber system used in our study by taking the values from the chamber outputs, assuming proper mixing inside the chambers. At eddy-covariance flux sites it might prove more difficult to find a representative location for a mean “ambient” value, since it should be a sample from the “fresh” air masses within the site. In particular sites with a high canopy (forests) could be challenging for this task.

Having a strong isotopic disequilibrium between the assimilation and the respiration flux at the sampling site keeps the fraction in equation (5a) far from 1 and makes equation (5a) robust to slight changes in δ_N and δ_R . This is generally given at sites where C3 photosynthetic pathway plants prevail, but might prove more difficult at sites with dominating or complete C4 vegetation, since the isotopic disequilibrium between δ_A and δ_R is smaller.

4.5.6 Pooling of data

4.5.6.1 Pooling of different (former) CO_2 treatments from FACE

The difference of 2‰ in $\delta^{13}\text{C}$ of soil organic matter (SOM) between the two former FACE CO_2 levels was thought to have the largest effect on above ground CO_2 during night time due to the respiratory release of CO_2 partially containing the isotopic signature of SOM (see above). No significant differences could be observed when calculating Keeling plot intercepts from each treatment (Student’s t test). There was not even a (non-significant) pattern to be found. The intercepts from the plots with more negative SOM $\delta^{13}\text{C}$ were more negative than the control plots on two occasions, May 11 and May 14, but not so on May 18. The underlying data sets for the Keeling plots consisted of twelve data points each, the intercepts therefore showed rather large associated errors between 0.5 and 2.3‰. With the present amount of samples it was therefore not possible to detect an effect of the 2‰ difference in SOM between different plots. This seems reasonable, since respiration of FACE-derived

SOM was shown to be only 40% of total soil respiration on these plots (see chapter 3). Together with the respiratory CO₂ release from plants the $\delta^{13}\text{C}$ signature of SOM is even more diluted within the total respiratory flux and was therefore not detectable within air samples.

4.5.6.2 Pooling of different nitrogen fertilization levels

Plant canopies which received a high nitrogen (N) fertilization had larger total leaf areas, this was reflected in lower intercepted photosynthetic active radiation (PAR) at 5 cm above ground: 2% for high N fertilization and 13% for low N fertilization (with respect to above canopy PAR). This might have resulted in a higher assimilation rate for the canopies with the larger leaf area, but is expected to have been at least partially compensated by a higher respiration rate. NEE of CO₂ and H₂O showed no significant differences between these treatments.

4.6 Conclusions

The calculation of Δ_{canopy} remains a crucial point in CO₂ flux partitioning studies besides finding the best Keeling plots. Establishing a more accurate model for the assessment of proportional transpiration fluxes using H₂¹⁸O could provide a useful alternative to the Penman-Monteith equation which is often used together with the eddy covariance measurements. According to our study the new model should consider non isotopic steady state conditions occurring during transpiration and account for leaf water $\delta^{18}\text{O}$ enrichment.

A close link between isotopic signature of assimilation and respiration during the following night was found, and, in addition, night time δ_R correlated to meteorological conditions (VPD) from 3-4 days backwards, prior to sampling. Night time Keeling plots showed a good stability when excluding the transition times around sunset and early morning, we suggest to start night time sampling not before complete darkness and to stop before early morning. A considerable variation of day time Keeling plot intercepts was observed. The time period from mid-morning to early evening (10.00 to 19.00 hours in our case) provided the most stable results and matched well with intercepts from the 12.00 to 14.00 hours period. Whole-day Keeling plots therefore provide a good means to determine mid-day δ_N .

Open-flow chamber studies provide a relatively well characterized environment in comparison to “open” field studies which are much more affected by changes in turbulence,

wind direction etc. Nevertheless, the partitioning approaches applied here to a chamber study are not very stable and are shown to be critically dependent on the models used. A sensitivity analysis where the used parameters to calculate the partitioning of CO₂ fluxes into F_A and F_R were varied, showed a strong dependence to isotopic values of “ambient” CO₂. Locations for sampling of ambient CO₂ should therefore be carefully chosen when designing sampling strategies. Sensitivity to changes in δ_N and δ_R was found to be low if a strong isotopic disequilibrium of several permil between the isotopic signature of the assimilation flux δ_A ($=\delta_a - \Delta_{canopy}$) and the respiration flux δ_R is present.

4.7 Acknowledgements

This study is supported by the COST 627 initiative “Carbon storage in European Grasslands” (Grant No. C01.0056), Federal office for education and Science. Meteorological data with thanks from Agrometeo Switzerland and MeteoSchweiz.

5 General Discussion

This study advances the field of ecosystem research with stable isotopes by contributing a novel tool for the automated collection of trace gas samples. Furthermore, a new calculation approach for the partitioning of net ecosystem fluxes of H₂O and CO₂ was tested and the associated uncertainties were broadly discussed. The application of the stable isotope ¹³C as a valuable system tracer was demonstrated with the results obtained from SOM within the former FACE site, where a contribution towards the open question concerning carbon sequestration and turnover under elevated CO₂ could be made.

5.1 A novel tool for air sampling

Studies on ecosystem CO₂ flux partitioning depend on a high frequency, high accuracy and large enough range of [CO₂] and δ¹³CO₂ measurements. This is needed to achieve a high precision when applying the two-component mixing model (Keeling plot, Keeling, 1958) used to determine net source values of the air within the investigated area. How high this precision must be has not been defined yet, but in general, values < 1‰ would seem acceptable. Pataki *et al.*, 2003 found mean standard errors of the source values of 1.2‰ by analyzing data from 146 Keeling plots. She also pointed out that the range of sampled CO₂ concentrations can be more important than the amount of samples and should be 75 ppm or larger. This is generally achieved only by sampling over several hours, this applies both for day and night time.

The computer controlled, automated air sampler (ASA) developed in our study allows for 33 air samples being taken in a programmed sequence. Subsequent analysis in the laboratory is fast and does not require additional handling of the samples. The ASA is computer-controlled also during analysis, like an autosampler. Analysis of 33 samples at a continuous-flow mass spectrometer takes less than six hours and the ASA is ready for the next sampling as soon as the analysis is finished. The achieved precision was shown to be twice as high as with manual single-flask analysis, 0.03‰ for δ¹³C and 0.02‰ for δ¹⁸O of CO₂ (standard errors *SE*, n=11). The ASA is also a useful tool for sampling and analysis of trace gases with concentrations up to 1000 times smaller than that of CO₂; e.g. CO and CH₄. Potentially it may also be used for non-carbon containing trace gases such as nitrous or sulphurous oxides, depending on the preparation peripherals at the mass spectrometer. The ASA has also been successfully used at the “High Altitude Research Station Jungfraujoch” and other locations in the Swiss Alps to

sample CO (unpublished data). Two current projects study the influence of wood burning in a remote area in southern Switzerland and the emissions of traffic in a large city, such as Basel.

5.2 CO₂ and H₂O flux partitioning

Flux partitioning of the net water vapor flux (evapotranspiration, ET) into transpiration (T) and soil evaporation (E) was done with the goal to further calculate canopy discrimination (Δ_{canopy}) there from. Δ_{canopy} is a crucial parameter when calculating the partitioning of CO₂ fluxes. The currently used model to assess the $\delta^{18}\text{O}$ composition of the T flux did not yield acceptable results for our data set. Only in a few studies evapotranspiration was partitioned and only in dryer climatic regions than in the current study (e.g. Yepez *et al.*, 2003, Williams *et al.*, 2004). The current model for $\delta^{18}\text{O}$ of T assumes isotopic steady state (ISS) of transpired water and source or xylem water, meaning the transpired water coming from the soil and flowing through the stem and evaporating from the leaves has the same isotopic composition despite the processes in between. Nevertheless, numerous studies have shown previously that leaf water is strongly enriched in $\delta^{18}\text{O}$ during the course of a day (Flanagan and Bain *et al.*, 1991, Harwood *et al.*, 1999). The newest literature discusses observed deviations from ISS (Farquhar *et al.*, 2005) and the need for an adapted model to calculate $\delta^{18}\text{O}$ of the T flux has become apparent. Our approach was to include the isotopic enrichment of leaf water to determine the $\delta^{18}\text{O}$ of the T flux. The obtained results for the H₂O flux partitioning with this new model were acceptable in their magnitude and yielded results for Δ_{canopy} which showed a close relation to water vapor pressure deficit (VPD) and net carbon assimilation. Still, the new model has to be further refined by laboratory experiments, but it should provide grounds for an in-depth discussion.

From our CO₂ data we could derive optimal time slots for CO₂ sampling campaigns within a day or a night. The mixing model (Keeling plot) became less accurate when transition times from day to night and night to day were included in the sampling. Night time ordinate intercepts were found to deviate up to 1.7‰ when including time periods around and shortly after sunset. Night time sampling, which is used to find the isotopic composition of the respiration flux, should commence not before 1-2 hours after sunset at the earliest and stop well before dawn. Day time sampling was found best when also excluding transition times, but, since $\delta^{13}\text{C}$ is subject to much stronger fluctuations during day than night time (due to photosynthesis), an even time distribution for sampling over the whole day is to be preferred.

We found a close link of $\delta^{13}\text{C}$ signatures between assimilation and respiration of the following night. Similar findings have also been made with non-isotope methods; Aeschlimann *et al.*, 2005 found a close interrelation between the magnitude of the daytime net assimilation and the respiration during the following night. These findings may not be directly compared but nevertheless show that processes during day time determine the processes of the subsequent night. Isotopic composition of the night time respiration fluxes during our field campaign showed a link to meteorological conditions (VPD) 3-4 days prior to sampling. This is a shorter time-lag than other investigators had recently found for forest ecosystems (Ekblad *et al.*, 2005, Knohl *et al.*, 2005) but reaction times are expected to be much shorter in a grassland compared to a forest due to the much smaller canopy and therefore smaller shoot-root distances.

5.3 Carbon sequestration

The question if grassland soils would be a sink for carbon under elevated CO_2 conditions cannot be answered conclusively since no significant change of the size of the soil carbon pool was found after ten years of FACE. Studies conducted four and six years prior to this study came to the same conclusion (Van Kessel *et al.*, 2000). Aeschlimann *et al.*, 2005 found a long-term stimulation of net CO_2 assimilation under elevated CO_2 after nine years of FACE, but this increase was compensated for by a concurrent stimulation of night time respiration. Net ecosystem carbon input was therefore not significantly increased. These findings do not support the theory that the soil is the “missing sink” for the amount of the carbon which is “missing” in the atmosphere (in relation to emission calculations). Since the fore mentioned studies, including our own, were all made on grassland, this can not be readily extrapolated to the entire terrestrial biome. But it raises the question if the magnitude of the calculated fluxes between biomes, that lead to the “missing sink” theory, is in fact correct. Since the rates of the individual fluxes within the global carbon cycle are subject to uncertainties, small errors could propagate and lead to erroneous estimates. Otherwise, the soil is a very heterogeneous system with a generally large “patchiness” regarding the distribution of compounds. This generally increases the uncertainties when calculating flux rates. And not to forget, the term “not significant” does not mean “not happening”; changes could be so small in magnitude that they are not detectable due to an unfavorable signal to noise ratio.

5.4 ^{13}C as a system tracer

The ^{13}C label within the soil organic matter (SOM), originating from CO_2 of fossil origin used in the FACE experiment, offered a unique opportunity to study SOM-related processes. A strong label of SOM in 0-12 cm depth (3.4‰) was found after ten years of fumigation with ^{13}C depleted CO_2 , which decreased by 50% within 960 days after the end of the fumigation according to our calculations. From this rapidly diminishing isotopic signal we could further estimate the annual carbon input to be $9.8 \pm 3.7 \text{ Mg ha}^{-1}$ which was slightly higher than the findings of Aeschlimann *et al.*, 2005 and Van Kessel *et al.*, 2000 (both 6.3 Mg ha^{-1}), but the studies did only calculate the input for 0-10 cm soil depth and not for 0-12 cm as we did. Furthermore, the associated errors were large ($> 1/3$ of the actual value) in all studies.

The formerly fumigated soils showing a strong ^{13}C label of SOM were in isotopic disequilibrium with the newly grown plants fixing “normal” undepleted atmospheric CO_2 after the fumigation was stopped. This allowed a separation based on the isotopic composition of soil CO_2 of respired carbon derived from labeled SOM and from fresh plant material. Rhizosphere respiration was thus calculated to account for 61% of total soil respiration. Again, as outlined above that night time respiration is driven by recent assimilation, this shows that ecophysiological factors driving plant activity are of considerable importance for below-ground processes.

5.5 Outlook

New advances for gathering $^{13}\text{CO}_2$ data from field sites have recently been made. Schnyder *et al.*, 2004 introduced a setup for high frequency *in situ* on-line measurements with a mass spectrometer. Bowling and Sargent *et al.*, 2003 tested tunable diode laser (TDL) technique for high frequency analysis of $^{13}\text{CO}_2$ based on the specific absorption of ^{13}C in the infrared spectrum. This seems to be a promising method if the associated technical effort can be reduced (need for liquid nitrogen, $\text{N}_2(l)$), and the precision increased (0.25‰ currently), in particular in combination with high-frequency eddy-covariance measurements for net CO_2 and H_2O ecosystem exchange. Nevertheless, the large amounts of data produced by these systems would also need to be handled.

The presented model for assessing the H_2^{18}O signature of the transpiration flux in plant canopies must be further developed. In a first step the new version of a leaf water enrichment model for H_2^{18}O should be included (Cernusak *et al.*, 2002). In a next step the back diffusion

of depleted water vapor from the ambient air through the stomata into the leaf needs to be considered. For a parametrisation and testing of this new model, laboratory scale gas exchange chamber measurements and experiments in phytotrons with H_2^{18}O marked soil water are needed. Differences in the $\delta^{18}\text{O}$ enrichment in leaves between species should be addressed as well as differences in soil evaporation between different soil types (e.g. sandy soils and loamy soils).

$\delta^{18}\text{O}$ of CO_2 has a large potential to improve the partitioning of carbon fluxes between the atmosphere and terrestrial ecosystems. The underlying processes leading to the isotopic signature are well known (^{18}O equilibration between the water body and the CO_2 with which it gets in contact) and the principles understood (Ogee *et al.*, 2004). The current associated problems evolve from the large scattering of $\delta^{18}\text{O}$ in these samples. This calls for an increased effort to improve the sampling methods. Recent attempts to use the $\delta^{18}\text{O}$ in CO_2 as a proxy for leaf and soil water enrichment are promising (Theis, unpublished data, Bowling, unpublished data).

In our study the basic applicability of water vapor and CO_2 flux partitioning on a temperate grassland site was demonstrated. There is need for further research in particular regarding the link of H_2O and CO_2 partitioning models. The combination of stable oxygen and carbon isotopes is a very useful and promising tool.

6 References

- Aeschlimann, U., 2003. Effects of elevated atmospheric pCO₂ on net ecosystem CO₂ exchange in managed grassland. *Thesis, ETH Zurich*, **15182**,
- Aeschlimann, U., Nösberger, J., Edwards, P. J., Schneider, M. K., Richter, M. *et al.*, 2005. Responses of net ecosystem CO₂ exchange in managed grassland to long-term CO₂ enrichment, N fertilization and plant species. *Plant, Cell and Environment*, **in press**,
- Amundson, R., Stern, L., Baisden, T. & Wang, Y., 1998. The isotopic composition of soil and soil-respired CO₂. *Geoderma*, **82**, 83-114.
- Baldocchi, D. D. & Bowling, D. R., 2003. Modelling the discrimination of ¹³CO₂ above and within a temperate broad-leaved forest canopy on hourly to seasonal time scales. *Plant, Cell and Environment*, **26**, 231-244.
- Baldocchi, D. D., Hicks, B. & Meyers, T., 1988. Measuring biosphere atmosphere exchanges of biologically related gases with micrometeorological methods. *Ecology*, **69**, 1331-1340.
- Balesdent, J. & Mariotti, A., 1987. Natural ¹³C abundance as a tracer for studies of soil organic matter dynamics. *Soil Biol. Biochem.*, **10**, 25-30.
- Balesdent, J., Wagner, G. H. & Mariotti, A., 1988. Soil organic matter turnover in long-term field experiments as revealed by carbon-13 natural abundance. *Soil Science Society of America Journal*, **52**, 118-124.
- Beer, J., Mende, W. & Stellmacher, R., 2000. The role of the sun in climate forcing. *Quaternary Science Reviews*, **19**, 403-415.
- Bond, G., Kromer, B., Beer, J., Muscheler, R., Evans, M. N. *et al.*, 2001. Persistent solar influence on north Atlantic climate during the Holocene. *Science*, **294**, 2130-2136.
- Boschker, H. T. S. & Middelburg, J. J., 2002. Stable isotopes and biomarkers in microbial ecology. *FEMS Microbiology Ecology*, **40**, 85-95.
- Bowling, D. R., McDowell, N. G., Bond, B. J., Law, B. E. & Ehleringer, J. R., 2002. ¹³C content of ecosystem respiration is linked to precipitation and vapor pressure deficit. *Oecologia*, **131**, 113-124.
- Bowling, D. R., Pataki, D. E. & Ehleringer, J. R., 2003. Critical evaluation of micrometeorological methods for measuring ecosystem-atmosphere isotopic exchange of CO₂. *Agricultural and Forest Meteorology*, **116**, 159-179.
- Bowling, D. R., Sargent, S. D., Tanner, B. D. & Ehleringer, J. R., 2003. Tunable diode laser absorption spectroscopy for stable isotope studies of ecosystem-atmosphere CO₂ exchange. *Agricultural and Forest Meteorology*, **118**, 1-19.
- Bowling, D. R., Tans, P. P. & Monson, R. K., 2001. Partitioning net ecosystem carbon exchange with isotopic fluxes of CO₂. *Global Change Biology*, **7**, 127-145.
- Broecker, W. S. & Peng, T. H., 1992. Interhemispheric transport of carbon dioxide by ocean circulation. *Nature*, **356**, 587-589.
- Buchmann, N., 2000. Biotic and abiotic factors controlling soil respiration rates in *Picea abies* stands. *Soil Biol. Biochem.*, **32**, 1625-1635.
- Bundt, M., Jäggi, M., Blaser, P., Siegwolf, R. T. W. & Hagedorn, F., 2001. Carbon and Nitrogen Dynamics in Preferential Flow Paths and Matrix of a Forest Soil. *Soil Science Society of America Journal*, **65**, 1529-1538.

- Cappa, C. D., Hendricks, M. B., DePaolo, D. J. & Cohen, R. C., 2003. Isotopic fractionation of water during evaporation. *Journal of Geophysical Research-Atmospheres*, **108**, 4525 doi:10.1029/2003JD003597.
- Cernusak, L. A., Pate, J. S. & Farquhar, G. D., 2002. Diurnal variation in the stable isotope composition of water and dry matter in fruiting *Lupinus angustifolius* under field conditions. *Plant, Cell and Environment*, **25**, 893-907.
- Craig, H. & Gordon, L., 1965. Deuterium and Oxygen-18 variations in the ocean and marine atmosphere. In: *Tongiorgi, E., (ed), Proceeding of a Conference on Stable Isotopes in Oceanographic Studies and Paleotemperatures, Laboratory of Geology and Nuclear Science, Spoleto, Italy. Lischi and Figli, Pisa*, 9-130.
- Craine, J. M., Wedin, D. A. & Chapin, F. S., 1999. Predominance of ecophysiological controls on soil CO₂ flux in a Minnesota grassland. *Plant and Soil*, **207**, 77-86.
- De Graaf, M.-A., Six, J., Harris, D., Blum, H. & Van Kessel, C., 2004. Decomposition of soil and plant carbon from pasture systems after 9 years of exposure to elevated CO₂: impact on C cycling and modeling. *Global Change Biology*, **10**, 1922-1935.
- Dongmann, G., Nurnberg, H. W., Forstel, H. & Wagener, K., 1974. On the Enrichment of H₂(18-O) in the Leaves of Transpiring Plants. *Radiation and Environmental Biophysics*, **11**, 41-52.
- Duranceau, M., Ghashghaie, J., Badeck, F., Deleens, E. & Cornic, G., 1999. delta C-13 of CO₂ respired in the dark in relation to delta C- 13 of leaf carbohydrates in *Phaseolus vulgaris* L-under progressive drought. *Plant Cell and Environment*, **22**, 515-523.
- Ekblad, A., Boström, B., Holm, A. & Comstedt, D., 2005. Forest soil respiration rate and d13C is regulated by recent above ground weather conditions. *Oecologia*, **143**, 136-142.
- Ekblad, A. & Högberg, P., 2001. Natural abundance of 13C in CO₂ respired from forest soils reveals speed of link between tree photosynthesis and root respiration. *Oecologia*, **127**, 305-308.
- Evans, J. R. & von Caemmerer, S., 1996. Carbon dioxide diffusion inside leaves. *Plant Physiology*, **110**, 339-346.
- Farquhar, G. D. & Cernusak, L. A., 2005. On the isotopic composition of leaf water in the non-steady state. *Functional Plant Biology*, **32**, 293-303.
- Farquhar, G. D., Ehleringer, J. R. & Hubick, K. T., 1989. Carbon Isotope Discrimination and Photosynthesis. *Annual Review of Plant Physiology and Plant Molecular Biology*, **40**, 503-537.
- Flanagan, L. B., Bain, J. F. & Ehleringer, J. R., 1991. Stable oxygen and hydrogen isotope composition of leaf water in C₃ and C₄ plant species under field conditions. *Oecologia*, **88**, 394-400.
- Flanagan, L. B., Brooks, R., Varney, G. T., Berry, S. C. & Ehleringer, J. R., 1996. Carbon isotope discrimination during photosynthesis and the isotope ratio of respired CO₂ in boreal forest ecosystems. *Global Biogeochemical Cycles*, **10**, 629-640.
- Flanagan, L. B. & Ehleringer, J. R., 1991. Stable isotope composition of stem and leaf water: applications to the study of plant water use. *Functional Ecology*, **5**, 270-277.
- Fontaine, S., Mariotti, A. & Abbadie, L., 2003. The priming effect of organic matter: a question of microbial competition? *Soil Biology and Biochemistry*, **35**, 837-843.
- Friedli, H., Löttscher, H., Oeschger, H., Siegenthaler, U. & Stauffer, B., 1986. Ice core record of the 13C/12C ratios of atmospheric CO₂ in the past two centuries. *Nature*, **324**, 237-238.

- Gat, J. R., 1996. OXYGEN AND HYDROGEN ISOTOPES IN THE HYDROLOGIC CYCLE. *Annu. Rev. Earth Planet. Sci.*, **24**, 225-262.
- Ghashghaie, J., Duranceau, M., Badeck, F. W., Cornic, G., Adeline, M. T. *et al.*, 2001. delta C-13 of CO₂ respired in the dark in relation to delta C-13 of leaf metabolites: comparison between *Nicotiana sylvestris* and *Helianthus annuus* under drought. *Plant Cell and Environment*, **24**, 505-515.
- Gifford, R. M., 1994. The global carbon cycle: a viewpoint on the missing sink. *Australian Journal of Plant Physiology*, **21**, 1-15.
- Harwood, K. G., Gillon, J. S., Roberts, A. & Griffiths, H., 1999. Determinants of isotopic coupling of CO₂ and water vapour within a *Quercus petraea* forest canopy. *Oecologia*, **119**, 109-119.
- Hebeisen, T., Lüscher, A., Zanetti, S., Fischer, B. U., Hartwig, U. A. *et al.*, 1997. Growth response of *Trifolium repens* L. and *Lolium perenne* L. as monocultures and bi-species mixture to free air CO₂ enrichment and management. *Global Change Biology*, **3**, 149-160.
- Hendrey, G. R., 1992. Global greenhouse studies: need for a new approach to ecosystem management. *Critical Reviews in Plant Sciences*, **11**, 61-74.
- Högberg, P., Nordgren, A., Buchmann, N., Taylor, A. F. S., Ekblad, A. *et al.*, 2001. Large-scale forest girdling shows that current photosynthesis drives soil respiration. *Nature*, **411**, 789-792.
- Houghton, J. T., Ding, Y., Griggs, D. J., Nogue, M., van der Linden, P. J. *et al.*, 2001. Climate Change 2001: The Scientific Basis. *Cambridge University Press, Cambridge*, 183-237.
- Hungate, B. A., Holland, E. A., Jackson, R. B., Chapin, F. S., Mooney, H. A. *et al.*, 1997. The fate of carbon in grasslands under carbon dioxide enrichment. *Nature*, **388**, 576-579.
- Jones, M. B. & Donnelly, A., 2004. Carbon sequestration in temperate grassland ecosystems and the influence of management, climate and elevated CO₂. *New Phytologist*, **164**, 423-439.
- Kato, T., Kimura, R. & Kamichika, M., 2004. Estimation of evapotranspiration, transpiration ratio and water-use efficiency from a sparse canopy using a compartment model. *Agricultural water management*, **65**, 173-191.
- Keeling, C. D., 1958. The concentration and isotopic abundances of atmospheric carbon dioxide in rural areas. *Geochimica et Cosmochimica Acta*, **13**, 322-334.
- Knohl, A., Werner, R. A., Brand, W. A. & Buchmann, N., 2005. Short-term variations in d13C of ecosystem respiration reveals link between assimilation and respiration in a deciduous forest. *Oecologia*, **142**, 70-82.
- Lai, C. T., Schauer, A. J., Owensby, C., Ham, J. M. & Ehleringer, J. R., 2003. Isotopic air sampling in a tallgrass prairie to partition net ecosystem CO₂ exchange. *Journal of Geophysical Research-Atmospheres*, **108**,
- Lamaud, E., Brunet, Y., Labatut, A., Lopez, A., Fontan, J. *et al.*, 1994. The Landes experiment: Biosphere-atmosphere exchanges of ozone and aerosol particles above a pine forest. *Journal of Geophysical Research-Atmospheres*, **99**, 16511-16521.
- Lin, G. H. & Ehleringer, J. R., 1997. Carbon isotopic fractionation does not occur during dark respiration in C-3 and C-4. *Plant Physiology*, **114**, 391-394.
- Maier-Reimer, E., Mikolajewicz, U. & Winguth, A., 1996. Future ocean uptake of CO₂: interaction between ocean circulation and biology. *Climate Dynamics*, 711-721.
- Majoube, M., 1971. Fractionnement en oxygène 18 et en deutérium entre l'eau et sa vapeur. *J. de Chim. Phys. et de Phys.-Chim. Biol*, **68**, 1423-1436.

- Mak, J. E. & Yang, W., 1998. Technique for analysis of air samples for ^{13}C and ^{18}O in carbon monoxide via continuous-flow isotope ratio mass spectrometry. *Analytical Chemistry*, **70**, 5159-5161.
- McNamara, N., Benham, D., Sleep, D., Grant, H. & Stott, A., 2002. Development of a trace gas stable isotope capture system in a mobile laboratory for temporal and spatial sampling of field and laboratory experiments. *Rapid Communications in Mass Spectrometry*, **16**, 2165-2171.
- Moreira, M. Z., Sternberg, L. D. L., Martinelli, L. A., Victoria, R. L., Barbosa, E. M. *et al.*, 1997. Contribution of transpiration to forest ambient vapour based on isotopic measurements. *Global Change Biol*, **3**, 439-450.
- Mortazavi, B. & Chanton, J. P., 2002. A rapid and precise technique for measuring $\text{d}^{13}\text{C}\text{-CO}_2$ and $\text{d}^{18}\text{O}\text{-CO}_2$ ratios at ambient CO_2 concentrations for biological applications and the influence of container type and storage time on the sample isotope ratios. *Rapid Communications in Mass Spectrometry*, **16**, 1398-1403.
- Nadelhoffer, K. J. & Fry, B., 1988. Controls on Natural Nitrogen-15 and Carbon-13 Abundances in Forest Soil Organic Matter. *Soil Science Society of America Journal*, **52**, 1633-1640.
- Nelson, S. T., 2000. Sample vial influences on the accuracy and precision of carbon and oxygen isotope ratio analysis in continuous flow mass spectrometric applications. *Rapid Communications in Mass Spectrometry*, **14**, 293-297.
- Nitschelm, J. J., Lüscher, A., Hartwig, U. A. & Van Kessel, C., 1997. Using stable isotopes to determine soil carbon input differences under ambient and elevated atmospheric CO_2 conditions. *Global Change Biology*, **3**, 411-416.
- Nobel, P. S., 1983. Biophysical Plant Physiology and Ecology. *W. H. Freeman, New York*, 393.
- Nösberger, J., Blum, H. & Fuhrer, J., 2000. Crop ecosystem responses to climatic change: productive grasslands. *In: Reddy, K.R., Hodges, H.F. (eds.), Climate Change and Global Crop Productivity. CAB International, Wallingford, Oxon*, pp. 271-291.
- Ogee, J., Peylin, P., Ciais, P., Bariac, T., Brunet, Y. *et al.*, 2003. Partitioning net ecosystem carbon exchange into net assimilation and respiration using $(\text{CO}_2)\text{-C-13}$ measurements: A cost-effective sampling strategy. *Global Biogeochemical Cycles*, **17**, art. no.-1070.
- Ogee, J., Peylin, P., Cuntz, M., Bariac, T., Brunet, Y. *et al.*, 2004. Partitioning net ecosystem carbon exchange into net assimilation and respiration with canopy-scale isotopic measurements: An error propagation analysis with $(\text{CO}_2)\text{-C-13}$ and $(\text{COO})\text{-O-18}$ data. *Global Biogeochemical Cycles*, **18**, art. no.-GB2019.
- O'Leary, M. H., 1981. Carbon isotope fractionation in plants. *Phytochemistry*, **20**, 553-567.
- Pataki, D. E., Ehleringer, J. R., Flanagan, L. B., Yakir, D., Bowling, D. R. *et al.*, 2003. The application and interpretation of Keeling plots in terrestrial carbon cycle research. *Global Biogeochemical Cycles*, **17**, 1022.
- Pearcy, R. W., Ehleringer, J. R., Mooney, H. A. & Rundel, P. W. e., 1989. Plant Physiological Ecology Field Methods and Instrumentation. *Chapman and Hall, London*,
- Pelz, O., Abraham, W.-R., Saurer, M., Siegwolf, R. T. W. & Zeyer, J., 2005. Microbial assimilation of plant-derived carbon in soil traced by isotope analysis. *Biol Fertil Soils*, **41**, 153-162.
- Petit, J. R., Jouzel, J., Raynaud, D., Barkov, N. I., Barnola, J.-M. *et al.*, 1999. Climate and atmospheric history of the past 420,000 years from the Vostok ice core, Antarctica. *Nature*, **399**, 429-436.
- Post, W. M., Emanuel, W. R., Zinke, P. J. & Stangenberger, A. G., 1982. Soil carbon pools and world life zones. *Nature*, **298**, 156-159.

- Ribas-Carbo, M., Still, C. & Berry, J., 2002. Automated system for simultaneous analysis of $\delta^{13}\text{C}$, $\delta^{18}\text{O}$ and CO_2 concentrations in small air samples. *Rapid Communications in Mass Spectrometry*, **16**, 339-345.
- Schauer, A. J., Lai, C.-T., Bowling, D. R. & Ehleringer, J. R., 2003. An automated sampler for collection of atmospheric trace gas samples for stable isotope analyses. *Agricultural and Forest Meteorology*, **118**, 113-124.
- Scheidegger, Y., Saurer, M., Bahn, M. & Siegwolf, R. T. W., 2000. Linking stable oxygen and carbon isotopes with stomatal conductance and photosynthetic capacity: a conceptual model. *Oecologia*, **125**, 350-357.
- Schimel, D. S., 1995. Terrestrial ecosystems and the carbon cycle. *Global Change Biology*, **1**, 77-91.
- Schneider, M. K., Lüscher, A., Richter, M., Aeschlimann, U., Hartwig, U. A. *et al.*, 2004. Ten years of free-air CO_2 enrichment altered the mobilization of N from soil in *Lolium perenne* L. swards. *Global Change Biology*, **10**, 1377-1388.
- Schnyder, H., Schäufele, R. & Wenzel, R., 2004. Mobile, outdoor continuous-flow isotope-ratio mass spectrometer system for automated high-frequency ^{13}C - and ^{18}O - CO_2 analysis for Keeling plot applications. *Rapid Communications in Mass Spectrometry*, **18**, 3068-3074 (DOI: 10.1002/rcm.1731).
- Sene, K. J., 1994. Parameterisations for energy transfers from a sparse vine crop. *Agricultural and Forest Meteorology*, **71**, 1-18.
- Shuttleworth, W. J. & Wallace, J. S., 1985. Evaporation from sparse crops - an energy combination theory. *Q. J. R. Meteorol. Soc.*, **111**, 839-855.
- Sims, P. L. & Risser, P. G., 2000. Grasslands. In: *Barbour M. G., Billings, W. G. (eds) Cambridge University Press, New York, pp 323-356*,
- Six, J., Carpentier, A., van Kessel, C., Merckx, R., Harris, D. *et al.*, 2001. Impact of elevated CO_2 on soil organic matter dynamics as related to changes in aggregate turnover and residue quality. *Plant and Soil*, **234**, 27-36.
- Smith, B. N. & Epstein, S., 1971. Two categories of $^{13}\text{C}/^{12}\text{C}$ ratios for higher plants. *Plant Physiology*, **47**, 380-384.
- Soe, A. R. B., Giesemann, A., Anderson, T. H., Weigel, H. J. & Buchmann, N., 2004. Soil respiration under elevated CO_2 and its partitioning into recently assimilated and older carbon sources. *Plant and Soil*, **262**, 85-94.
- Sokal, R. R. & Rohlf, F. J., 1995. Biometry. *W. H. Freeman, New York*,
- Soussana, J. F., Loiseau, P., Vuichard, N., Ceschia, E., Balesdent, J. *et al.*, 2004. Carbon cycling and sequestration opportunities in temperate grasslands. *Soil Use and Management*, **20**, 219-230.
- Steinmann, K., Siegwolf, R. T. W., Saurer, M. & Körner, C., 2004. Carbon fluxes to the soil in a mature temperate forest assessed by ^{13}C isotope tracing. *Oecologia*, **141**, 489-501.
- Tcherkez, G., Nogues, S., Bleton, J., Cornic, G., Badeck, F. *et al.*, 2003. Metabolic Origin of Carbon Isotope Composition of Leaf Dark-Respired CO_2 in French Bean. *Plant Physiology*, **131**, 237-244.
- Theis, D. E., Saurer, M., Blum, H., Frossard, E. & Siegwolf, R. T. W., 2004. A portable automated system for trace gas sampling in the field and stable isotope analysis in the laboratory. *Rapid Communications in Mass Spectrometry*, **18**, 2106-2112 (DOI: 10.1002/rcm.1596).
- Van Groenigen, K. J., Six, J., Harris, D., Blum, H. & Van Kessel, C., 2003. Soil C-13-N-15 dynamics in an N-2-fixing clover system under long-term exposure to elevated atmospheric CO_2 . *Global Change Biology*, **9**, 1751-1762.

- Van Kessel, C., Nitschelm, J., Horwath, W. R., Harris, D., Walley, F. *et al.*, 2000. Carbon-13 input and turn-over in a pasture soil exposed to long-term elevated atmospheric CO₂. *Global Change Biology*, **6**, 123-135.
- Wang, W. J., Dalal, R. C., Moody, P. W. & Smith, C. J., 2003. Relationships of soil respiration to microbial biomass, substrate availability and clay content. *Soil Biology and Biochemistry*, **35**, 273-284.
- Wang, X.-F. & Yakir, D., 2000. Using stable isotopes of water in evapotranspiration studies. *Hydrological Processes*, **14**, 1407-1421.
- Wardle, D. A. & Parkinson, D., 1990. Interactions between microclimatic variables and the soil microbial biomass. *Biol Fertil Soils*, **9**, 273-280.
- Webb, T., Howe, S. E., Bradshaw, R. H. W. & Heide, K. M., 1981. Estimating plant abundance from pollen percentages: the use of regression analysis. *Review of Palaeobotany and Palynology*, **34**, 269-300.
- Williams, D. G., Cable, W., Hultine, K., Hoedjes, J. C. B., Yezpez, E. A. *et al.*, 2004. Evapotranspiration components determined by stable isotope, sap flow and eddy covariance techniques. *Agricultural and Forest Meteorology*, **125**, 241-258.
- Xie, Z., Cadisch, G., Edwards, G., Baggs, E., M. & Blum, H., 2005. Carbon dynamics in a temperate grassland soil after 9 years exposure to elevated CO₂ (Swiss FACE). *Soil Biol. Biochem.*, **37**, 1387-1395.
- Yakir, D. & Sternberg, L. D. L., 2000. The use of stable isotopes to study ecosystem gas exchange. *Oecologia*, **123**, 297-311.
- Yakir, D. & Wang, X. F., 1996. Fluxes of CO₂ and water between terrestrial vegetation and the atmosphere estimated from isotope measurements. *Nature*, **380**, 515-517.
- Yezpez, E. A., Williams, D. G., Scott, R. L. & Lin, G. H., 2003. Partitioning overstory and understory evapotranspiration in a semiarid savanna woodland from the isotopic composition of water vapor. *Agricultural and Forest Meteorology*, **119**, 53-68.
- Zanetti, S., Hartwig, U. A., Lüscher, A., Hebeisen, T., Frehner, M. *et al.*, 1996. Stimulation of Symbiotic N₂ Fixation in *Trifolium repens* L. under Elevated Atmospheric pCO₂ in a Grassland Ecosystem. *Plant Physiology*, **112**, 575-583.

Appendix

A short introduction to stable isotopes and their applications

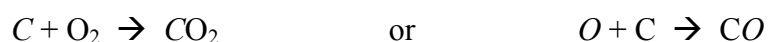
Definition

The number of protons within an atom determines its basic chemical properties, which for example, makes a certain atom to be a “carbon” or a “sulfur” atom. Chemical reactions and bonds between atoms take place in the electron cloud around its nucleus, which corresponds to the nucleus in electric charge (with the exceptions of ions, where charges deviate). The second component of the nucleus are neutrons, with no electric charge. Isotopes are defined as atoms with the same number of protons but a different number of neutrons. The name “isotope” is derived from Greek, meaning “same place”; this refers to the “same place” in the periodic table of the elements. This means that isotopes of a single element do not differ in basic chemical, but rather in physical properties due to their different mass and can be detected with the appropriate instrumentation, for example a mass spectrometer.

There are chemically stable and unstable forms of isotopes. Unstable isotopes, for example ^{14}C , decay over time and are a source of radioactive radiation and are therefore called “radionuclides”. Stable isotopes, in contrast, for example ^{13}C , do not decay and are distinguishable by mass from the “main” isotope of an element (e.g. ^{12}C). Abundances of stable isotopes are a percentage fraction or less, for instance ^{13}C accounts for 1.1 % of the total carbon ($^{12}\text{C} + ^{13}\text{C} + ^{14}\text{C}$, the latter is a radionuclide) and ^{18}O for 0.2 % of the total oxygen ($^{16}\text{O} + ^{17}\text{O} + ^{18}\text{O}$, all stable). Since their mass differs slightly, physical processes like phase change, diffusion and adsorption lead to accumulation or depletion of stable isotopes within different compartments in nature. This is referred to as a “fractionation” process.

Mass spectrometry

Isotopes are measured with mass spectrometers, which have a history of almost one hundred years. Since then, mass spectrometry has been continuously improved in measurement precision. Since only gaseous compounds can be analyzed directly, solid and liquid samples need first to be transferred to a gaseous state. For the example of carbon and oxygen, this is done by either pyrolysis or oxidative combustion. The resulting gases contain the original carbon or oxygen atoms but now coupled to newly introduced carbon or oxygen atoms, giving either carbon dioxide (CO_2) or carbon monoxide (CO), depending on the atom of interest.



The obtained gas is ionized in high vacuum by a cathode beam and then accelerated by a high-voltage electric field (3-5 kV). Focused to a thin ion beam by two parallel plates, the positively charged ions are deflected in a strong (adjustable) magnetic field (Figure 1). The isotopes, differing in mass, are deflected from their flight path proportionally to their mass and hit the detector at different points. The intensity of the ion beam at each detection point is then calculated into a ratio for the isotopes. Measurements are always made relative to a standard gas which needs to be injected with every sample. The obtained ratio is then expressed relative to an international standard; VPDB for carbon or SMOW for oxygen as an example.

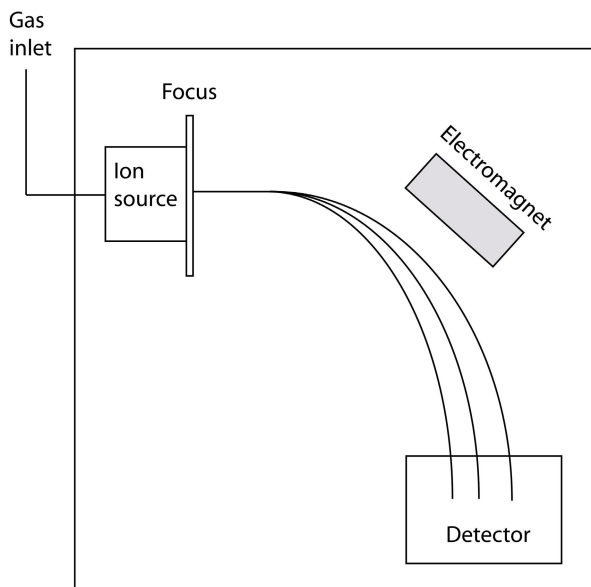


Figure 1 Schematic of an isotope ratio mass spectrometer

The notation used to express the ratio of a sample relative to a standard is the “ δ ” which itself is dimensionless but is expressed as a ‰ fraction, here shown for ^{13}C :

$$\delta^{13}\text{C} = \left[\frac{R(\text{sample})}{R(\text{standard})} - 1 \right] * 1000 \quad \text{with} \quad R = \frac{^{13}\text{C}}{^{12}\text{C}}$$

Positive values for δ therefore mean a sample is enriched relative to the standard, whereas zero means equality and negative values indicate depletion. As an example: the standard for ^{13}C (VPDB) contains an absolute amount of 1.1237‰ of ^{13}C . An air sample of CO_2 which contains 1.1147‰ of ^{13}C , therefore has a $\delta^{13}\text{C}$ value of -8‰.

Applications

As pointed out above, abundances of isotopes of the same atom can vary within different compartments due to physical or physico-chemical fractionation processes.

Plants discriminate the heavy ^{13}C isotope over the ^{12}C isotope during the photosynthetic process (98.9% of the carbon is ^{12}C). This means that plant biomass is depleted in ^{13}C relative to the CO_2 in the atmosphere. All plants and plant-derived products show this depletion: humus in soils, fossil fuels, all higher organisms.

Water shows fractionation processes between ^{18}O and ^{16}O during evaporation and condensation processes, making rainfall more depleted in ^{18}O the further away it falls from the evaporating source, which often is the ocean (Figure 2).

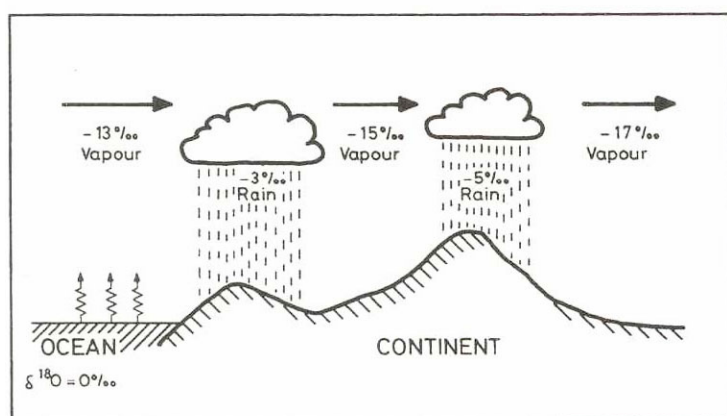


Figure 2 Oxygen isotope fractionation of water in the atmosphere (after Siegenthaler 1979)

There are numerous possible applications for stable isotopes. They can be used as system tracers (natural or added) providing information of processes within a system, e.g. biological systems or as an example the hydrological cycle. They are widely applied in geosciences for climate reconstruction from ice cores (long term) or tree rings (short term). Numerous applications in life sciences and even forensic medicine make stable isotopes a unique and valuable tool.

Further reading:

Hoefs, J., 1996. Stable isotope geochemistry. *Springer, Berlin*

Griffiths, H., 1998. Stable isotopes: The integration of biological, ecological and geological processes. *Bios scientific publishers, Oxford, UK*

Broecker, W., 1985. How to build a habitable planet. *Eldigio Press, Palisades, NY*

Acknowledgements

Thanks goes out to all the wonderful beings who made this work possible and for providing a good atmosphere to work with: the group in the Laboratory of Atmospheric Chemistry at the Paul Scherrer Institute, the people in Eschikon from the group of Plant Nutrition and the Grassland Science group at ETH Zürich. A special thanks goes out to Rolf Siegwolf for his faith and support. Many thanks also to Herbert Blum for sharing fun and tough hours in the field and keeping cool in hectic times. Thanks to all of you from the Stable Isotope Research Group at the Paul Scherrer Institute: Maya, Matthias, Sonja, Christina, Eva. Thanks to Doris for all the good laughs and discussions.

And this goes out to my family and friends.

Without you, all this would be meaningless.

Curriculum vitae

Daniel Ethan Theis

born 29th August 1972 in Zürich, Switzerland

citizen of Winterthur (ZH) and Schaffhausen (SH)

2002 - 2005	Ph.D. in Environmental Sciences at the Paul Scherrer Institute (PSI, ETH Zürich), Villigen, Switzerland
1999 - 2002	Scientific collaborator, Institute for Computational Science, ETH Zürich
1999	Thesis (M. Sc. Microbiology), University of Zürich “Influence of suspended erosion particles on the microbiota in an oligotrophic high mountain lake”
1994 - 1999	Studies of Microbiology and Environmental Sciences at the University of Zürich Major: Microbiology Minor: Limnology and Plant Sciences
1991 - 1994	Commercial clerk in various companies
1987 - 1991	Gymnasium (High School) Type C (Mathematical), Kantonsschule im Lee, Winterthur (ZH)
1979 - 1987	Primary and Secondary School (Primar and Sekundarschule), Winterthur (ZH)